Instituto de Tecnologia Química e Biológica
da Universidade Nova de Lisboa

NMR STUDIES OF TETRAHAEM CYTOCHROMES FROM *D. DESULFURICANS* AND *S. FRIGIDIMARINA*

VÍTOR MANUEL BORDONA DE SOUSA PAIXÃO

Dissertation Presented to obtain the Ph.D. in Biochemistry.

OEIRAS, SEPTEMBER 2010

To my grandparents:
Virgínia and Ilídio, Almerinda and Jorge

ACKNOWLEDGEMENTS

No scientific work is ever the product of one person's efforts, and certainly this one was no different. I have been very fortunate over the years to collaborate with many supportive friends and colleagues without whom this work would not have been possible.

My biggest thanks go to my supervisors; Prof. António Xavier for the enlightened leadership, warm encouragement and guidance and to Prof. David Turner for his patience, advice and expertise.

I am also deeply grateful to Prof. Carlos Salgueiro, upon whose assistance I have called far more often than is reasonable, for his friendship, generosity and support over the years. A special thanks goes to Dr. Miguel Pessanha for all the help with NMR spectra and the useful suggestions in the darkest hours.

I would like to thank Dr. Ricardo Louro for introducing me to NMR spectroscopy and for valuable assistance during the first years in the lab; and Isabel Pacheco for the growth and help with the purification of cytochrome c_3 from *D. desulfuricans*. I would also like to thank Fátima Madeira for her generosity and help with the bureaucratic affairs and to all the former members of Prof. Xavier's group; Prof. Teresa Catarino, Dr. Catarina Paquete, Dr. Patricia Pereira, Dr. Ilídio Correia and Prof. António Aguiar for their friendship and excellent working environment.

During the writing of this thesis I held a position at Instituto Gulbenkian de Ciência in the neurobiology of action group. I am particularly grateful to Dr. Rui Costa for his patience, support and understanding even when the manuscript took time from the work in the laboratory.

Last but not least I want to thank my family and friends for the unconditional support and encouragement. A special mentioning to my mother and Dino for being there when I needed the most, and to Vanessa for persistently *persuade* me to finish what it seemed like a never ending work.

Finally, I must acknowledge the ITQB for providing the excellent conditions under which this work took place and Fundação para a Ciência e Tecnologia for the funding.

Oeiras, August 2010
Vitor Paixão

RESUMO

Os citocromos tetrahémicos são proteínas solúveis com cerca de 80-120 aminoácidos em que os quatro grupos hemo se encontram coordenados axialmente por dois resíduos de histidina. Estas proteínas foram identificadas pela primeira vez na década de 1950 na bactéria *Desulfovibrio vulgaris* e, mais recentemente, em outros microrganismos.

As estruturas determinadas até à data por cristalografia de raios-X ou por ressonância magnética nuclear (RMN) para citocromos tetrahémicos isolados de *Desulfovibrio* spp. (Dc_3), mostram que o núcleo central destas proteínas, formado pelos quatro grupos hemos, bem como o enrolamento das proteínas, é conservado em todos os Dc_3 apesar da baixa homologia das suas sequências de aminoácidos. A pequena dimensão destas proteínas, e a concomitante proximidade dos diferentes grupos hemo, fazem com que o estado de oxidação de um hemo altere o potencial de redução de um hemo vizinho (interações redox), os quais são também afectados pelo pH (interações redox–Bohr).

Deste modo, os citocromos tetrahémicos constituem um excelente modelo para investigação dos processos cooperativos associados à transferência electrónica e transdução de energia nos sistemas biológicos. Tendo em vista a elucidação dos mecanismos estruturais/funcionais associados a estes processos utilizou-se a técnica de RMN para determinar as estruturas tridimensionais em solução de dois citocromos tetrahémicos de dois microrganismos diferentes.

No Capítulo 1 desta Tese, apresenta-se uma breve revisão das características mais relevantes do ponto de vista biológico e bioquímico dos microrganismos e proteínas em estudo. Neste primeiro capítulo são ainda apresentados alguns aspectos da técnica de RMN, com particular ênfase no cálculo dos desvios dipolares e dos tensores de susceptibilidade magnética em proteínas paramagnéticas. No Capítulo 2 descrevem-se os conceitos básicos da espectroscopia bi-dimensional de RMN e métodos de cálculo de estruturas em solução.

No Capítulo 3 apresentam-se as estruturas em solução da forma reduzida e oxidada do citocromo tetrahémico c_3 de *Desulfovibrio desulfuricans* ATCC 27774. Este citocromo desempenha um papel fundamental no metabolismo energético deste organismo acoplando a transferência de electrões e protões para a hidrogenase e de todos os Dc_3 já estudados é o único que apresenta dois centros redox-Bohr distintos. As estruturas na forma reduzida e oxidada foram determinadas a valores de pH inferiores aos pK_a dos grupos envolvidos no efeito redox-Bohr, de forma a garantir que as variações encontradas entre as duas estruturas reflectissem apenas modificações associadas à alteração do estado redox da proteína. As alterações conformacionais observadas explicam a cooperatividade positiva entre os hemos 1 e 2.

Finalmente, no Capítulo 4 apresenta-se a estrutura de um novo citocromo tetrahémico isolado da bactéria *Shewanella frigidimarina* (*Sfc*) o qual se encontra envolvido na cadeia de transporte electrónico conducente à redução de Fe(III). A estrutura apresentada é a primeira estrutura em solução de uma proteína multihémica a ser descrita para *Shewanella* spp. A análise da estrutura do *Sfc* revelou a existência de um motivo estrutural claramente distinto do existente nos Dc_3. O motivo estrutural identificado para *Sfc* apresenta uma disposição dos hemos e enrolamento geral da cadeia polipeptídica semelhantes aos encontrados para o citocromo tetrahémico homólogo de *Shewanella oneidensis* e para o domínio N-terminal dos flavocitocromos de *S. frigidimarina* e *S. oneidensis*, cujas estruturas foram determinadas por cristalografia de raios-X. Os resultados obtidos sugerem que a arquitectura dos centros redox é extremamente conservada entre os membros do género *Shewanella*, apesar da grande variabilidade verificada na sequência dos aminoácidos e potenciais de redução dos diferentes grupos hemo.

SUMMARY

Tetrahaem cytochromes are small soluble proteins with four non-planar haems with bis-histidinyl axial coordination that were first isolated from *Desulfovibrio vulgaris* in the 1950s and subsequently in several other bacteria. Even though the sequence homology, the amino acid composition and the thermodynamic properties of the several tetrahaem cytochromes may be different; the overall haem core architecture and the general fold of the protein established by X-ray crystallography and nuclear magnetic resonance (NMR) are highly conserved.

Because of their small size, haem close proximity, redox and redox-Bohr (pH dependent) interactions, these cytochromes are an appropriate model to study cooperative processes in biological systems. In this Thesis NMR was used to determine three-dimensional solution structures of two tetrahaem cytochromes from two different organisms.

In Chapter One we present a basic introduction concerning the organisms and proteins studied in this work as well as some relevant topics of NMR, including the calculation of dipolar shifts and magnetic susceptibility tensor calculation for paramagnetic proteins. Chapter Two deals mostly with the description of two-dimensional NMR spectroscopy concepts and NMR solution structure calculation methods.

In Chapter Three we present the structures of cytochrome c_3 from *Desulfovibrio desulfuricans* ATCC 27774 in the reduced (diamagnetic) and oxidised (paramagnetic) forms obtained from homonuclear NMR spectra. This cytochrome plays a central role in the energetic metabolism of its organism by coupling the transfer of electrons and protons to hydrogenase. The studies were carried out at pH values below those of the groups involved in redox-Bohr interactions to ensure that conformational changes detected between both families of structures will depend only on redox state. From all the cytochromes c_3 from *Desulfovibrio* spp. (Dc_3) characterized so far this one presents a distinctive pH dependence of its reduction potentials, involving two separate redox-Bohr centres

instead of just one in all of the other Dc_3 studied so far. This work allowed us to infer critical information on the functional significance of the conformational modifications involved in the positive cooperativities observed in this cytochrome.

Chapter Four reports the structure determination of a novel tetrahaem cytochrome isolated from *Shewanella frigidimarina* that is thought to play a central role in the Fe (III) reduction pathways of this organism. This is the first solution structure of a multihaem cytochrome isolated from *Shewanella* spp. The haem spatial disposition and the general fold of the protein show close similarities with the homolog tetrahaem cytochrome from *Shewanella oneidensis* (*Soc*) and the N-terminal domain from the periplasmic flavocytochromes isolated from *S. frigidimarina* and *S. oneidensis*. However this conserved structural motif is distinct from that of Dc_3, suggesting a highly conserved haem core architecture for the members of the *Shewanellaceae* family in spite of the considerable diversity in their primary structure and haem reduction potentials.

PHYSICAL CONSTANTS

Planck constant	h	$6.626\ 068\ 76(52) \times 10^{-34}$ J s
$h/(2\pi)$	$\hbar$	$1.054\ 571\ 596(82) \times 10^{-34}$ J s
Molar gas constant	R	$8.314\ 472(15)$ J mol^{-1} K^{-1}
Boltzmann constant	k	$1.380\ 650\ 3(24) \times 10^{-23}$ J K^{-1}
Bohr magneton	μ_B	$9.274\ 008\ 99(37) \times 10^{-24}$ J T^{-1}
Electron magnetic moment	μ_e	$-9.284\ 763\ 62(37) \times 10^{-24}$ J T^{-1}
in Bohr magnetons	μ_e/μ_B	$-1.001\ 159\ 652\ 186\ 9(41)$
Electron gyromagnetic ratio	γ_e	$1.760\ 859\ 794(71) \times 10^{11}$ s^{-1} T^{-1}
Electron g-factor	g_e	$-2.002\ 319\ 304\ 3737(82)$
Proton magnetic moment	μ_p	$1.410\ 606\ 633(58) \times 10^{-24}$ J T^{-1}
in Bohr magnetons	μ_p/μ_B	$1.521\ 032\ 203(15) \times 10^{-3}$

ABBREVIATIONS AND SYMBOLS

1D - One dimensional
2D - Two dimensional
CO - Carbon monoxide
COSY - Correlation spectroscopy
Dc$_3$ - Cytochromes c_3 from *Desulfovibrio spp.*
Dd27c$_3$ - Cytochrome c_3 from *Desulfovibrio desulfuricans* ATCC 27774
DvHc$_3$ - Cytochrome c_3 from *Desulfovibrio vulgaris* Hildenborough, NCIB 8303
FID - Free induction decay
I (italic) - Spin quantum number
I (bold) - Angular momentum (vector)
IUPAC - International Union of Pure and Applied Chemistry
lol - Lower distance limit
lov - Lower distance volume
NMR - Nuclear Magnetic resonance
NOE - Nuclear Overhauser effect
NOESY - Nuclear Overhauser enhancement spectroscopy
PDB - Protein data bank
Ppm - Parts per million
RF - Radiofrequency
Rms - Root-mean-square
RMSD - Root-mean-square deviation
SA - Simulated annealing
Sfc - Tetrahaem cytochrome *c* from *Shewanella frigidimarina*
Sffcc$_3$ - Flavocytochrome c_3 isolated from *Shewanella frigidimarina*
TAD - Torsion angle dynamics
TpIc_3 - Type I cytochrome c_3
TpII-c_3 - Type II cytochrome c_3
TOCSY - Total correlation spectroscopy
upl - Upper distance limit
upv - Upper distance volume

μ_B - Electron Bohr magneton
g_e - Free-spin electron g factor

AMINO ACID ABBREVIATIONS

Alanine	Ala	A
Arginine	Arg	R
Asparagine	Asn	N
Aspartate	Asp	D
Cysteine	Cys	C
Glutamate	Glu	E
Glutamine	Gln	Q
Glycine	Gly	G
Histidine	His	H
Isoleucine	Ile	I
Leucine	Leu	L
Lysine	Lys	K
Methionine	Met	M
Phenylalanine	Phe	F
Proline	Pro	P
Serine	Ser	S
Threonine	Thr	T
Tryptophan	Trp	W
Tyrosine	Tyr	Y
Valine	Val	V

CONTENTS

FIGURES INDEX

TABLES INDEX

1

INTRODUCTION

CONTENTS

HAEM PROTEINS

Haem-containing proteins are one of the most functionally diverse groups of proteins that exist in nature, spreading from archaea to eukaryotes, and from aerobes to anaerobes [1].

By using the simple arrangement of a haem prosthetic group linked to a polypeptide backbone, haem-proteins can perform a wide range of different functions such as: oxygen transport and storage (haemoglobin and myoglobin) [2], nitric oxide production [3] and transport (nitric oxide synthase and nitrophorin) [4], electron transport (*c-type* cytochromes) [5], and reduction of dioxygen to water by terminal oxidases (cytochrome *c*-oxidase) [6].

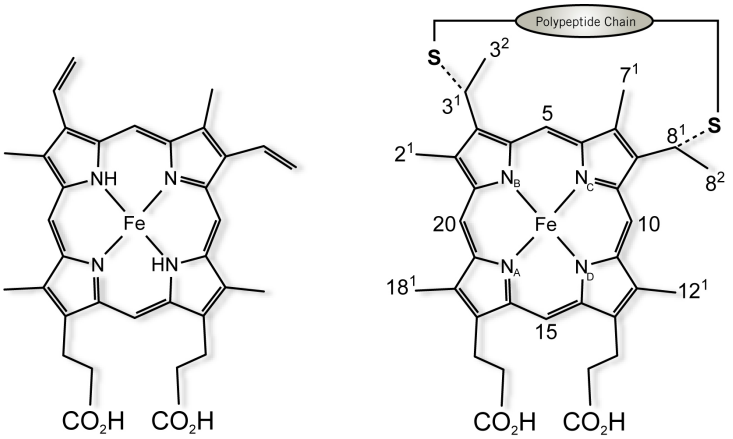

FIGURE 1.1 - Structure of protoporphyrin IX of haem group *c*. A haem numbered according to IUPAC-IUB nomenclature for tetrapyrroles [7] is showed on the right.

This diversity of functions is due to the versatility of the haem group and the variety of interactions with the polypeptide chain that generate different haem environments. The haem group is formed by a protoporphyrin IX ring (Figure 1.1) that binds the iron equatorially via the four pyrrole nitrogens, in a nearly square planar geometry. Additionally, the iron is axially coordinated by one or two ligands. According to the nature of the protoporphyrin IX pyrrole rings substituents define the haem type groups.

c-type cytochromes

An extremely important family of haem proteins present in most living organisms are the *c*-type cytochromes. They are primarily involved in vital processes for life such as electron transport in both anaerobic and aerobic respiratory pathways [8] and cover a nearly 800 mV range of reduction potentials (from -400 to +400 mV) [9, 10].

All these cytochromes contain at least one *c*-type haem covalently linked to two cysteine residues in the protein backbone *via* thioether bonds in position 3 and 8 of the haem ring (IUPAC-IUB recommended nomenclature [7]). The typical haem binding amino acid sequence is the conserved motif -Cys-X-X-(X-X)-Cys-His-, where the X represents an arbitrary amino acid residue and the histidine residue is the fifth ligand (proximal). Recently an unprecedented $CX_{15}CH$ sequence involved in haem *c* binding was described for a multihaem cytochrome MccA from *Wolinella succinogenes* [11].

Both five- and six-coordinated haem-iron axial ligand sets have been observed for *c*-type cytochromes. The sixth ligand (distal) is usually a histidine [12-15] or a methionine [5, 8, 16] however other type of ligands, such as lysine [17] and asparagine [18] have been described. Six coordinated haems are usually diamagnetic in the reduced form and low spin paramagnetic in the oxidised form.

An important group of proteins that have gained relevance in the last two decades are the multihaem *c*-type cytochromes, not only because they participate in crucial bioenergetic processes in bacteria but also because their function seems to go beyond that of a mere electron transfer protein [13, 19-22].

Multihaem *c*-type cytochromes ranging from two to twenty seven haems have already been identified, and methodologies to characterize them at the microscopic level both thermodynamically and structurally have been developed revealing the tremendous importance of these proteins [9, 12, 14-17, 23-35].

Tetrahaem cytochromes c_3

Tetrahaem cytochromes c_3 were first isolated in 1954 from *Desulfovibrio vulgaris* [36, 37], the term was originally used to classify the third type of cytochromes discovered. Subsequently several tetrahaem cytochromes were isolated from the *Desulfovibrionaceae* family and in particular from the genus *Desulfovibrio* and *Desulfomicrobium*. To date, several of these proteins isolated mostly from *Desulfovibrio* genus (Dc_3), but also from *Desulfomicrobium*, have been characterized in detail [19]. In the last decade tetrahaem cytochromes isolated from the genus *Shewanella* were also identified [38, 39].

They are small (~15kDa), soluble and very stable globular proteins with polypeptide chains with 102-118 amino-acid residues and four non-planar haems with bis-histidinyl coordination.

The structures of several tetrahaem cytochromes have been determined both by X-ray and NMR and in spite of the low homology in terms of their amino-acid sequence; the haem core architecture is strictly conserved as well as the general folding of the proteins [14, 15, 30, 31, 34, 40-46].

The conserved pattern of consecutive axial ligands for haem I (fifth ligand) and haem II (sixth ligand) in the sequence is an important constraint that is largely responsible for the haem core architecture adopted by these cytochromes. In a protein with an average of 30-40 amino-acid residues per haem [47] the fold is restrained by the need to bind the four haems in a compact assembly in which haems II and III are perpendicular to each other and to haems I and IV which are approximately parallel (Figure 1.2).

The conserved four-haem structural motif is also observed in domains of eight-haem [48], nine-haem [33] and sixteen-haem cytochromes c_3 [35]. In cytochrome c_3 from *D. desulfuricans*, *D. vulgaris* and *D. gigas* there is a clear patch of positive charges provided mostly by lysine side

chains close to haem IV which has been proposed to be the docking site of the redox partners [49-54].

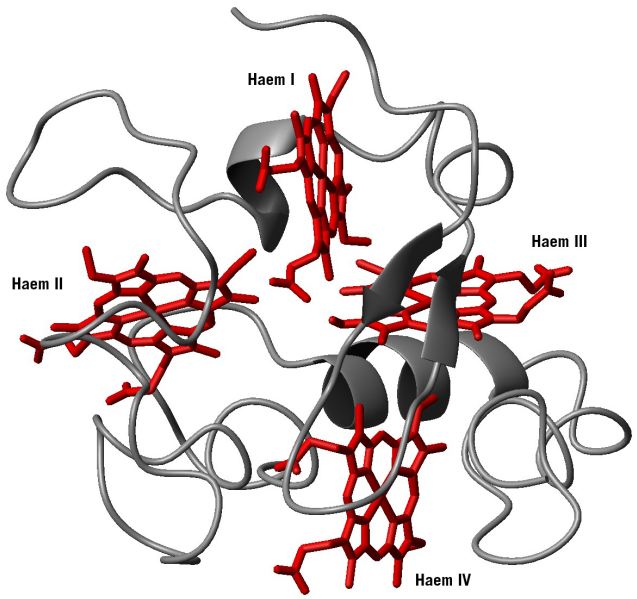

FIGURE 1.2 - Ribbon diagram of cytochrome c_3 oxidised structure by NMR from *Desulfovibrio desulfuricans* ATCC 27774 (*Dd27*c_3) (Chapter 3). Haem architecture and the general fold of the protein are conserved among cytochromes c_3 family. Haems highlighted in red.

Cytochromes c_3 belong to Class III according to the classification of Ambler [55]. An additional division into two types was proposed based on genetic, structural and functional features [56]. Differences between Type I and II cytochromes c_3 (TpI-c_3 and TpII-c_3) relate mostly to their structure and surface charge distribution. TpII-c_3 displays minor activity towards hydrogenases and does not show the characteristic lysine patch around haem IV which is considered to be the interaction site between TpI-c_3 and hydrogenase [56]. All the haem binding sites in TpII-c_3 are of the form C-X-X-C-H as opposed to TpI-c_3, where they are of the type C-X-X-(X-X)-C-H.

Due to the small size of these cytochromes, the close proximity of the haems with Fe-Fe distances ranging from 1.1 to 1.8nm [19] causes the reduction potential of one particular haem to be affected by the reduction of a neighboring one (redox interactions); in addition the haem reduction potentials are pH dependent (redox-Bohr interactions) [57-59]. All in all this makes these proteins a model system well suited to study cooperative processes in biological systems [60, 61].

Physiological role and thermodynamic properties of *Dc*$_3$

Tetrahaem cytochromes c_3 from *Desulfovibrio* spp. (*Dc*$_3$) are present in large quantities in the bacterial periplasm where they act as a coupling protein to hydrogenase [62]. Experimental data suggests that cytochromes c_3 play fundamental roles in the metabolism of the host organisms, by linking the electron and proton flow in the bioenergetic pathways [58].

In different metabolic models such as the hydrogen cycling mechanism [63], the CO cycling mechanism [64] or the more general unified model [65], it has been proposed that these cytochromes act as mediators between periplasmic hydrogenases and transmembrane electron complexes (Figure 1.3).

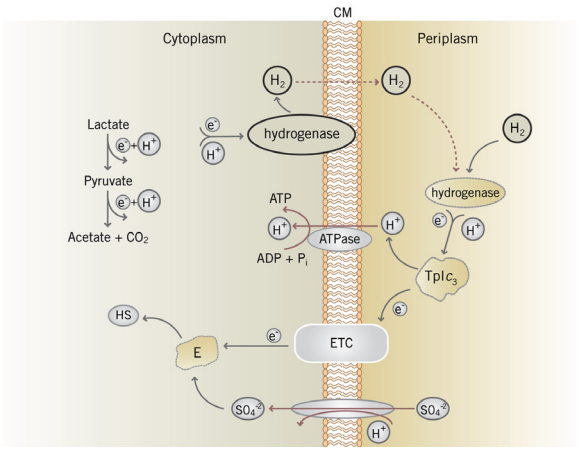

FIGURE 1.3 - Proposed physiological model for the metabolism of genus *Desulfovibrio* according to the hydrogen cycling hypothesis [63]. ATPase, ATP synthase; ETC, electron transfer complex; TpIc_3, type I cytochrome c_3; E, enzymes involved in sulphate reduction; H_2, molecular hydrogen; e^-, electrons; CM, cytoplasmic membrane.

It was proposed [20] that the characteristic thermodynamic properties of TpI-c_3 allow it to act as an energy transduction device by accepting low energy protons (high pK_a) and high energy electrons (low redox potential) and converting them into high energy protons that drive ATP synthase and lower energy electrons for sulphate reduction.

In multihaem proteins macroscopic analysis such as visible redox titrations and voltammetry is insufficient to discriminate the individual haem reduction potentials and the redox interactions between redox centres. However, by combining such analysis with NMR measurements it is possible to characterize these proteins at the microscopic level. Such characterizations have been obtained for multihaem cytochromes containing up to four low spin *c*-type haem groups [21, 28]. The methodology relies on three main steps: (i) the self-consistent assignment of the sets of haem signals in the reduced proteins [66-70]; (ii) identification of the haem oxidation patterns via 2D-NMR redox titrations and (iii) redox titrations followed by visible spectroscopy.

The self-consistent assignment of the haem signals in the fully reduced proteins is based on the methodology described for horse heart ferrocytochromes *c* by Keller and Wüthrich (1978) which relies on the identification of the NOE connectivities between the haem methyl groups and meso-proton resonances [71].

The 2D-NMR redox titration explores the paramagnetic shift originated by the iron spin state change from S=0 to S=1/2 upon oxidation [61, 67]. Indeed, during the oxidation of a tetrahaem cytochrome, four consecutive reversible steps of one-electron transfer convert the fully reduced protein (stage 0) into fully oxidised (stage 4). Therefore, five oxidation stages can be defined each containing the microstates with the same number of oxidised haems [60, 61, 68]. The total number of microstates is 16 distributed according to the Pascal's triangle rule for binomial coefficients as 1:4:6:4:1, respectively for oxidation stages 0-4 [72]. For each acid–base centre considered within the model the number of microstates is duplicated following the same rule.

On the NMR time scale, in conditions of fast intramolecular electron exchange (between the different microstates within the same oxidation stage) and slow intermolecular electron exchange (between different oxidation stages) the individual haem signals in the different oxidation

stages can be discriminated. Since the intrinsic paramagnetic shifts of the haem substituents are proportional to the oxidation fraction of that particular haem, they can be used to obtain the relative microscopic reduction potentials of the haems [61, 67]. Because NMR data only defines the relative haem reduction potentials and haem redox interactions it is necessary to calibrate these values with redox titrations monitored by visible spectroscopy [57].

The pH dependence of the haem substituent chemical shifts provides data to define the parameters of the thermodynamic model which for the simplest case of four haems and one acid-base centre are: four haem reduction potentials, the deprotonation energy of the acid-base centre, six redox-interactions and 4 redox-Bohr interactions. The thermodynamic properties of several Dc_3 members have been determined [43, 57, 73-75].

The relative reduction potentials of the haems for several Dc_3 are indicated in Table 1.1 and are different among the Dc_3 of different *Desulfovibrio* species.

TABLE 1.1 - Haem oxidation order in cytochromes c_3. Boldface indicates the haem with the strongest redox-Bohr effect. Adapted from [19].

Organism	Order of oxidation
D. gigas	**I**, II/III, IV
D. vulgaris (Hildenborough)	III, II/**I**, IV
D. vulgaris (Miyazaki F)	III, II/**I**, IV
D. desulfuricans (ATCC 27774)	**I/II**, IV, III
Desulfomicrobium norvegicum	II, **I**/IV, III
Desulfomicrobium baculatum	II, **I**/IV, III

A compilation of the thermodynamic data obtained from the different Dc_3 is presented in the Appendix. Within the error of the measurements, all the haems show different and negative interaction energies with the protonatable centre(s) (heterotropic cooperativity). On the contrary, for

the haem-haem interactions (homotropic cooperativities), mostly positive energies are observed. In both cases the sign of the energies is expected in electrostatic terms. Nevertheless in the case of *D. gigas* and *D. vulgaris* Hildenborough some of the haems show large negative redox interaction energies. Such results can only be explained by the existence of redox related conformational changes [14, 15, 76].

Although several crystal structures have been reported for this class of proteins [30, 31, 34, 40, 44], solution structures were obtained in both oxidised and reduced states only for cytochromes c_3 from *D. vulgaris* (Hildenborough -*Dv*H) and *D. gigas* (*Dg*), allowing the description of the structural bases for homotropic cooperativity in solution [14, 15, 76].

Out of all the Dc_3 studied, the tetrahaem cytochrome isolated from *D. desulfuricans* ATCC 27774 ($Dd27c_3$) is unique in terms of its thermodynamic properties. Indeed, the model considering five centres (four haems and one redox-Bohr centre) was able to describe very well the experimental data for all Dc_3 with the exception of $Dd27c_3$ where a second acid-base centre had to be included in the model to explain the modulation of its redox proprieties [73, 77]. To understand the thermodynamic and kinetic properties, which are essential to understand the electron-transfer properties of a protein it is essential to obtain structural information. The solution structure of the tetrahaem cytochrome c_3 isolated from *D. desulfuricans* ATCC 27774 in both oxidised and reduced states will be addressed in Chapter 3 of the Thesis.

Physiological role and thermodynamic properties of tetrahaem cytochrome from *Shewanella* spp

Shewanella spp. are Gram-negative bacteria belonging to the γ-Proteobacteria subgroup; they are motile facultative anaerobes and extremely versatile in terms of electron donors and acceptors including even insoluble metal oxides such as Fe(III) and Mn(IV)[78-84].

Terminal metal oxide electron acceptors are insoluble and therefore cannot diffuse inside the cells. As a consequence the transport of electrons outside the cell is required for the reduction of the terminal electron acceptor.

As described earlier, type I tetrahaem cytochromes from *Desulfovibrio* spp. (Dc_3) are important to the hydrogenase activity and are proposed to function as mediators between periplasmic hydrogenases and transmembrane electron transfer complexes.

On the other hand, tetrahaem cytochromes isolated from *Shewanella* spp. seem to have a completely different function. In fact, it was found that the growth rate of *S. frigidimarina* under anaerobiosis with Fe(III) as sole acceptor is severely reduced if the tetrahaem cytochrome (here after *Sfc*) is removed by gene disruption [38].

A proposed model for the electron transport pathway in *Shewanella* spp. for dissimilatory reduction of Fe(III) is given in Figure 1.4. In general terms the electrons are transferred from dehydrogenase to a quinone pool in the cytoplasmic membrane and from there to a cytoplasmic membrane bound tetrahaem cytochrome CymA [85-87] and then transferred to periplasmic *c*-type cytochromes and finally to the periplasmic electron carriers [85, 88-90].

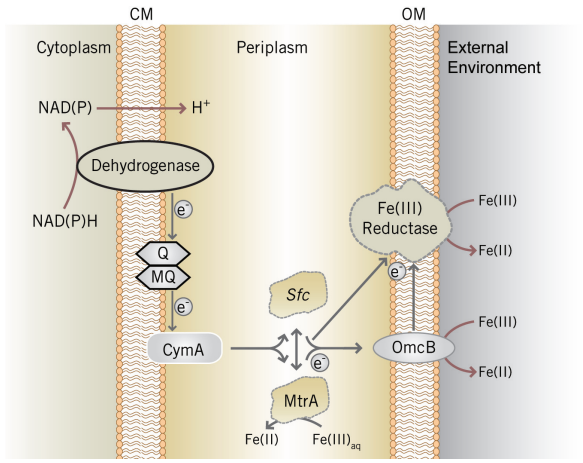

FIGURE 1.4 - Physiological model of the biochemistry suggested to be involved in electron transfer to extracellular insoluble Fe(III) oxides in *Shewanella* spp. CymA, cytoplasmic membrane-bound c-type tetrahaem cytochrome; *Sfc* periplasmic cytochrome *c*; e^-, electrons; MtrA, periplasmic decahaem *c*-type cytochrome; OmcB, outer membrane-bound cytochrome; MQ, menaquinone; CM, cytoplasmic membrane; OM, outer membrane. Adapted from [93].

Two *c*-type cytochromes that may act as potential electron carriers necessary for Fe(III) reduction in *Shewanella* spp. have been identified in the periplasm, *Sfc* and MtrA [91, 92].

The tetrahaem cytochrome *Sfc* is a small periplasmic *c*-type tetrahaem

cytochrome [38, 94] that is thought to have a central role in bridging the electron transfer between the cytoplasm and the outside of cell where reduction of extracellular iron takes place [39].

This cytochrome has 86 residues (11.8 kDa) and four low-spin haems with bis-histidinyl ligation. For the thermodynamic properties of *Sfc*, it was shown that the haem redox potentials are modulated by redox interactions between the four haems and also by redox-Bohr interactions between the haems and an ionisable centre proposed to be close to haem III [95]. However in this case and again in contrast to the Dc_3, haem III is now the most affected by the protonation state of the protein and by the oxidation of the other haems. Moreover all the interactions between the five centres are clearly dominated by electrostatic effects (Appendix).

When the primary sequence of this cytochrome is compared with type I cytochromes c_3 from *Desulfovibrio* spp. remarkable differences emerge (Figure 1.5), particularly, in *Sfc* the haem binding motif of all the haems

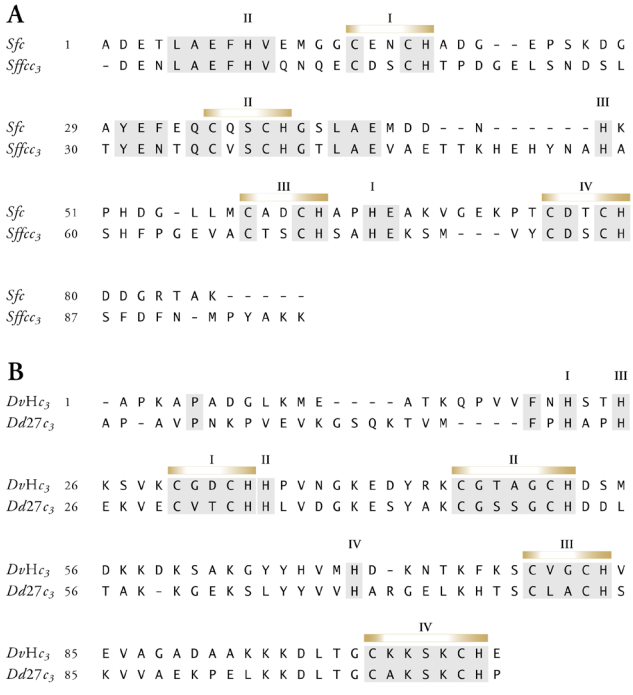

FIGURE 1.5 - Comparison between the relative positions of the haem binding motifs and haem axial ligands in both the tetrahaem (*Sfc*) and the N-terminal cytochrome domain of flavocytochrome c_3 (*Sffcc*$_3$) isolated from *S. frigidimarina* and the *Desulfovibrio* spp. cytochromes c_3.
A- Sequence alignment for *Sfc* and *Sffcc*$_3$. The grey shadowed letters indicate the conserved residues in both proteins.
B- Sequence alignment for two cytochromes c_3 isolated from *Desulfovibrio* species: *DvHc*$_3$ (*Desulfovibrio vulgaris* Hildenborough, NCIB 8303), *Dd27c*$_3$ (*Desulfovibrio desulfuricans* ATCC 27774). The grey shadowed letters indicate the residues conserved in all Dc_3s. The bold roman numbers in (A) and (B) indicate the haem binding motifs (CXX(XX)CH) and the sixth axial ligand of each haem.

is CXXCH in contrast with all the Dc_3 where at least one of the haems shows the CXXXXCH motif [15, 96-102]. Additionally the conserved pattern of two consecutive haem axial ligands observed in all Dc_3 is not found in *Sfc*.

Simply based upon sequence alignment it was suggested that the haem core of both proteins was distinct. Indeed, the preliminary model for the *Sfc* haem core [12] showed that the haems had a nearly linear arrangement as opposed to those found in Dc_3 (Figure 1.6). A similar but not identical architecture was found for the haem core in the N-terminal domain of the fumarate reductase flavocytochrome c_3 isolated from *S. frigidimarina* and *S. oneidensis* [13, 22] (Figure 1.6).

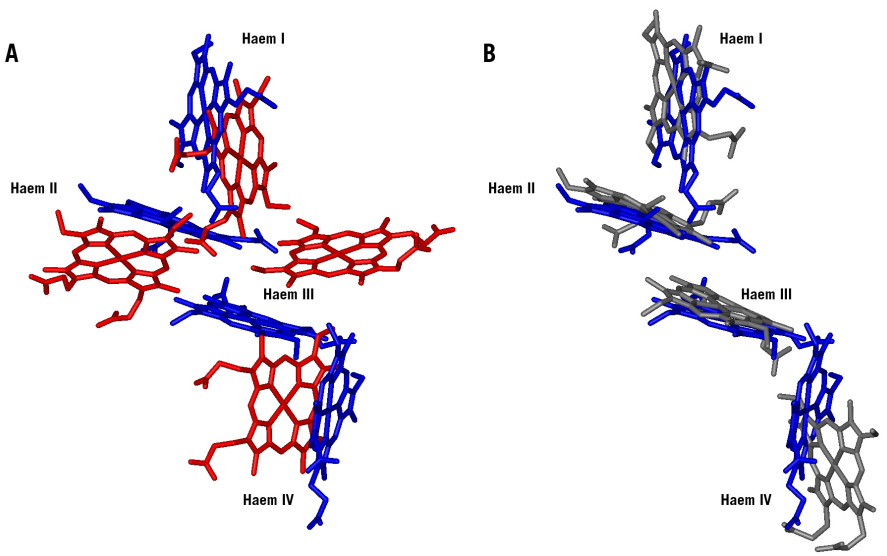

FIGURE 1.6 - Haem core comparisons between tetrahaem cytochrome *c* from *S. fridigimarina* (*Sfc*), cytochrome c_3 from *D. desulfuricans* ($Dd27c_3$) and the N-terminal domain of the fumarate reductase flavocytochrome c_3 isolated from *S. frigidimarina* ($Sffcc_3$). A - *Sfc* haem core showed in blue and $Dd27c_3$ in red. B - *Sfc* haem core showed in blue and $Sffcc_3$ showed in grey.

The preliminary model of the haem core model from Pessanha et al. [12], anticipated a different structural motif from those reported for Dc_3. The solution structure determination of *Sfc* is one of the aims of this Thesis and will be described in Chapter 4, where the structural fea-

tures of *Sfc* are compared with those of Dc_3 and used to interpret the thermodynamic properties of this cytochrome.

NUCLEAR MAGNETIC RESONANCE

Space quantization

Let us consider a system with conserved angular momentum, like an isolated atom in vacuum. Such a system could in principle (as the Earth spinning on its axis) be spinning around any desired direction. For a given spin, each particular direction of the angular momentum axis would correspond to a different *state* with each of the *states* possessing the same energy.

So, in the classical theory, for a given angular momentum there is an infinite number of possible states, all with the same energy.

However in quantum mechanics, several important differences happen:

- The number of observable states such a system can have is now limited.

- A state cannot be described by knowing the direction of its angular momentum. Only by giving the *component* of the angular momentum along some direction – z axis direction for example.

In classical mechanics, an object with angular momentum **I**, could have for its z-component of angular momentum any value from I to –I. In quantum mechanics, the measured z-component of angular momentum can only have certain discrete values.

Any nucleus, has a characteristic number I – called the spin quantum number, or just spin – so that the observable z-component of the angular momentum is given by the set of values:

$$I\hbar, (I-1)\hbar, ..., -(I-1)\hbar, -I\hbar = m\hbar \quad \{1.1\}$$

in which m= (-*I*, ... , *I*).

The fact that the z direction was chosen is totally arbitrary. For a given system with spin *I*, the component of angular momentum along *any* axis can only be observed to have one of the values stated above. The characteristic spin *I* of a nucleus can have one of the following values:

$$I = 0, \frac{1}{2}, 1, \frac{3}{2}, 2, ...$$

spin values for common nuclei are shown in Table 1.2.

Protons, neutrons and electrons all have $I = ½$ and are called 'spin-½' particles. For any given *I* there are $2I+1$ different states all with the same energy.

It's worth noting that two very common nuclei; ^{12}C and ^{16}O, have zero spin number, and therefore zero magnetic moment, and so are invisible in magnetic resonance.

The magnitude of the angular momentum is also a quantized value that depends on *I*:

$$\|\mathbf{I}\| = \sqrt{I(I+1)}\ \hbar \quad \{1.2\}$$

TABLE 1.2 - Magnetic properties of selected particles. γ_I is the gyromagnetic ratio in units of rad $T^{-1}s^{-1}$. Adapted from [103].

Isotope	Spin (*I*)	Natural abundance (%)	γ_I	NMR Freq. (MHz at 2.3488 T)
^{1}H	1/2	99,98	$2{,}67x10^{8}$	100.00
^{2}H	1	$1{,}56x10^{-2}$	$4{,}10x10^{7}$	15,35
^{13}C	1/2	1,108	$6{,}73x10^{7}$	25,15
^{15}N	1/2	0,37	$-2{,}71x10^{7}$	10,14
^{19}F	1/2	100	$2{,}51x10^{8}$	94,13
^{23}Na	3/2	100	$7{,}08x10^{7}$	26,46

Nuclear magnetization

Nuclei with non zero spin angular momentum also possess a magnetic moment. The magnetic moment **μ** is collinear and directly proportional to **I** with a proportionality constant γ, known as the gyromagnetic ratio:

$$\mu = \gamma I \qquad \{1.3\}$$

$$\mu_z = \gamma I_z = \gamma \hbar m \qquad \{1.4\}$$

As we can see the nuclear magnetic moment, like the angular momentum, has both magnitude and orientation quantized.

In the presence of an external magnetic field B the energy of the system can be written as:

$$E = -\mu \bullet \mathbf{B} \qquad \{1.5\}$$

and the minimum energy corresponds to the maximum projection of μ onto B.

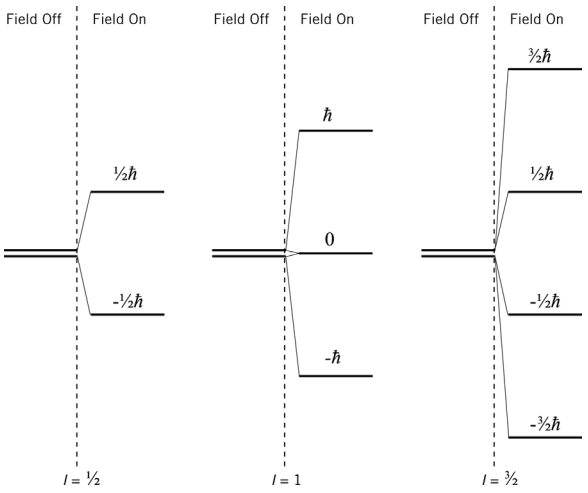

FIGURE 1.7 - Nuclear spin energy levels of spin-1/2, spin 1 and spin 3/2 nucleus respectively. In the absence and when an external magnetic field is turned on.

For an external field oriented along the z axis, equation {1.5} reduces to:

$$E_m = -\gamma I_z B_0 = -m\gamma\hbar B_0 \qquad \{1.6\}$$

Consider a system with spin I=3/2. In the absence of an external magnetic field, the system has four different (Figure 1.7) possible states corresponding to the values of I_z, all of them with the exact same energy (said to be degenerate). When the magnetic field is turned on, there is an additional energy of interaction that separates these states into four different levels. The energies of these levels are proportional to B multiplied by $\hbar$ times 3/2, 1/2, -1/2 and –3/2 as given by equation {1.6}. The splitting of energies for systems with spins 1/2, 1 and 3/2 are shown in Figure 1.7. The $2I$+1 states (called Zeeman levels) for a spin 1/2 nucleus are equally spaced with energy gap of $\gamma\hbar$B.

The allowed transitions between adjacent energy levels have the energy:

$$\Delta E = E_\beta - E_\alpha = \frac{1}{2}\gamma\hbar B - (-\frac{1}{2}\gamma\hbar B) = \gamma\hbar B$$

or using E=$h\nu$:

$$\nu = \frac{\gamma B}{2\pi} \qquad \{1.7\}$$

where ν is the frequency of electromagnetic radiation.

That is, when we apply an external magnetic field to a nucleus of nonzero spin, its energy splits into a number of different levels. Furthermore the phase of the wavefunction varies in a manner analogous to the classical precession of the nucleus about the direction of the field. This effect is caused by the interaction of the nuclear angular momentum vector with the applied magnetic field.

The precessional motion (called Larmor frequency) depends on the type of nucleus (its value of γ) and it is proportional to the applied field:

$$\nu_L = \frac{\gamma B}{2\pi} \qquad \{1.8\}$$

NMR spectroscopy

In a very basic form, nuclear magnetic resonance (NMR) is the study of the properties of molecules that have magnetic nuclei, by the appli-

cation of a magnetic field and observing the frequency at which they come into resonance with an oscillating electromagnetic field.

With the magnetic field strengths normally employed in magnetic resonance experiments, the Larmor frequencies of equation {1.8}(for ^1H nuclei) lie in the radiofrequency region of the electromagnetic spectrum.

A typical magnetic field strength used in NMR would be 18.8 T. From equation {1.8} and for the proton we get a frequency of $8x10^8$ Hz, or 800 MHz.

Because proton is by far the most popular NMR nucleus, NMR spectrometers are usually classified by their proton frequencies rather than the strengths of their magnetic fields.

Population of energy levels

Molecular and atomic systems possess energy in a variety of different forms. It can be associated with the vibrational, rotational or translational motions of the molecules, or with the interactions between electrons and nuclei.

One common characteristic shared by all these forms of energy is that each one of them separately is restricted only to certain quantized values (energy levels). And for each particular type of energy, the gaps between allowed (existing) levels are characteristic of the system. Therefore the measure of energy gaps in atoms or molecules is one of the most important ways of testing models of their internal structure.

In a general spectroscopy experiment, the system is irradiated with a range of frequencies of electromagnetic radiation, the interactions between the sample and the radiation will result in the promotion of some atoms or molecules to higher energy levels, with absorption of energy at the corresponding frequency of radiation. The analysis of the emerging radiation from the sample will reveal the missing frequencies and therefore the energy gaps present in the sample.

The occupancy of the energy levels at equilibrium (the way the sample molecules are distributed among the available energy states) is given by the Boltzmann relation: If we consider two states, s_1 and s_2 with populations η_1 and η_2 respectively, separated by an energy gap ΔE, the ratio of

their populations is given by:

$$\frac{\eta_2}{\eta_1} = e^{-(\Delta E/kT)} \qquad \{1.9\}$$

where k is the Boltzmann constant and T the absolute temperature.

When ΔE is large in relation to kT the population of the upper energy state may be assumed to be negligible. On the contrary, when ΔE is small compared to kT, (as in the case of NMR) the population ratio is close to unity, which means that upper and lower states are almost, although not quite, equally populated.

For protons in a 18.8T field at 300K temperature the ratio of populations given by equation {1.9}, and using $\Delta E=\gamma\hbar B$, gives $\Delta E=5.3\text{x}10^{-25}$J ($kT=4.14\text{x}10^{-21}$ J).

Therefore we have a population ratio of about $\eta_2=0.9998\eta_1$, or 1 part in 10,000 for the population differences.

In NMR spectroscopy it is as if we can only detect one nucleus in every 10^4 (or even 10^5 depending on the magnetic field strength). If we add to this the fact that higher frequency spectroscopy is more sensitive (because it is easier to detect higher energy particles) it is easy to see why the NMR signals are intrinsically weak.

This is the reason why the optimisation of signal strength is so important, by using the strongest magnetic fields possible, strong gyromagnetic ratio nuclei and high natural abundance.

Various methods are used to improve the comparative sizes of NMR signal and noise – *the signal to noise ratio*. Signal averaging is one way of improving this. Because NMR signals occur in the same place every time, while noise is random, the spectrum is recorded more than once and the results are added, so the signal builds up. In *n* repetitions the signal-to-noise ratio improves by a factor of $\sqrt{n}$.

There is the possibility to extract a complete frequency response in one go, by using a short intense burst of radiofrequency radiation, instead (as in the early years of NMR spectroscopy) of using a weak fixed amplitude radiofrequency while slowly sweeping the magnetic field strength in order to bring spins with different chemical shifts into resonance.

Following the pulse, the NMR response, referred to as *free induction decay* (FID) fades over a period of time (in an analogous manner to any damped vibration). After sufficient repetitions have been made, all data contains information about all the frequencies in the NMR spectrum. To obtain a spectrum of amplitude as function of frequency we need to use a Fourier transform to interconvert between time and frequency data.

Magnetization

In a large equilibrium population of identical nuclei at equilibrium, the z-components of each individual magnetic moment almost cancel out. However the alignment along B_0 of the small excess of spins in the lower energy level, means that a net magnetization exists in this direction, called M_z (Figure 1.8).

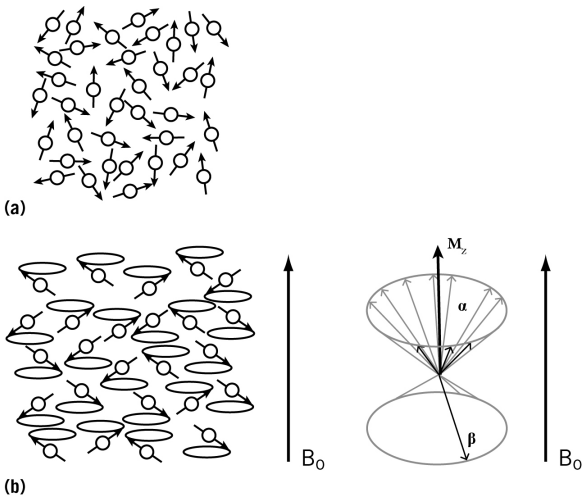

FIGURE 1.8 - Spin populations, a) disordered in the absence of an external magnetic field; b) in the presence of the magnetic field there is a net magnetization along the z axis. Although the magnetization is stationary along the z axis (the magnetic field direction), the individual spin moments rotate about the axis.

The magnetic moment component along the x and y axis (Figure 1.8) averages out since it is randomly distributed. It is the total magnetization M_z and not the magnetic moment of each spin that determines the NMR signal.

For our NMR experiment we will apply a short radiofrequency (RF) pulse at the Larmor frequency to induce transitions between the allowed energy states. Although the probability is the same for either direction, more transitions exist from the lower to the higher energy level, which will reduce the population difference between the states and consequently reducing M_z.

Depending on how long the RF pulse is applied the population difference and therefore M_z could even be inverted (Figure 1.9-c). These transitions caused by the applied pulse (also called the B_1 field) bring the spins into phase with B_1, so they precess together with phase coherence. So the resultant magnetization M_{xy} in the x-y plane is no longer zero.

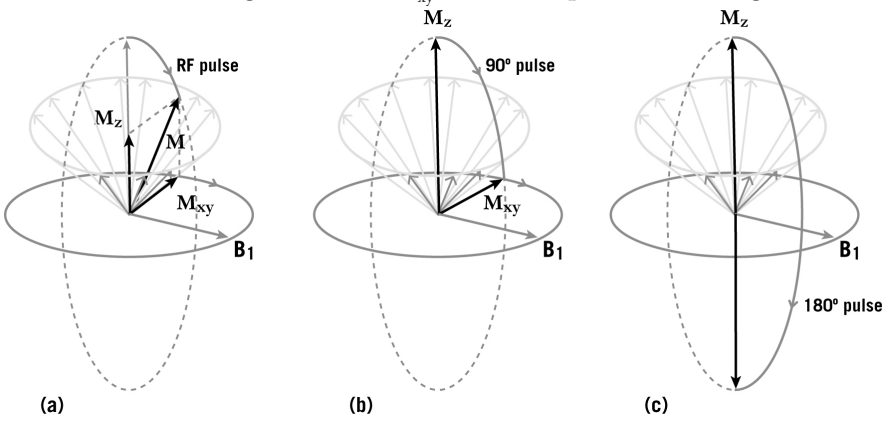

FIGURE 1.9 - a) Resultant magnetization M of M_z and M_{xy} in a frame of reference rotating at the Larmor frequency; b) 90º pulse; c) 180º pulse.

The detection of this rotating magnetization is the purpose of an NMR spectrometer. Its creation, decay and exchange will provide us with the molecular information that we seek.
Thus, as we have seen the RF pulse reduces or inverts M_z and introduces M_{xy}. The resultant of these two magnetizations is called M. We can think of M as the result of tilting M_z away from the z-axis. (Figure 1.9)

By controlling the strength and the duration of the pulse it is possible to control the magnitude of the tilt angle, and we can speak of a 30º or 60º pulse for example. A 90º pulse is associated with a zero M_z and non-zero

M_{xy}; a 180° pulse inverts M_z from its original direction and has zero M_{xy} (Figure 1.9).

When the RF pulse B_1 ends, the spin system returns over a period of time to its original state; this is called relaxation.

The chemical shift

One of the main characteristics of NMR spectroscopy is that the observed nuclear resonance frequencies depend on the position of the nucleus in the molecule, or to be more precise, on the local electron distribution and therefore differ slightly from the frequencies predicted by equation {1.7}:

$$\nu = \frac{\gamma B_0}{2\pi} \text{ or } \omega = \gamma B_0 \qquad \{1.10\}$$

The effect of chemical shift arises because the external field B_0 induces electron motions that generate secondary magnetic fields. The net magnetic field at the nucleus in an atom or molecule depends on the static magnetic and secondary magnetic fields. The effect of these secondary fields, also called nuclear shielding, can enhance or oppose the main field.

In isotropic liquid solution, the shielding effects on a particular nucleus can be considered, rearranging {1.10} as:

$$\omega = \gamma(1-\sigma)B_0 \qquad \{1.11\}$$

where σ is the average, isotropic shielding constant of the nucleus.

Resonance frequencies of the nuclei will reflect variations in σ due to different electronic environments. It is common practice to measure chemical shifts in parts per million (p.p.m. or δ) relative to a reference resonance signal from a standard molecule:

$$\delta = \frac{10^6(\nu - \nu_{ref})}{\nu_{ref}} \qquad \{1.12\}$$

in which ν is the nucleus of interest resonance and ν_{ref} the reference resonance. The frequency difference ν-ν_{ref} is divided by ν_{ref} so that δ is a molecular property independent of the magnetic field used in the measurement.

The reference signal is usually obtained by adding a small amount of a suitable compound to the NMR sample. For the ^{1}H and ^{13}C spectra this is usually tetramethylsilane $(CH_3)_4Si$ or TMS, which is soluble in most organic compounds, inert and gives a single strong resonance signal from its 12 identical protons. A secondary reference compound that has a known chemical shift with respect to TMS may be used. Water is a convenient secondary reference for biological samples but it is necessary to take account of the temperature dependence of its shift with respect to TMS.

Scalar and dipolar couplings

The appearance of high resolution NMR spectra is not solely due to the chemical shift. The magnetic interactions between nuclei, also known as couplings, cause splitting of the lines.

Ramsey and Purcell [104] suggested that the multiplicity of NMR resonances (multiplets) was due to the indirect interactions mediated by the electrons forming the chemical bonds between nuclei.

This interaction, known as spin-spin coupling or scalar coupling, is measured by the scalar coupling constant $^{n}J_{ab}$ (Hz), where *n* stands for the number of covalent bonds separating the two nuclei *a* and *b*.

Scalar coupling is the effect caused on a nuclear spin *I* by the local magnetic field of a neighbour nuclear spin *S*.
The orientation of spin *S* in the magnetic field induces a small polarization mostly on the s orbitals around spin *S*. The electron density distribution of spin *I*, bonded to spin *S* will be affected by this polarization.

Since this interaction depends on the electron density of the s orbitals surrounding both nuclei, the electron density must be related, therefore in Fermi contact. As a consequence, scalar spin-spin coupling propagates only along chemical bonds.

If we consider two spin ½ nuclei (e.g. two ^{1}H spins) designated *I* and *S* with resonance frequencies ω_I and ω_S respectively:

$$\omega_I = \gamma_I(1-\sigma_I)\mathbf{B}_0 \qquad \omega_S = \gamma_S(1-\sigma_S)\mathbf{B}_0 \qquad \{1.13\}$$

In the absence of scalar coupling between the spins, the two spin system is described by the energies of the four states, given by:

$$E_1 = -\frac{1}{2}\hbar\omega_I - \frac{1}{2}\hbar\omega_S \quad E_2 = -\frac{1}{2}\hbar\omega_I + \frac{1}{2}\hbar\omega_S$$
$$E_3 = \frac{1}{2}\hbar\omega_I - \frac{1}{2}\hbar\omega_S \quad E_4 = \frac{1}{2}\hbar\omega_I + \frac{1}{2}\hbar\omega_S \qquad \{1.14\}$$

In Figure 1.10-a, we can see the energy-level diagram for a two-spin system in the absence of scalar coupling.

Spin system refers to a group of nuclei coupled through spin-spin coupling.

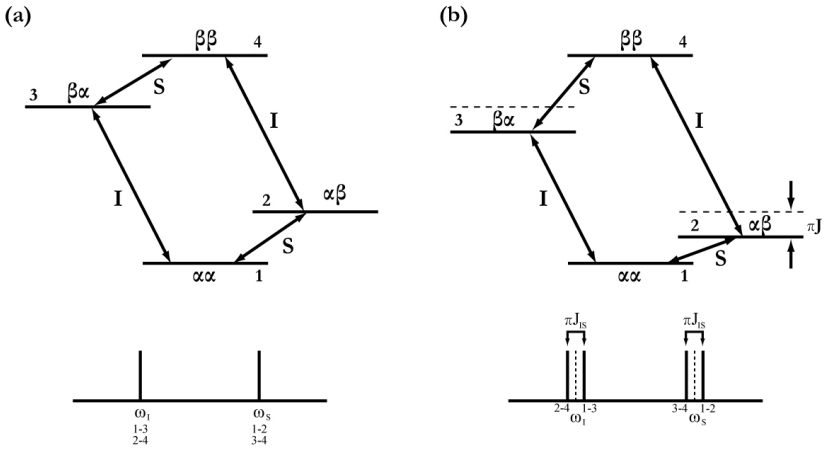

FIGURE 1.10 - Energy levels and spectrum of a two spin system (a) with no spin coupling and (b) with J coupling. The allowed transitions are indicated between arrows. The dashed lines in (b) represent the energy levels or frequency positions without J couplings. Adapted from [105]

The allowed transitions occur between levels 1 and 2, 3 and 4 (corresponding to a change in the spin state of *S*), and between levels 2 and 4, and 1 and 3 (corresponding to a change in the spin state of *I*). Therefore the NMR spectra consists of one resonance line at ω_I (due to transitions 1-3, and 2-4) and one resonance line at ω_S (corresponding to transitions 1-2, and 3-4).

If we now introduce the scalar coupling J_{IS} (which can be positive or negative) between *I* and *S*, the energy levels are given by:

$$E_1 = -\frac{1}{2}\hbar\omega_I - \frac{1}{2}\hbar\omega_S + \frac{1}{2}\pi\hbar J_{IS} \quad E_2 = -\frac{1}{2}\hbar\omega_I + \frac{1}{2}\hbar\omega_S - \frac{1}{2}\pi\hbar J_{IS}$$
$$E_3 = \frac{1}{2}\hbar\omega_I - \frac{1}{2}\hbar\omega_S - \frac{1}{2}\pi\hbar J_{IS} \quad E_4 = \frac{1}{2}\hbar\omega_I + \frac{1}{2}\hbar\omega_S + \frac{1}{2}\pi\hbar J_{IS} \qquad \{1.15\}$$

The energy level diagram for the spin-spin coupled system now shows four lines corresponding to the new transition frequencies (Figure 1.10-b):

$$\omega_{12} = \omega_S - \pi J_{IS} \qquad \omega_{34} = \omega_S + \pi J_{IS}$$
$$\omega_{13} = \omega_I - \pi J_{IS} \qquad \omega_{24} = \omega_I + \pi J_{IS} \qquad \{1.16\}$$

The dipolar coupling is a dipole-dipole interaction between spatially near nuclei. This coupling is a direct through space rather than through a molecular bond as in J coupling. In solution, dipolar line splitting is not observable because the orientational term of the dipolar interaction with respect to the magnetic field direction is averaged to zero by rapid molecular tumbling.
The effect of dipolar interaction on molecular relaxation however is still present, which is the origin of the NOE (see below).

Relaxation

A perturbed spin system relaxes over a period of time to its equilibrium state.

- The relaxation of M_z occurs along the direction of the applied field B_0: It is called *longitudinal relaxation* and the characteristic relaxation time is denoted T_1.

- The M_{xy} decays exponentially to zero. This is called transverse relaxation and has a characteristic time T_2.

Relaxation is caused by state transitions of many individual nuclei, which restore the original Boltzmann populations (thus M_z returning to its equilibrium value) in the case of longitudinal relaxation and disrupts the precession phase coherence of the nuclear spins, reducing M_{xy} to zero in transverse relaxation. During T_1 relaxation the nuclear spins exchange energy with the fluctuating magnetic or electric fields in the environment ("lattice"). T_2 relaxation can occur due to mutual energy exchange between two nuclei or by inhomogeneities in the local mag-

netic fields, and contrary to T_1 relaxation does not involve net changes in the energy of the system.

Both forms of relaxation depend on oscillating magnetic fields that arise from sources including nuclear dipole-dipole interactions, chemical shift anisotropy, and interaction with unpaired electrons in the case of paramagnetic samples, which are modulated by molecular motions in liquid samples.

T_1 interaction arises from the fact that each nucleus is surrounded by other magnetic nuclei in the same or neighbouring molecules. The energy exchange is caused by the time dependent fluctuation of magnetic field produced by vibrational, rotational and translational motions of surrounding nuclei, changes in chemical shielding or unpaired electrons.

The time average of the correlation between the fluctuating magnetic field measured at time t and the same field at time (t+τ) is the autocorrelation function G(τ), which essentially characterizes the memory that the system has of a particular arrangement of spins in the sample.

For times τ much shorter than the time it takes the system to rearrange itself G(τ) will be close to its maximum. For longer times when the initial arrangement gets more disturbed G(τ) value falls. For sufficiently long times, G(τ) tends to zero.
The simplest form for G(τ) is:

$$G(\tau) = G(0)\, e^{(-\tau/\tau_c)}$$

where τ_c is the correlation time, the decay time constant of the autocorrelation time function.
For times much less than τ_c the spins have not moved much and the correlation function is close to its initial value; for times of the order of τ_c spins have gone through significant rearrangements and the correlation function falls to about half its original value. For times much longer than τ_c spins have moved to completely new positions and the correlation function has fallen close to zero.

As the correlation function is a function of time its Fourier transform will give a function of frequency which is called the spectral density J(ω). This function gives a measure of the amount of motion present at different frequencies. For a simple exponential correlation function the spectral density is of the form:

$$e^{(-\tau/\tau_c)} \xrightarrow{\text{Fourier Transform}} \frac{2\tau_c}{1+\omega^2\tau_c^2}$$

We can think of correlation time τ_c as the mean time between reorientation of a molecule or the rate of its random motions. Because random motions of molecules are dependent on molecular size, the magnitude of correlation time τ_c is substantially dependent on molecular weight.

The dominant mechanism for spin-lattice relaxation for protons is dipole-dipole interaction, which although averaged to zero in solution, its field at any given instant is not. It is dependent on the inverse cube of the distance between the two nuclei and the direction of the vector joining them. For an aqueous solution of normal viscosity, as the molecules tumble, the direction of this vector changes and so does the dipole-dipole interaction. Spin-lattice relaxation is proportional to the square of the coupling and it is given by [106] in the case of isotropic motion:

$$R_1 = \frac{1}{T_1} = \frac{3}{10}\left(\frac{\mu_0}{4\pi}\right)^2 \frac{\gamma^4\hbar^2}{r^6}\left(\frac{\tau_c}{1+\omega^2{\tau_c}^2} + \frac{4\tau_c}{1+4\omega^2{\tau_c}^2}\right) \qquad \{1.17\}$$

where r is the distance between the nuclei (with like-spins), τ_c is the cor-

relation time, ω is the Larmor frequency and γ the gyromagnetic ratio.

In paramagnetic systems the presence of unpaired electrons will add new efficient relaxation pathways dominated by the coupling of the magnetic dipole of the target nucleus and the fluctuating magnetic fields of unpaired electrons. The fluctuation in low spin iron is usually dominated by the rate of electron spin relaxation. Nuclear spin relaxations occur now not only at the nuclear Larmor frequency ω_I, but also at the frequencies of the transitions involving both nuclear and electronic spin levels; $\omega_I + \omega_S$ and $\omega_I - \omega_S$. Therefore the expression for the overall nuclear spin-lattice relaxation rate has the form [107]:

$$R_1 = \frac{1}{T_1} = \frac{1}{10}\left(\frac{\mu_0}{4\pi}\right)^2 \frac{\gamma_I^2 \gamma_S^2 \hbar^2}{r^6}\left(\frac{3\tau_S}{1+\omega_I^2 {\tau_S}^2} + \right.$$
$$\left. + \frac{\tau_S}{1+\left(\omega_I - \omega_S\right)^2 {\tau_S}^2} + \frac{6\tau_S}{1+\left(\omega_I + \omega_S\right)^2 {\tau_S}^2}\right) \qquad \{1.18\}$$

Here, τ_S is the correlation time for electron spin relaxation and γ_I, γ_S, ω_I and ω_S are the gyromagnetic ratio and the Larmor frequencies for the nuclei and the unpaired electron respectively.

In T_2 or spin-spin relaxation the energy of the system is not altered because this relaxation does not cause population changes, the energy is exchanged between nuclei. Due to the intrinsic inhomogeneity of the applied magnetic field each nucleus of the sample will experience a slightly different B_0 field. As a consequence some of the nuclei will precess faster and some slower, which will lead to a fanning out of individual magnetization and the result is a loss of phase coherence. Thus the spin-spin relaxation has an additional component that depends on frequencies close to zero.

Spin-spin relaxation is given by [106]:

$$R_2 = \frac{1}{T_2} = \frac{3}{20}\left(\frac{\mu_0}{4\pi}\right)^2 \frac{\gamma^4 \hbar^2}{r^6}\left(3\tau_c + \frac{5\tau_c}{1+\omega^2 {\tau_c}^2} + \frac{2\tau_c}{1+4\omega^2 {\tau_c}^2}\right) \qquad \{1.19\}$$

And for a paramagnetic system [107]:

$$R_2 = \frac{1}{T_2} = \frac{1}{20}\left(\frac{\mu_0}{4\pi}\right)^2 \frac{\gamma_I^2 \gamma_S^2 \hbar^2}{r^6}\left(4\tau_S + \frac{3\tau_S}{1+\omega_I^2 {\tau_S}^2} + \right.$$
$$\left. + \frac{\tau_S}{1+(\omega_I - \omega_S)^2 {\tau_S}^2} + \frac{6\tau_S}{1+(\omega_I + \omega_S)^2 {\tau_S}^2} + \frac{6\tau_S}{1+\omega_S^2 {\tau_S}^2}\right) \quad \{1.20\}$$

Spin exchanges are more efficient the longer the spins stay "close together", therefore T_2 gets shorter when molecules are slow moving, i.e. with longer correlation times.

Nuclear Overhauser Effect (NOE)

When a spin resonance is perturbed by saturation (equalisation of upper and lower energy state populations by RF irradiation) or magnetisation inversion, it may produce a change in the intensities of other resonances. This phenomenon is called the Nuclear Overhauser Effect (NOE).

Consider a two spin ½ system with dipolar coupling interaction but no spin coupling present. Figure 1.11-a shows the energy states denoted as 1 to 4, with 1 as the lower energy level. Transitions 1-3 and 2-4 correspond to spin *I* and 1-2 and 3-4 to spin *S*.

Since J coupling is considered to be zero, both transitions for spin *I* have the same frequency, as do the two transitions of spin *S*.

If we assume that at equilibrium the populations of the energy levels 1 to 4 are respectively proportional to 1, 0, 0 and –1, when spin *S* transitions are saturated (i.e. levels 1 and 2 and levels 3 and 4 have equalised populations) populations are changed to ½, ½, -½ and -½ (Figure 1.11-b). The fractions represent the populations in relation to levels 2 or 3 in equilibrium, which were considered zero for simplicity.

After the perturbation the system will relax back to equilibrium through any of the allowable relaxation pathways (labelled *w* in Figure 1.11-b).

The normal relaxation pathway, labelled w_1 in Figure 1.11-b, does not alter the population difference for spin *S*, because both transitions have the same relaxation rate, there is no change in population difference between the spin states. Therefore the w_1 relaxation does not change the intensity of spin *I*.

However in addition to the above mentioned w_1 relaxation there exist two other relaxation processes (labelled w_0 and w_2 in Figure 1.11-b), that

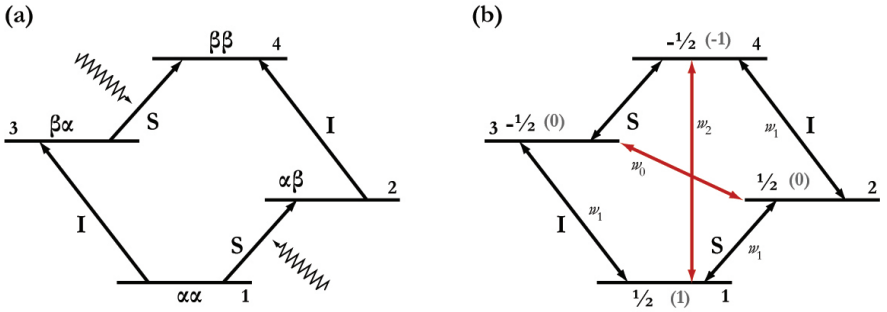

FIGURE 1.11 - Energy levels and population of a two spin system with no spin coupling. (a) The 4 states are labelled 1 to 4 corresponding to αα, αβ, βα and ββ respectively. The S transitions are saturated by RF irradiation. (b) The relaxation pathways are represented by w_0, w_1 and w_2. The fractions indicate the populations after saturation. The numbers in parenthesis indicate the initial equilibrium values. Adapted from [108].

in spite of not being directly observable in the NMR spectrum, are allowed pathways for spin relaxation due to an exchange of magnetization between spins, known as cross-relaxation.

These relaxation pathways are important when two spins are close enough to each other (~5Å) to have a significant dipolar interaction. Both w_0 and w_2 alter the intensity of spin *I*. Whether the intensity is enhanced or reduced after saturation is dependent on which relaxation pathway is dominant.

Considering Figure 1.11-b, when the system relaxes back to equilibrium only through w_0 pathway the populations of levels 2 and 3 reach equilibrium, and now we have the population distribution for each level respectively ½, 0, 0, -½. Therefore spin *I* intensity is reduced, because the population difference for transitions 1-3 and 2-4 is decreased to ½

from the initial equilibrium state of 1.

Alternatively, if the system relaxes via w_2 pathway the final populations at levels 4 and 1 reach equilibrium (1 and –1 respectively) but levels 2 and 3 do not relax. The distribution is now 1, ½, -½, -1 and since the population difference for transitions 1-3 and 2-4 increases to 1 ½ from the equilibrium value of 1 the intensity of spin *I* is increased by the NOE.

The NOE enhancement η is given by the ratio of the cross-relaxation rate to the total relaxation of spin *I*:

$$\eta = \frac{\gamma_S}{\gamma_I}\ \frac{w_2 - w_0}{2w_1 + w_2 + w_0} = \frac{\gamma_S \sigma_{I(J)}}{\gamma_I \rho_{I(J)}} \qquad \{1.21\}$$

in which γ have their usual meaning, $(2w_1+w_2+w_0)$ represents the dipolar spin relaxation ρ, and (w_2-w_0) the cross relaxation rate, σ. In the case of two homonuclear spins ($\gamma_I=\gamma_S=\gamma$) *I* and *S*, dipolar coupled and completely isolated from other spins the equations for σ and ρ are [103]:

$$\sigma_{I(J)} = \frac{1}{10}\left(\frac{\mu_0}{4\pi}\right)^2 \frac{\gamma^4\hbar^2}{r^6}\left(\frac{6\tau_c}{1+4\omega^2\tau_c{}^2} - \tau_c\right) \qquad \{1.22\}$$

$$\rho_{I(J)} = \frac{1}{10}\left(\frac{\mu_0}{4\pi}\right)^2 \frac{\gamma^4\hbar^2}{r^6}\left(\tau_c + \frac{3\tau_c}{1+\omega^2\tau_c{}^2} + \frac{6\tau_c}{1+4\omega^2\tau_c{}^2}\right) \qquad \{1.23\}$$

The cross relaxation rate constant σ is proportional to the inverse sixth power of the distance between the two interacting spins. For values of $\omega\tau_c \ll 1$, equation {1.22} reduces to:

$$\sigma_{I(J)} = \left(\frac{\mu_0}{4\pi}\right)^2 \frac{\gamma^4\hbar^2\tau_c}{2r^6} \qquad \{1.24\}$$

And when $\omega\tau_c \gg 1$,

$$\sigma_{I(J)} = -\frac{1}{10}\left(\frac{\mu_0}{4\pi}\right)^2 \frac{\gamma^4\hbar^2\tau_c}{r^6} \qquad \{1.25\}$$

So, for small molecules in non viscous solution (short correlation times) NOE's are positive, and for large molecules or viscous solutions (long correlation times) NOE's are negative.

The main use of NOE in biological NMR spectroscopy is for the determination of distances between pairs of protons. For short mixing times the slope of the initial buildup rates of the NOE enhancement gives the cross relaxation rate, which is related to the distances between the protons and therefore can be used for the valuable distance information.

Mixing time: One experiment used to reveal the NOE is to invert one of the coupled spins with a selective 180° pulse.

Since the *S* spin is not at equilibrium magnetization is transferred to spin *I* by cross-relaxation. After a suitable period, called the mixing time τ_m a non selective 90° pulse is applied and the spectrum recorded.

Hyperfine shift

The NMR spectrum of a paramagnetic protein, which has at least one unpaired electron, is dependent on the electron-nucleus interaction. The electron magnetic moment (658 times bigger than that of a proton) of the unpaired electron(s) gives rise to a contribution to the chemical shift that is called the hyperfine shift.

The hyperfine shift is defined as the difference between the chemical shift in a paramagnetic system and that in an analogous diamagnetic system and it consists of two contributions.

The Fermi contact term that results from the effect of the unpaired electron spin density on the resonating nucleus; the magnetic field from the electron magnetic moment generates an additional magnetic field at the nucleus.

In the case of haem proteins the Fermi contact shift is only important for the haem and its ligands. The electron density of the unpaired electron is delocalized from the iron orbitals into the π-molecular orbitals of the porphyrin and the axial ligands and then it is transferred directly or by hyperconjugation to the haem substituents [109, 110].

The second contribution to the hyperfine interaction is the pseudocontact shift, also called the dipolar shift because it is a through space interaction between the unpaired electron and the nucleus, which can be described by the dipolar interaction of two magnetic dipoles. Being a

through-space interaction, this shift influences the chemical shifts of both ligated and nonligated nuclei.

Applying the metal-centred dipole approximation [107], for the pseudocontact shift we have[111]:

$$\delta_i^{pc} = \frac{10^6}{12\pi r^3}\left[\Delta\chi_{ax}(3\cos^2\theta - 1) + \frac{3}{2}\Delta\chi_{eq}\sin^2\theta\cdot\cos 2\phi\right] \qquad \{1.26\}$$

Where $\Delta\chi_{ax} = \chi_z - (\chi_x + \chi_y)/2$; $\Delta\chi_{eq} = \chi_x - \chi_y$ and θ, ϕ and r are the spherical polar coordinates with respect to the principal axes of the magnetic susceptibility tensor, and $\Delta\chi_{ax}$, $\Delta\chi_{eq}$ are the axial and equatorial anisotropies respectively. If the susceptibility were isotropic or the electron relaxation were slow then the interaction would average to zero as the molecules rotate isotropically and if there is no Fermi contact interaction, as the internuclear dipolar interaction does. For the calculation of pseudocontact shifts the anisotropy of the magnetic susceptibility tensor and the orientation of its principal axes with respect to the protein are necessary.

For the NMR spectrum of a paramagnetic protein, the total observed chemical shift is given by:

$$\delta = \Delta\delta_{dia} + \delta_{pc} + \delta_{FC} \qquad \{1.27\}$$

Where δ_{dia} is the diamagnetic shift (we are assuming that the difference in the diamagnetic shift on going from the diamagnetic to the paramagnetic state is negligible), δ_{PC} is the metal centred pseudocontact shift and δ_{FC} is the Fermi contact shift.

The dipolar shifts of protons from a known structure of a low-spin haem protein can be used to determine the magnetic susceptibility tensor, since the metal position is rigidly defined, with the diamagnetic state used to provide the reference shifts [112]. From the shift difference between the oxidised and reduced protein we can identify redox-related structural changes if any and test the accuracy of a structure [113].

Determination of the magnetic susceptibility tensor

The pseudocontact shifts are extracted by subtracting the diamagnetic chemical shift from the paramagnetic chemical shift, once the assignments for proton resonances in the paramagnetic and diamagnetic reference state of the metalloprotein in question are known. Providing that the atomic coordinates of the nuclei with respect to the metal centres are available from a structural model, the magnetic susceptibility tensor can be determined.

To do this the axial and equatorial anisotropies $\Delta\chi_{ax}$, $\Delta\chi_{eq}$ must be known as well as the three Euler rotation angles that relate the molecular coordinate system to the coordinate system defined by the principal axes of the magnetic susceptibility tensor (Figure 1.12).

Based on the set of observed pseudocontact shifts and the atomic coordinates from the preliminary NMR structures, the five parameters of the magnetic susceptibility tensors are fitted iteratively [114].

The fit quality is associated with several uncertainties from the experimental and calculation procedures. Assuming that the observed shifts are purely dipolar, the *experimental uncertainty* from the measured shifts in the reduced and oxidised forms is δS. The uncertainties associated with the atomic coordinates affect the *calculated values* of the fit and are assumed to have a standard deviation of 0.05 nm for the heavy atoms. The uncertainty in the calculated shifts may be defined by the change that would arise from a movement of 0.05 nm in the direction of the maximum gradient of the pseudocontact shift field. The sum of the squares of the three orthogonal gradients, multiplied by 0.0025 nm then gives the variance of each calculated value.

Finally, the standard deviation of the difference between each pair of observed and calculated values is given by:

$$\sigma(\exp - calc) = \sqrt{2\delta S^2 + 0,0025(\delta pc_x{}^2 + \delta pc_y{}^2 + \delta pc_z{}^2)} \qquad \{1.28\}$$

where δpc_x, δpc_y and δpc_z represents the orthogonal gradient of the pseudocontact shift field.

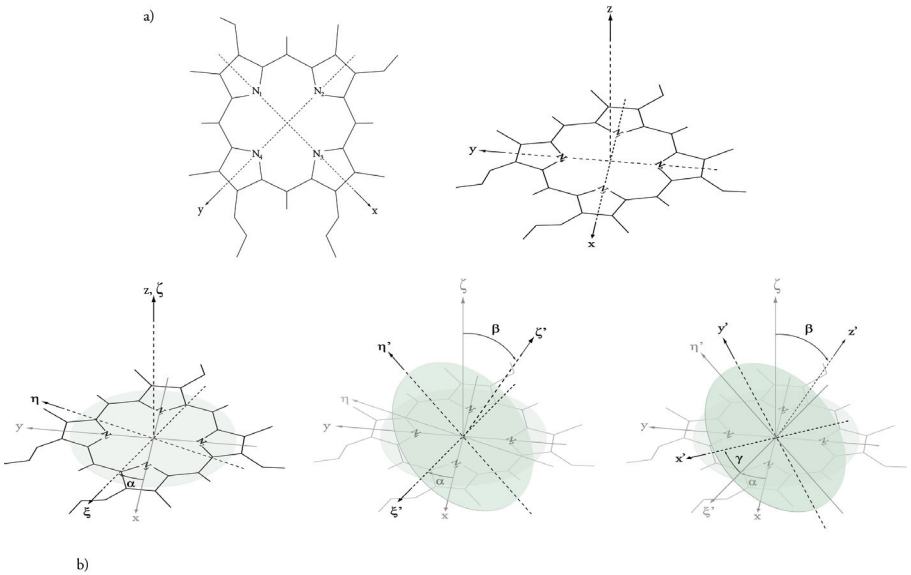

FIGURE 1.12 - a) The molecular axis system. The x axis is taken along the mean of the positions of nitrogens N1-N3, y axis taken along the vectors N2-N4 and the z axis taken normal to the two vectors N1-N3 and N2-N4. A small adjustment was made to the vector N2-N4 to ensure orthogonality [113]. b) Representation of the Euler angles α, β, γ that relate the axis system of the magnetic susceptibility tensor to the molecular axis system.

If the coordinates and the redox-related shifts are well defined by the model, the complete set of scaled differences should have variance equal to one. When this doesn't happen, the largest deviation is rejected and the standard deviation of the remaining shifts is recalculated, repeating the procedure until the standard deviation of the remaining shifts is one. Alternatively, the magnetic susceptibility tensors of the haems can be fitted simultaneously with a structure determination, as described in chapter 3.

REFERENCES

1. Chapman, S., Daff, S., and Munro, A., *Heme: The most versatile redox centre in biology?*, in *Metal Sites in Proteins and Models*. 1997. 39-70.

2. Perutz, M., *Mechanisms of Cooperativity and Allosteric Regulation in Proteins*. 1990, Cambridge: Cambridge University Press.

3. Stuehr, D.J., *Mammalian nitric oxide synthases.* Biochim Biophys Acta, 1999. **1411**: 217-30.

4. Ribeiro, J.M., Hazzard, J.M., Nussenzveig, R.H., Champagne, D.E., and Walker, F.A., *Reversible binding of nitric oxide by a salivary heme protein from a bloodsucking insect.* Science, 1993. **260**: 539-41.

5. Moore, G.R. and Pettigrew, G.W., *Cytochromes* c*: evolutionary, structural, and physicochemical aspects*. Springer series in molecular biology. 1990, Berlin; New York: Springer-Verlag.

6. Namslauer, A. and Brzezinski, P., *Structural elements involved in electron-coupled proton transfer in cytochrome* c *oxidase.* FEBS Lett, 2004. **567**: 103-10.

7. Moss, G.P., *Nomenclature of tetrapyrroles.* Eur J Biochem, 1988. **178**: 277-328.

8. Pettigrew, G.W. and Moore, G.R., *Cytochromes* c*: biological aspects*. Springer series in molecular biology. 1987, Berlin; New York: Springer-Verlag.

9. Pereira, A.C., Teixeira, M., and Xavier, A.V., *Hemeproteins in anerobes*. Structure & Bonding. 1998, Heidelberg: Springer Berlin.

10. Fraústo da Silva, J.R.R. and Williams, R.J.P., *The biological chemistry of the elements : the inorganic chemistry of life*. 1993, Oxford [England]; New York: Clarendon Press ; Oxford University Press.

11. Hartshorne, R.S., Kern, M., Meyer, B., Clarke, T.A., Karas, M., Richardson, D.J., and Simon, J., *A dedicated haem lyase is required for the maturation of a novel bacterial cytochrome* c *with unconventional covalent haem binding.* Mol Microbiol, 2007. **64**: 1049-60.

12. Pessanha, M., Brennan, L., Xavier, A.V., Cuthbertson, P.M., Reid, G.A., Chapman, S.K., Turner, D.L., and Salgueiro, C.A., *NMR structure of the haem core of a novel tetrahaem cytochrome isolated from* Shewanella frigidimarina*: identification of the haem-specific axial ligands and order of oxidation.* FEBS Lett, 2001. **489**: 8-13.

13. Taylor, P., Pealing, S.L., Reid, G.A., Chapman, S.K., and Walkinshaw, M.D., *Structural and mechanistic mapping of a unique fumarate reductase.* Nat Struct Biol, 1999. **6**: 1108-12.

14. Messias, A.C., Kastrau, D.H., Costa, H.S., LeGall, J., Turner, D.L., Santos, H., and Xavier, A.V., *Solution structure of* Desulfovibrio vulgaris *(Hildenborough) ferrocytochrome* c_3*: structural basis for functional cooperativity.* J Mol Biol, 1998. **281**: 719-39.

15. Brennan, L., Turner, D.L., Messias, A.C., Teodoro, M.L., LeGall, J., Santos, H., and Xavier, A.V., *Structural basis for the network of functional cooperativities in cytochrome* c_3 *from* Desulfovibrio gigas*: solution structures of the oxidised and reduced states.* J Mol Biol, 2000. **298**: 61-82.

16. Pokkuluri, P.R., Londer, Y.Y., Duke, N.E., Erickson, J., Pessanha, M., Salgueiro, C.A., and Schiffer, M., *Structure of a novel* c_7*-type three-heme cytochrome domain from a multidomain cytochrome* c *polymer.* Protein Sci, 2004. **13**: 1684-92.

17. Mowat, C.G., Rothery, E., Miles, C.S., McIver, L., Doherty, M.K., Drewette, K., Taylor, P., Walkinshaw, M.D., Chapman, S.K., and Reid, G.A., *Octaheme tetrathionate reductase is a respiratory enzyme with novel heme ligation.* Nat Struct Mol Biol, 2004. **11**: 1023-4.

18. Klarskov, K., Van Driessche, G., Backers, K., Dumortier, C., Meyer, T.E., Tollin, G., Cusanovich, M.A., and Van Beeumen, J.J., *Ligand Binding and Covalent Structure of an Oxygen-Binding Heme Protein from* Rhodobacter sphaeroides*, a Representative of a New Structural Family of* c*-Type Cytochromes.* Biochemistry, 1998. **37**: 5995-6002.

19. Louro, R.O., *Proton thrusters: overview of the structural and functional features of soluble tetrahaem cytochromes* c_3. J Biol Inorg Chem, 2007. **12**(1): 1-10.

20. Louro, R.O., Catarino, T., LeGall, J., and Xavier, A.V., *Redox-Bohr effect in electron/proton energy transduction: cytochrome* c_3 *coupled to hydrogenase works as a 'proton thruster' in* Desulfovibrio vulgaris. J Biol Inorg Chem,

1997. **2**: 488-91.

21. Pessanha, M., Morgado, L., Louro, R.O., Londer, Y.Y., Pokkuluri, P.R., Schiffer, M., and Salgueiro, C.A., *Thermodynamic characterization of triheme cytochrome PpcA from* Geobacter sulfurreducens*: evidence for a role played in* e^-/H^+ *energy transduction.* Biochemistry, 2006. **45**: 13910-7.

22. Leys, D., Tsapin, A.S., Nealson, K.H., Meyer, T.E., Cusanovich, M.A., and Van Beeumen, J.J., *Structure and mechanism of the flavocytochrome* c *fumarate reductase of* Shewanella putrefaciens *MR-1.* Nat Struct Biol, 1999. **6**: 1113-7.

23. Field, S.J., Dobbin, P.S., Cheesman, M.R., Watmough, N.J., Thomson, A.J., and Richardson, D.J., *Purification and magneto-optical spectroscopic characterization of cytoplasmic membrane and outer membrane multiheme* c*-type cytochromes from* Shewanella frigidimarina *NCIMB400.* J Biol Chem, 2000. **275**: 8515-22.

24. Methe, B.A., Nelson, K.E., Eisen, J.A., Paulsen, I.T., Nelson, W., Heidelberg, J.F., Wu, D., Wu, M., Ward, N., Beanan, M.J., Dodson, R.J., Madupu, R., Brinkac, L.M., Daugherty, S.C., DeBoy, R.T., Durkin, A.S., Gwinn, M., Kolonay, J.F., Sullivan, S.A., Haft, D.H., Selengut, J., Davidsen, T.M., Zafar, N., White, O., Tran, B., Romero, C., Forberger, H.A., Weidman, J., Khouri, H., Feldblyum, T.V., Utterback, T.R., Van Aken, S.E., Lovley, D.R., and Fraser, C.M., *Genome of* Geobacter sulfurreducens*: metal reduction in subsurface environments.* Science, 2003. **302**: 1967-9.

25. Butler, J.E., Kaufmann, F., Coppi, M.V., Nunez, C., and Lovley, D.R., *MacA, a diheme* c*-type cytochrome involved in Fe(III) reduction by* Geobacter sulfurreducens. J Bacteriol, 2004. **186**: 4042-5.

26. Leang, C., Coppi, M.V., and Lovley, D.R., *OmcB, a* c*-type polyheme cytochrome, involved in Fe(III) reduction in* Geobacter sulfurreducens. J Bacteriol, 2003. **185**: 2096-103.

27. Pokkuluri, P.R., Londer, Y.Y., Duke, N.E., Long, W.C., and Schiffer, M., *Family of cytochrome* c_7*-type proteins from* Geobacter sulfurreducens*: structure of one cytochrome* c_7 *at 1.45 A resolution.* Biochemistry, 2004. **43**: 849-59.

28. Correia, I.J., Paquete, C.M., Louro, R.O., Catarino, T., Turner, D.L., and Xavier, A.V., *Thermodynamic and kinetic characterization of trihaem cytochrome* c_3 *from* Desulfuromonas acetoxidans. Eur J Biochem, 2002. **269**: 5722-30.

29. Morris, C.J., Black, A.C., Pealing, S.L., Manson, F.D., Chapman, S.K., Reid, G.A., Gibson, D.M., and Ward, F.B., *Purification and properties of a novel cytochrome: flavocytochrome* c *from* Shewanella putrefaciens. Biochem J, 1994. **302**: 587-93.

30. Matias, P.M., Frazao, C., Morais, J., Coll, M., and Carrondo, M.A., *Structure analysis of cytochrome* c_3 *from Desulfovibrio vulgaris Hildenborough at 1.9 A resolution.* J Mol Biol, 1993. **234**: 680-99.

31. Matias, P.M., Morais, J., Coelho, R., Carrondo, M.A., Wilson, K., Dauter, Z., and Sieker, L., *Cytochrome* c_3 *from* Desulfovibrio gigas*: crystal structure at 1.8 A resolution and evidence for a specific calcium-binding site.* Protein Sci, 1996. **5**: 1342-54.

32. Einsle, O., Messerschmidt, A., Stach, P., Bourenkov, G.P., Bartunik, H.D., Huber, R., and Kroneck, P.M., *Structure of cytochrome* c *nitrite reductase.* Nature, 1999. **400**: 476-80.

33. Matias, P.M., Saraiva, L.M., Soares, C.M., Coelho, A.V., LeGall, J., and Carrondo, M.A., *Nine-haem cytochrome* c *from* Desulfovibrio desulfuricans *ATCC 27774:primary sequence determination, crystallographic refinement at 1.8 and modelling studies of its interaction with the tetrahaem cytochrome* c_{3}. J Biol Inorg Chem, 1999. **4**: 478-94.

34. Nørager, S., Legrand, P., Pieulle, L., Hatchikian, C., and Roth, M., *Crystal structure of the oxidised and reduced acidic cytochrome* c_3 *from* Desulfovibrio africanus. J Mol Biol, 1999. **290**: 881-902.

35. Matias, P.M., Coelho, A.V., Valente, F.M., Placido, D., LeGall, J., Xavier, A.V., Pereira, I.A., and Carrondo, M.A., *Sulfate respiration in* Desulfovibrio vulgaris *Hildenborough. Structure of the 16-heme cytochrome* c *HmcA at 2.5A resolution and a view of its role in transmembrane electron transfer.* J Biol Chem, 2002. **277**: 47907-16.

36. Ishimoto, M., Koyama, J., and Nagai, Y., *A Cytochrome and a Green Pigment of Sulfate-reducing Bacteria.*

Bull Chem Soc Jpn, 1954. **27**: 564b-5.

37. Postgate, J.R., *Dependence of Sulphate Reduction and Oxygen Utilization on a Cytochrome in Desulphovibrio.* Biochem J, 1954. **58**: ix.

38. Gordon, E.H., Pike, A.D., Hill, A.E., Cuthbertson, P.M., Chapman, S.K., and Reid, G.A., *Identification and characterization of a novel cytochrome* c_3 *from* Shewanella frigidimarina *that is involved in Fe(III) respiration.* Biochem J, 2000. **349**: 153-8.

39. Leys, D., Meyer, T.E., Tsapin, A.S., Nealson, K.H., Cusanovich, M.A., and Van Beeumen, J.J., *Crystal structures at atomic resolution reveal the novel concept of "electron-harvesting" as a role for the small tetraheme cytochrome* c. J Biol Chem, 2002. **277**: 35703-11.

40. Czjzek, M., Payan, F., Guerlesquin, F., Bruschi, M., and Haser, R., *Crystal structure of cytochrome* c_3 *from* Desulfovibrio desulfuricans *Norway at 1·7 Å resolution.* J Mol Biol, 1994. **243**: 653-67.

41. Simões, P., Matias, P.M., Morais, J., Wilsonc, K., Dauterc, Z., and Carrondo, M.A., *Refinement of the three-dimensional structures of cytochrome* c_3 *from* Desulfovibrio vulgaris *Hildenborough at 1.67 Å resolution and from* Desulfovibrio desulfuricans *ATCC 27774 at 1.6 Å resolution* Inorg Chim Acta, 1998. **273**: 213-24.

42. Einsle, O., Foerster, S., Mann, K., Fritz, G., Messerschmidt, A., and Kroneck, P.M., *Spectroscopic investigation and determination of reactivity and structure of the tetraheme cytochrome* c_3 *from* Desulfovibrio desulfuricans *Essex 6.* Eur J Biochem, 2001. **268**: 3028-35.

43. Correia, I.J., Paquete, C.M., Coelho, A., Almeida, C.C., Catarino, T., Louro, R.O., Frazao, C., Saraiva, L.M., Carrondo, M.A., Turner, D.L., and Xavier, A.V., *Proton-assisted two-electron transfer in natural variants of tetraheme cytochromes from* Desulfomicrobium *Sp.* J Biol Chem, 2004. **279**: 52227-37.

44. Bento, I., Matias, P.M., Baptista, A.M., da Costa, P.N., van Dongen, W.M., Saraiva, L.M., Schneider, T.R., Soares, C.M., and Carrondo, M.A., *Molecular basis for redox-Bohr and cooperative effects in cytochrome* c_3 *from* Desulfovibrio desulfuricans *ATCC 27774: crystallographic and modeling studies of oxidized and reduced high-resolution structures at pH 7.6.* Proteins, 2004. **54**: 135-52.

45. Coutinho, I.B., Turner, D.L., Legall, J., and Xavier, A.V., *Revision of the haem-core architecture in the tetraheam cytochrome* c_3 *from* Desulfovibrio baculatus *by two-dimensional* ^1H *NMR.* Eur J Biochem, 1992. **209**: 329-33.

46. Morais, J., Palma, P.N., Frazao, C., Caldeira, J., LeGall, J., Moura, I., Moura, J.J., and Carrondo, M.A., *Structure of the tetraheme cytochrome from* Desulfovibrio desulfuricans *ATCC 27774: X-ray diffraction and electron paramagnetic resonance studies.* Biochemistry, 1995. **34**: 12830-41.

47. Badziong, W. and Thauer, R.K., *Vectorial electron transport in* Desulfovibrio vulgaris *(Marburg) growing on hydrogen plus sulfate as sole energy source.* Arch Microbiol, 1980. **125**: 167-74.

48. Czjzek, M., Guerlesquin, F., Bruschi, M., and Haser, R., *Crystal structure of a dimeric octaheme cytochrome* c_3 *(M(r) 26,000) from* Desulfovibrio desulfuricans *Norway.* Structure, 1996. **4**: 395-404.

49. Dolla, A., Leroy, G., Guerlesquin, F., and Bruschi, M., *Identification of the site of interaction between cytochrome* c_3 *and ferredoxin using peptide mapping of the cross-linked complex.* Biochim Biophys Acta, 1991. **1058**: 171-7.

50. Matias, P.M., Soares, C.M., Saraiva, L.M., Coelho, R., Morais, J., Le Gall, J., and Carrondo, M.A., *[NiFe] hydrogenase from* Desulfovibrio desulfuricans *ATCC 27774: gene sequencing, three-dimensional structure determination and refinement at 1.8 Å and modelling studies of its interaction with the tetrahaem cytochrome* c_3. J Biol Inorg Chem, 2001. **6**: 63-81.

51. ElAntak, L., Morelli, X., Bornet, O., Hatchikian, C., Czjzek, M., Dolla, A., and Guerlesquin, F., *The cytochrome* c_3*-[Fe]-hydrogenase electron-transfer complex: structural model by NMR restrained docking.* FEBS Lett, 2003. **548**: 1-4.

52. Yahata, N., Saitoh, T., Takayama, Y., Ozawa, K., Ogata, H., Higuchi, Y., and Akutsu, H., *Redox interaction of cytochrome* c_3 *with [NiFe] hydrogenase from* Desulfovibrio vulgaris *Miyazaki F.* Biochemistry, 2006. **45**: 1653-62.

53. Stewart, D.E., LeGall, J., Moura, I., Moura, J.J., Peck, H.D., Jr., Xavier, A.V., Weiner, P.K., and Wampler,

J.E., *A hypothetical model of the flavodoxin-tetraheme cytochrome* c_3 *complex of sulfate-reducing bacteria.* Biochemistry, 1988. **27**: 2444-50.

54. Palma, P.N., Moura, I., LeGall, J., Van Beeumen, J., Wampler, J.E., and Moura, J.J., *Evidence for a ternary complex formed between flavodoxin and cytochrome* c_3*: ^{1}H-NMR and molecular modeling studies.* Biochemistry, 1994. **33**: 6394-407.

55. Ambler, R.P., *The structure and classification of cytochromes* c_3, in *From cyclotrons to cytochromes*, N.O. Kaplan and A. Robinson, Editors. 1980, Academic Press: NY USA, London UK. 263-79.

56. Valente, F.M., Saraiva, L.M., LeGall, J., Xavier, A.V., Teixeira, M., and Pereira, I.A., *A membrane-bound cytochrome* c_3*: a type II cytochrome* c_3 *from Desulfovibrio vulgaris Hildenborough.* Chembiochem, 2001. **2**: 895-905.

57. Turner, D.L., Salgueiro, C.A., Catarino, T., Legall, J., and Xavier, A.V., *NMR studies of cooperativity in the tetrahaem cytochrome* c_3 *from* Desulfovibrio vulgaris. Eur J Biochem, 1996. **241**: 723-31.

58. Xavier, A.V., *Energy transduction coupling mechanisms in multiredox center proteins* J Inorg Biochem, 1986. **28**: 239-43.

59. Moura, J.J., Santos, H., Moura, I., LeGall, J., Moore, G.R., Williams, R.J., and Xavier, A.V., *NMR redox studies of* Desulfovibrio vulgaris *Cytochrome* c_3*. Electron transfer mechanisms.* Eur J Biochem, 1982. **127**: 151-5.

60. Coletta, M., Catarino, T., LeGall, J., and Xavier, A.V., *A thermodynamic model for the cooperative functional properties of the tetraheme cytochrome* c_3 *from* Desulfovibrio gigas. Eur J Biochem, 1991. **202**: 1101-6.

61. Santos, H., Moura, J.J., Moura, I., LeGall, J., and Xavier, A.V., *NMR studies of electron transfer mechanisms in a protein with interacting redox centres:* Desulfovibrio gigas *cytochrome* c_3. Eur J Biochem, 1984. **141**: 283-96.

62. Bell, G.R., Lee, J.P., Peck Jr, H.D., and Le Gall, J., *Reactivity of* Desulfovibrio gigas *hydrogenase toward artificial and natural electron donors or acceptors.* Biochimie, 1978. **60**: 315-20.

63. Odom, J.M. and Peck, H.D., *Hydrogen cycling as a general mechanism for energy coupling in the sulfate-reducing bacteria,* Desulfovibrio *sp.* FEMS Microbiol Lett, 1981. **12**: 47-50.

64. Voordouw, G., *Carbon monoxide cycling by* Desulfovibrio vulgaris *Hildenborough.* J Bacteriol, 2002. **184**: 5903-11.

65. Noguera, D.R., Brusseau, G.A., Rittmann, B.E., and Stahl, D.A., *A unified model describing the role of hydrogen in the growth of* Desulfovibrio vulgaris *under different environmental conditions.* Biotechnol Bioeng, 1998. **59**: 732-46.

66. Louro, R.O., Pacheco, I., Turner, D.L., LeGall, J., and Xavier, A.V., *Structural and functional characterization of cytochrome* c_3 *from* D. desulfuricans *ATCC 27774 by ^{1}H-NMR.* FEBS Lett, 1996. **390**: 59-62.

67. Salgueiro, C.A., Turner, D.L., Santos, H., LeGall, J., and Xavier, A.V., *Assignment of the redox potentials to the four haems in* Desulfovibrio vulgaris *cytochrome* c_3 *by 2D-NMR.* FEBS Lett, 1992. **314**: 155-8.

68. Turner, D.L., Salgueiro, C.A., LeGall, J., and Xavier, A.V., *Structural studies of* Desulfovibrio vulgaris *ferrocytochrome* c_3 *by two-dimensional NMR.* Eur J Biochem, 1992. **210**: 931-6.

69. Coutinho, I.B., Turner, D.L., LeGall, J., and Xavier, A.V., *Characterization of the structure and redox behaviour of cytochrome* c_3 *from* Desulfovibrio baculatus *by ^{1}H-nuclear-magnetic-resonance spectroscopy.* Biochem J, 1993. **294**: 899-908.

70. Picarra-Pereira, M.A., Turner, D.L., LeGall, J., and Xavier, A.V., *Structural studies on* Desulfovibrio gigas *cytochrome* c_3 *by two-dimensional ^{1}H-nuclear-magnetic-resonance spectroscopy.* Biochem J, 1993. **294**: 909-15.

71. Keller, R.M. and Wuthrich, K., *Assignment of the heme* c *resonances in the 360 MHz H NMR spectra of cytochrome* c. Biochim Biophys Acta, 1978. **533**: 195-208.

72. Palmer, G. and Olson, J.S., *Chapter 5*, in *Molybdenum and molybdenum- containing enzymes*, M.P. Coughlan, Editor. 1980, Pergamon Pr.: Oxford [u.a.].

73. Louro, R.O., Catarino, T., LeGall, J., Turner, D.L., and Xavier, A.V., *Cooperativity between electrons and protons in a monomeric cytochrome* c_3*: the importance of mechanochemical coupling for energy transduction.* Chembiochem,

2001. **2**: 831-7.

74. Louro, R.O., Catarino, T., Turner, D.L., Picarra-Pereira, M.A., Pacheco, I., LeGall, J., and Xavier, A.V., *Functional and mechanistic studies of cytochrome* c_3 *from* Desulfovibrio gigas*: thermodynamics of a "proton thruster".* Biochemistry, 1998. **37**: 15808-15.

75. Paquete, C.M., Pereira, P.M., Catarino, T., Turner, D.L., Louro, R.O., and Xavier, A.V., *Functional properties of type I and type II cytochromes* c_3 *from* Desulfovibrio africanus. Biochim Biophys Acta, 2007. **1767**: 178-88.

76. Messias, A.C., Aguiar, A.P., Brennan, L., Salgueiro, C.A., Saraiva, L.M., Xavier, A.V., and Turner, D.L., *Solution structures of tetrahaem ferricytochrome* c_3 *from* Desulfovibrio vulgaris *(Hildenborough) and its K45Q mutant: the molecular basis of cooperativity.* Biochim Biophys Acta, 2006. **1757**: 143-53.

77. Paquete, C.M., Turner, D.L., Louro, R.O., Xavier, A.V., and Catarino, T., *Thermodynamic and kinetic characterisation of individual haems in multicentre cytochromes* c_3. Biochim Biophys Acta, 2007. **1767**: 1169-79.

78. Nealson, K.H., Belz, A., and McKee, B., *Breathing metals as a way of life: geobiology in action.* Antonie Van Leeuwenhoek, 2002. **81**: 215-22.

79. Myers, C.R. and Nealson, K.H., *Bacterial Manganese Reduction and Growth with Manganese Oxide as the Sole Electron Acceptor.* Science, 1988. **240**: 1319-21.

80. Nealson, K.H. and Saffarini, D., *Iron and manganese in anaerobic respiration: environmental significance, physiology, and regulation.* Annu Rev Microbiol, 1994. **48**: 311-43.

81. Gordon, E.H., Pealing, S.L., Chapman, S.K., Ward, F.B., and Reid, G.A., *Physiological function and regulation of flavocytochrome* c_3*, the soluble fumarate reductase from* Shewanella putrefaciens *NCIMB 400.* Microbiology, 1998. **144**: 937-45.

82. Reid, G.A. and Gordon, E.H., *Phylogeny of marine and freshwater* Shewanella*: reclassification of S*hewanella putrefaciens *NCIMB 400 as* Shewanella frigidimarina. Int J Syst Bacteriol, 1999. **49**: 189-91.

83. Reid, G.A., Gordon, E.H., Hill, A.E., Doherty, M., Turner, K., Holt, R., and Chapman, S.K., *Structure and function of flavocytochrome* c_3*, the soluble fumarate reductase from* Shewanella *NCIMB400.* Biochem Soc Trans, 1998. **26**: 418-21.

84. Moser, D.P. and Nealson, K.H., *Growth of the facultative anaerobe* Shewanella putrefaciens *by elemental sulfur reduction.* Appl Environ Microbiol, 1996. **62**: 2100-5.

85. Myers, C.R. and Myers, J.M., *Role of menaquinone in the reduction of fumarate, nitrate, iron(III) and manganese(IV) by* Shewanella putrefaciens *MR-1.* FEMS Microbiol Lett, 1993. **114**: 215-22.

86. Myers, C.R. and Myers, J.M., *Cloning and sequence of cymA, a gene encoding a tetraheme cytochrome* c *required for reduction of iron(III), fumarate, and nitrate by S*hewanella putrefaciens *MR-1.* J Bacteriol, 1997. **179**: 1143-52.

87. Myers, J.M. and Myers, C.R., *Role of the tetraheme cytochrome CymA in anaerobic electron transport in cells of* Shewanella putrefaciens *MR-1 with normal levels of menaquinone.* J Bacteriol, 2000. **182**: 67-75.

88. Newman, D.K. and Kolter, R., *A role for excreted quinones in extracellular electron transfer.* Nature, 2000. **405**: 94-7.

89. Myers, C.R. and Myers, J.M., Shewanella oneidensis *MR-1 restores menaquinone synthesis to a menaquinone-negative mutant.* Appl Environ Microbiol, 2004. **70**: 5415-25.

90. Saffarini, D.A., Blumerman, S.L., and Mansoorabadi, K.J., *Role of menaquinones in Fe(III) reduction by membrane fractions of* Shewanella putrefaciens. J Bacteriol, 2002. **184**: 846-8.

91. Beliaev, A.S. and Saffarini, D.A., Shewanella putrefaciens *mtrB encodes an outer membrane protein required for Fe(III) and Mn(IV) reduction.* J Bacteriol, 1998. **180**: 6292-7.

92. Pitts, K.E., Dobbin, P.S., Reyes-Ramirez, F., Thomson, A.J., Richardson, D.J., and Seward, H.E., *Characterization of the* Shewanella oneidensis *MR-1 decaheme cytochrome MtrA: expression in* Escherichia coli *confers the ability to reduce soluble Fe(III) chelates.* J Biol Chem, 2003. **278**: 27758-65.

93. Weber, K.A., Achenbach, L.A., and Coates, J.D., *Microorganisms pumping iron: anaerobic microbial iron oxidation and reduction.* Nat Rev Microbiol, 2006. **4**: 752-64.

94. Dobbin, P.S., Butt, J.N., Powell, A.K., Reid, G.A., and Richardson, D.J., *Characterization of a flavocytochrome that is induced during the anaerobic respiration of Fe_3^+ by S*hewanella frigidimarina *NCIMB400.* Biochem J, 1999. **342** : 439-48.

95. Pessanha, M., Louro, R.O., Correia, I.J., Rothery, E.L., Pankhurst, K.L., Reid, G.A., Chapman, S.K., Turner, D.L., and Salgueiro, C.A., *Thermodynamic characterization of a tetrahaem cytochrome isolated from a facultative aerobic bacterium,* Shewanella frigidimarina*: a putative redox model for flavocytochrome* c_3. Biochem J, 2003. **370**: 489-95.

96. Ambler, R.P., *The amino acid sequence of cytochrome* c_3 *from* Desulfovibrio vulgaris*. (N.C. I.B. 8303).* Biochem J, 1968. **109**: 47P-8P.

97. Ambler, R.P., Bruschi, M., and Le Gall, J., *The amino acid sequence of cytochrome* c_3 *from* Desulfovibrio desulfuricans *(strain el agheila Z, NCIB 8380).* FEBS Lett, 1971. **18**: 347-50.

98. Ambler, R.P., *Bacterial Cytochromes c and Molecular Evolution.* Syst Zool, 1973. **22**: 554-65.

99. Shinkai, W., Hase, T., Yagi, T., and Matsubara, H., *Amino acid sequence of cytochrome* c_3 *from* Desulfovibrio vulgaris*, Miyazaki.* J Biochem, 1980. **87**: 1747-56.

100. Simões, P., Matias, P.M., Morais, J., Wilson, K., Dauter, Z., and Carrondo, M.A., *Refinement of the three-dimensional structures of cytochrome* c_3 *from* Desulfovibrio vulgaris *Hildenborough at 1.67 A resolution and from* Desulfovibrio desulfuricans *ATCC 27774 at 1.6 A resolution.* Inorg Chim Acta, 1998. **273**: 213-24.

101. Magro, V., Pieulle, L., Forget, N., Guigliarelli, B., Petillot, Y., and Hatchikian, E.C., *Further characterization of the two tetraheme cytochromes* c_3 *from* Desulfovibiro africanus*: nucleotide sequences, EPR spectroscopy and biological activity.* Biochim Biophys Acta, 1997. **1342**: 149-63.

102. Salgueiro, C.A., *Caracterizacão estrutural e termodinâmica do citocromo* c_3 *de* D. vulgaris*, Ph.D. Thesis*. Ph.D. Thesis. 1998, Lisboa: Universidade Nova de Lisboa.

103. Banci, L., Bertini, I., and Luchinat, C., *Nuclear and electron relaxation : the magnetic nucleus-unpaired electron coupling in solution*. 1991, New York, N.Y.: VCH.

104. Ramsey, N.F. and Purcell, E.M., *Interactions between Nuclear Spins in Molecules.* Physical Review, 1952. **85**: 143.

105. Cavanagh, J., *Protein NMR spectroscopy : principles and practice*. 1996, San Diego: Academic Press.

106. Solomon, I., *Relaxation Processes in a System of Two Spins.* Phys Rev, 1955. **99**: 559.

107. Bertini, I., Luchinat, C., and Parigi, G., *Solution NMR of paramagnetic molecules : applications to metallobiomolecules and models*. Curr Methods Inorg Chem, v. 2. 2001, Amsterdam; New York: Elsevier Science Ltd.

108. Teng, Q., *Structural biology : practical NMR applications*. 2005, New York: Springer.

109. Turner, D.L., Brennan, L., Messias, A.C., Teodoro, M.L., and Xavier, A.V., *Correlation of empirical magnetic susceptibility tensors and structure in low-spin haem proteins.* Eur Biophys J, 2000. **29**: 104-12.

110. Karplus, M., *Contact Electron-Spin Coupling of Nuclear Magnetic Moments.* J of Chem Phys, 1959. **30**: 11-5.

111. Turner, D.L., Brennan, L., Chamberlin, S.G., Louro, R.O., and Xavier, A.V., *Determination of solution structures of paramagnetic proteins by NMR.* Eur Biophys J, 1998. **27**: 367-75.

112. Keller, R.M. and Wuthrich, K., *The electronic g-tensor in cytochrome* b_5*: high resolution proton magnetic resonance studies.* Biochim Biophys Acta, 1972. **285**: 326-36.

113. Williams, G., Clayden, N.J., Moore, G.R., and Williams, R.J., *Comparison of the solution and crystal structures of mitochondrial cytochrome* c*. Analysis of paramagnetic shifts in the nuclear magnetic resonance spectrum of ferricytochrome* c*.* J Mol Biol, 1985. **183**: 447-60.

114. Turner, D.L. and Williams, R.J.P., *^{1}H- and ^{13}C-NMR investigation of redox-state-dependent and temperature-dependent conformation changes in horse cytochrome* c*.* Eur J Biochem, 1993. **211**: 555-62.

2

MATERIALS AND METHODS

CONTENTS

TWO-DIMENSIONAL NMR SPECTROSCOPY

Due to severe overlapping, the proton signals of a protein in a one-dimensional NMR experiment cannot be completely assigned. To overcome this, a second frequency dimension is introduced, which spreads the signals over two frequency dimensions, giving rise to two-dimensional NMR spectrum and improving the resolution of spectral assignment.

In a one dimensional NMR experiment, the acquired FID, which is a function of one time variable is Fourier transformed to obtain a function of one frequency variable called a spectrum. In two-dimensional NMR (2D-NMR) the recorded signal, now function of two time variables t_1 and t_2 is Fourier transformed twice resulting in a spectrum function of two frequency variables usually called F_1 and F_2.

The general scheme for 2D NMR spectroscopy can be summarized in the same basic pattern of four stages: *preparation*, *evolution*, *mixing* and *acquisition*.

During the preparation time period, the sample is excited by one or more pulses. The resulting magnetization evolves for the period t_1, called the evolution time. This consists of a variable time delay that increases during the course of the 2D experiment from an initial value to a final value in *m* increments. For each *m* value of the delay the same pulse sequence is executed and an FID is recorded, and so on for the required number of increments in t_1, maintaining all other parameters the same.

In the mixing time period which may comprise several RF pulses and time delays, the magnetization is transferred between spins. During detection period the signal is recorded as a function of the second time variable t_2. After Fourier transformation in both dimensions a 2D spectrum is obtained with the resolution in the F_1 dimension limited by the number of t_1 increments and in the F_2 dimension limited by the number of digitised data points during the t_2 period.

The mixing period is the crucial point in establishing the type of information content in the spectrum. The three experiments presented in Figure 2.1 have distinct evolution and mixing times. In all cases the preparation period consists of a delay interval and single 90º pulse at the end to induce spin *coherence*. In 2D correlation spectroscopy (COSY) the mixing period is simply the 90º pulse separating detection and evolution (Figure 2.1B). The COSY experiment gives correlation maps displaying spin-spin coupling connectivities therefore providing information on neighbouring nuclei along chemical bonds [1-3]

The recording of a two-dimensional signal is done in the following way: t_1 is firstly set to zero, the pulse sequence is executed and the FID recorded. Spins are allowed to return to equilibrium, t_1 is set to the interval $2\Delta_1$ the sequence repeated and a new FID is recorded and stored separately from the first.

After the spins reach equilibrium once again t_1 is now set to $2\Delta_1$, the pulse sequence repeated and the FID recorded and stored with the whole process repeated for $t_1 = 3\Delta_1$, $4\Delta_1$ and so forth until sufficient data is recorded.

Therefore the recording of a 2D data set consists of a repeating pulse sequence for increasing values of t_1 while recording a FID as a function of t_2 for each value of t_1. The result of two Fourier transformations is a 2D-NMR spectrum with two frequency axes and an intensity axes on the third dimension usually plotted as contours.

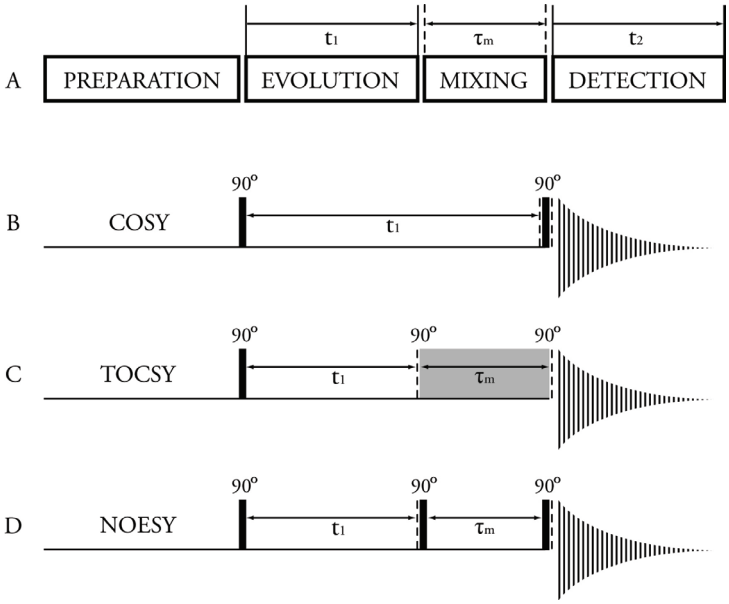

FIGURE 2.1 - (A) General scheme for two-dimensional NMR spectroscopy. (B) - (D) Experimental schemes for COSY, TOCSY and NOESY experiments. The dotted lines indicate the bounds of the mixing time period. The mixing period in the TOCSY experiment can contain a variety of pulse sequences; represented in grey.

Another experiment outlining through-bond scalar spin-spin connectivities is the total correlation spectroscopy (TOCSY) [4-6]. The fundamental difference from the COSY experiment is that the second pulse of the sequence is replaced by a mixing interval consisting of a series

or sequences of pulses that generate an average Hamiltonian without a chemical shift term, said to be *isotropic mixing sequences* (Figure 2.1C). Since magnetization transfer via the strong coupling interaction is efficient only if all chemical shift terms of the Hamiltonian governing the spin system have identical values for each of the two spins *I* and *S* - the so called *Hartmann-Hahn condition* [7] - the absence of chemical-shift terms ensures that the Hartmann-Hahn condition is always satisfied.

As the duration of the mixing time interval increases the extent to which transfer between coupled spins can occur is enhanced. When mixing intervals reach a sufficient length, responses for all members of a spin system even without direct coupling can be observed.

In 2D nuclear Overhauser enhancement spectroscopy (NOESY) the mixing consists of two 90º pulses separated by the *mixing time* τ_m (Figure 2.1D) during which magnetization is transferred between neighbouring spins via cross relaxation. The cross-peaks on a NOESY spectrum indicate dipole-dipole coupling between spins in close spatial proximity, which gives rise to NOE's [8].

In the NOESY experiment the NOE's build up during the mixing time. The initial magnetization build up can be used for internuclear distance measurements. Hence, the cross peak volumes in a NOESY spectrum can be used to obtain distance constraints for model structure calculation. The NOESY experiment is the basis for the use of NMR as a tool for molecular structure calculation.

NMR STRUCTURE DETERMINATION

The basic protocol of NMR structure determination can be divided in several distinct steps: *sample preparation*, *acquisition of NMR spectra* and *structural interpretation of the NMR data*.

The structural interpretation of NMR data can be further divided into; sequence specific assignments, determination of structural constraints,

structure calculation and structure refinement. In practice these four processes are part of an interactive methodology in which structure calculations are repeated several times and the calculated structures obtained with initial restraints are used to evaluate input restraints, correct misassignments and assign new constraints.

Sample preparation

For the type of probe used in the acquisition of spectra (5mm probe head) a minimum of 550µl of solution is needed to achieve good resolution. The sample should be clear without aggregation or deposits and care should be taken in order to avoid the presence of contaminants, since it reduces sensitivity. Contaminants are due mostly to the metabolic activity of bacteria within the sample, which can usually be avoided by using antibiotics to prevent their growth.

The different sample preparations used in the work presented here are described in detail in the corresponding chapters.

Spectra acquisition and resonance assignment

The proteins used in this work were not enriched with any isotope and the classical assignment strategy described by Wüthrich [9] was followed.

The general procedure starts with the identification of the different amino acid spin systems through the analysis of 2D-COSY and 2D-TOCSY spectra. In these experiments each cross-peak represents a through-bond spin-spin coupling connectivity. Given that each spin system contains an amide proton (H^N), an α-proton (H^α) and the side chain protons all connected by three or less covalent bonds, the identification of simple geometric patterns (Figure 2.2) allows the assignment of cross-peaks to individual amino acid types. With the only exceptions being the aromatic amino acid residues (His, Phe, Trp and Tyr) and the side chains

amide protons of Arg, Asn and Gln for which two spin systems are found, and proline which does not have an amide proton.

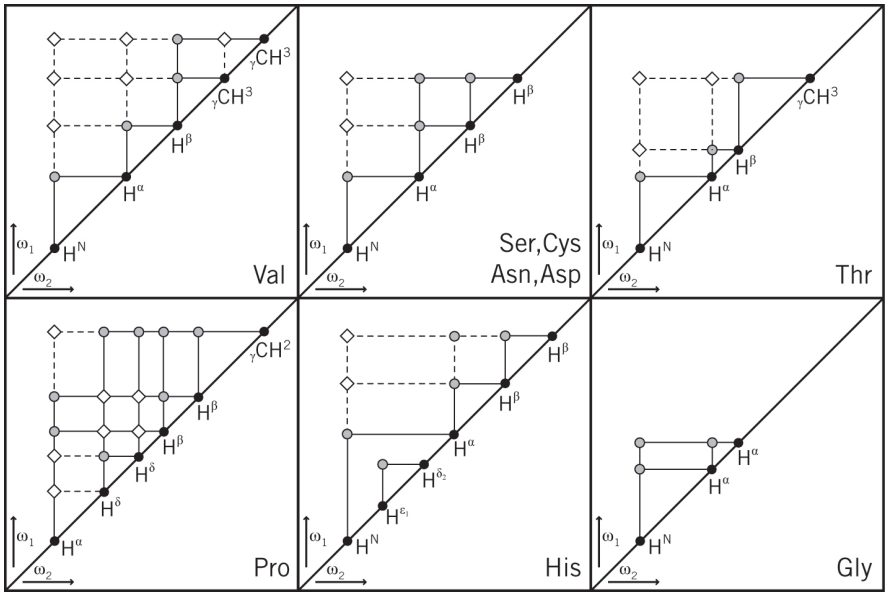

FIGURE 2.2 - Connectivity diagrams for some spin-systems of common amino acid residues. Each square represents a 2D spectrum for an amino acid residue or a group of residues. Diagonal peaks are represented by filled circles, COSY connectivities by open circles and solid lines, TOCSY connectivities by open diamonds and broken lines.

Additionally, hydrogen atoms from neighbouring residues within the polypeptide sequence are separated by at least four covalent bonds and can only be linked by the NOEs that originate from short through-space distances (like d_{NN} and $d_{\alpha N}$ in Figure 2.3).The strongest cross-peaks in a 2D-NOESY experiment will arise from the nearest neighbours along the sequence. By using the sequential inter-residue NOE connectivities in combination with the intraresidual proton connectivities obtained from scalar spin-spin couplings it is possible to achieve a progressive resonance assignment. Eventually the connected sequence of residues will match a unique section of the known primary polypeptide structure which will allow the sequence specific assignment.

In the case of haem proteins the haem proton resonances must also be assigned. Adopting the strategy previously described by Turner et al [10]

the short range intrahaem characteristic connectivity patterns can be followed around the porphyrin ring in a short- mixing time (~50 ms) 2D-NOESY spectra. Thioether methyl groups are unambiguously assigned through the spin-spin connectivities with thioether methine protons in 2D-TOCSY spectra.

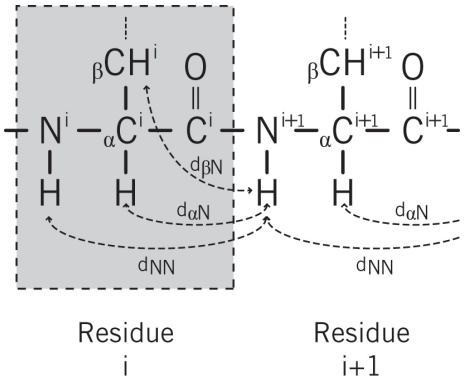

FIGURE 2.3 - Spin systems of neighbouring residues can be linked by the intervening H^{α}-H^{N} or H^{N}-H^{N} sequential NOE connectivities.

Once all the direct nearest neighbour NOE cross peak assignments are made there will be some still unaccounted for that arise from secondary structure contacts such as helical and beta structures and also from long range contacts, i.e. protons close in space but distant along the protein sequence. These supply the crucial distance constraints from which the tertiary fold of the protein will be deduced.

Determination of structural constraints

Obtaining quantitative distance measurements from the observed NOEs is intrinsically difficult because the experimental NOE data depends not only on proton-proton distance *r*, but also on the effective correlation time τ_c [9]:

$$\mathrm{NOE} \propto \frac{1}{\langle r^6 \rangle} \cdot f(\tau_c) \qquad \{2.1\}$$

The correlation function $f(\tau_c)$ exhibits the influence of motional averaging processes on the NOE, which depend not only on the overall rotational molecular motion (that depend on the size and shape of the

protein and on the viscosity of the solvent) but also on intramolecular motions. As a consequence in a protein $f(\tau_c)$ may differ for different pairs of hydrogen atoms. In addition the accuracy of experimental NOE measurements have limitations since a macromolecule has a network of spins and individual NOEs that can be influenced by competitive relaxation processes, such as spin diffusion, chemical exchange or proximity of paramagnetic metal ions.

In the earliest structure determinations, the conversion of NOE intensities into distances classified NOEs in different ranges depending on the intensity (for example backbone, sidechain and methyl) and a distance range was applied to each class.

In this work the measured NOEs were used to provide both upper distance limits (upls) and lower distance limits (lols) with a modified version of the program DYANA [11], called PARADYANA [12] which uses automatic calibration of the conversion from volumes to distance constraints. Separate calibration classes for proton-proton, proton-methyl, methyl-methyl and backbone proton-proton interactions were defined for both upls and lols and optimised iteratively for each structure.

Automatic calibration avoids the need for manual calibration and the possible introduction of bias caused by the use of a single set of scaling factors for all structures.

Structure calculation and refinement

The Cartesian coordinates of a molecular structure can be obtained by searching for the molecular geometries consistent with standard bond lengths of covalently linked atoms and the experimentally determined NOE distance constraints from NMR data.

Distance geometry algorithms can be used to identify the conformations compatible with the inequality:

$$L_{ij} \leq \left| r_i - r_j \right| \leq U_{ij} \qquad \{2.2\}$$

where L_{ij} and U_{ij} are lower and upper bounds respectively on the distance $|r_i - r_j|$ between points r_i and r_j.

Two methods that have been used to search for protein conformations satisfying inequality {2.2} are: (i) metric matrix methods [13, 14], where bounds matrices containing upper and lower bounds consistent with distance limits are used to calculate an initial global structure which is refined at later steps; and (ii) variable target function methods [15, 16] that uses dihedral angles to generate random initial starting conformations, then by changing the dihedral angles to fulfil the experimental distance constraints the initial conformation is adjusted, first by satisfying local constraints and gradually considering longer range constraints. The first method has been implemented in programs such as DISGEO [17] and DSPACE [18], while the second in DISMAN [15] and DIANA [19] for example.

For both these methods each calculation ends with the minimization of an error function that equals zero if all experimental restraints are fulfilled; the residual error function value can be used to evaluate the quality of the fit of the calculated structure to the experimental input data.

Because distance geometry methods take downhill steps the calculations get trapped in local minima, which translates into a low yield of converged structures. One way of addressing this problem is by using molecular dynamics methods such as torsion angle dynamics (TAD) [20-23]. The TAD algorithm implemented in the program DYANA [11] works with internal coordinates rather than Cartesian coordinates, thus the degrees of freedom are solely torsion angles, this way the covalent structure parameters (bond lengths, bond angles and chiralities) are kept fixed at their optimal values during calculations, which decrease the number of degrees of freedom by tenfold [11]. DYANA also raises the temperature of the system followed by slow cooling to overcome local minima; a molecular dynamic method known as simulated annealing (SA) [24].

An extended version of DYANA named PARADYANA [12] was used for all structure calculations presented in this thesis. PARADYANA was modified to allow the automatic calibration of NOE data and the determination of magnetic properties of paramagnetic proteins.

The evaluation of the *uniqueness* of a calculated structure is done by repeating the calculation with different starting conditions and the same input data. The precision of the calculations can be assessed by the tightness of the fit between the ensemble of the resulting conformers. Usually hundreds of conformers are calculated and a small sub-group (~20) with the lowest target function and small root mean square deviation (RMSD) are selected to represent the NMR structure of the protein.

SPIN DIFFUSION

In large molecules the relationship between NOE intensity and distance can be complicated due to the indirect transfer of magnetization via the numerous neighbouring protons [25], the so called spin diffusion effect.

One approach to try to account for this effect involves the calculation of NOE cross-peak intensities and comparison with the experimental spectrum [26] by solving the matrix:

$$a(\tau_m) = \chi \exp(-\lambda\tau_m)\chi^{-1} \qquad \{2.3\}$$

here **a** is the matrix whose elements give the cross-peaks intensities, χ is the matrix containing eigenvectors of the rate matrix R (given by $R=\chi\lambda\chi^{-1}$) which describes the relaxation behaviour of the system, and λ is a diagonal matrix giving the eigenvalues of that system. To obtain this, first the spectral densities are calculated, and then from preliminary structures the matrix R is determined. The eigenvalues and eigenvectors of the matrix R are then used to build the NOE matrix giving the cross-peak intensities.

A different approach is to use the opposite procedure in which the back transformation of the NOE matrix allows one to obtain the relaxation matrix [27].

$$R = \chi\lambda\chi^{-1} = -\chi\left[\ln\frac{\chi^{-1}a(\tau_m)\chi}{\tau_m}\right] = -\chi\left[\ln\frac{D}{\tau_m}\right] \qquad \{2.4\}$$

However, although in theory it is possible to obtain the matrix R from the measured NOE intensities; in practice this is not possible since for large molecules the NOE matrix is always incomplete.

One method to overcome this problem is known as IRMA (iterative relaxation matrix analysis)[28, 29]. In these calculations the relaxation matrix is build from initial structures, the NOE matrix is then constructed using equation {2.3} and combined with experimental NOEs. This new mixed NOE matrix is back-transformed to the relaxation matrix which can be used to calculate new distances and generate new starting structures to repeat the whole process.

A modified version of the program CORMA (complete relaxation matrix analysis)[30] called DYRMA that reads in DYANA coordinate files plus upper and lower volume limits was used in this work. DYRMA works in a similar way as described for IRMA where the calculated NOE intensities in the matrix are replaced by averaged intensities obtained from the observed lower and upper limit volumes.

The observed intensities are scaled using a scaling factor defined as follows:

$$sf = \frac{\sum_n I_{ij}^{calc}}{\sum_n I_{ij}^{obs}} \qquad \{2.5\}$$

here, n is the number of experimental intensities where there is both an upper and lower limit, I_{ij}^{calc} is the calculated intensity and I_{ij}^{obs} is the experimental intensity.

The calculated distances are compared to the lower and upper limit dis-

tances and the rms deviation is calculated. Calculated distances fall between limits, since we are using experimental upper and lower volume limits with associated error bars. With this calculation we then have an indication on how much the volume restraints should be loosened so that the restraints calculated from the isolated spin pair approximation capture the distances determined from the full relaxation matrix calculation. This procedure is used in preference to the adjustment of individual restraints because the spin diffusion pathways are extremely sensitive to details of the structure which are themselves uncertain.

This way we can use information obtained from initial structures as an indication on how much to *soften* the distance constraints to make sure that the spin diffusion effect is taken into account without the need to replace any experimental distances.

PARAMAGNETIC LEAKAGE CORRECTION

In paramagnetic proteins the protons near the haems have higher relaxation rates due to coupling to the unpaired electrons of the haems iron atoms, resulting in reduced NOE intensities and consequently distorted distance limits.

As we have seen the contribution to the nuclear dipolar relaxation rate between the unpaired electron and the nuclear spin is given by equation {1.18}, or using $\gamma_S \hbar = g_e \mu_B$

$$\rho_I^{\text{para}} = \frac{1}{10}\left(\frac{\mu_0}{4\pi}\right)^2 \frac{\gamma_I^2 g_e^2 \mu_B^2}{r^6}\left(\frac{3\tau_S}{1+\omega_I^2\tau_S{}^2} + \frac{\tau_S}{1+(\omega_I-\omega_S)^2\tau_S{}^2} + \frac{6\tau_S}{1+(\omega_I+\omega_S)^2\tau_S{}^2}\right) \{2.6\}$$

where μ_B is the electron Bohr magneton and g_e the electron g factor.

Through the modification of the program DYRMA mentioned in the previous section, the paramagnetic effects could be included. In this modified program called PARMA the electron-nucleus dipolar relaxation (equation {2.6}) is added to the diagonal elements of the relaxation

matrix R and from there the NOE intensities can be calculated.

All the constants of equation {2.6} can be combined into a single parameter *k*, and for a molecule with *n* paramagnetic metal centres the enhancement of the nuclear relaxation of proton *i* is given by:

$$\rho_{iI}^{\text{para}} = \sum_{l}^{n} \rho_{il}^{\text{para}} = \sum_{l}^{n} \frac{k}{r_{il}^{6}} \qquad \{2.7\}$$

r_{il} is the distance between the proton and the metal centre *l*.

The non-diagonal elements were calculated using averaged distances from preliminary structure families. The NOE intensities *without* the inclusion of paramagnetic effects were then calculated, obtaining for each cross-peak a correction factor of the form:

$$c_{ij} = \frac{I_{ij}^{\text{para}}}{I_{ij}^{\text{dia}}} \qquad \{2.8\}$$

where, I_{ij}^{para} is the calculated intensity with the paramagnetic effects inclusion and I_{ij}^{dia} the calculated intensity without the paramagnetic effects. Finally each upper and lower limit volume is divided by its correction factor and hence taking into account a paramagnetic effect correction for both upper and lower limit distances used in the calculation.

REFERENCES

1. Aue, W.P., Bartholdi, E., and Ernst, R.R., *Two-dimensional spectroscopy. Application to nuclear magnetic resonance.* J Chem Phys, 1976. **64**: 2229-46.

2. Bax, A. and Freeman, R., *Investigation of complex networks of spin-spin coupling by two-dimensional NMR.* J Magn Reson, 1981. **44**: 542-61.

3. Nagayama, K., Kumar, A., Wüthrich, K., and Ernst, R.R., *Experimental techniques of two-dimensional correlated spectroscopy.* J Magn Reson, 1980. **40**: 321-34.

4. Griesinger, C., Otting, G., Wuethrich, K., and Ernst, R.R., *Clean TOCSY for proton spin system identification in macromolecules.* J Am Chem Soc, 1988. **110**: 7870-2.

5. Davis, D.G. and Bax, A., *Assignment of complex proton NMR spectra via two-dimensional homonuclear Hartmann-Hahn spectroscopy.* J Am Chem Soc, 1985. **107**: 2820-1.

6. Bearden, D.W., Macura, S., and Brown, L.R., *Suppression of cross relaxation in TOCSY experiments on macromolecules.* J Magn Reson, 1988. **80**: 534-8

7. Hartmann, S.R. and Hahn, E.L., *Nuclear Double Resonance in the Rotating Frame.* Phys Rev, 1962. **128**: 2042-53.

8. Kumar, A., Ernst, R.R., and Wüthrich, K., *A two-dimensional nuclear Overhauser enhancement (2D NOE) experiment for the elucidation of complete proton-proton cross-relaxation networks in biological macromolecules.* Biochem Biophys Res Commun, 1980. **95**: 1-6.

9. Wüthrich, K., *NMR of Proteins and Nucleic Acids*. 1986, John Wiley and Sons: NY. 30-1, 130-61.

10. Turner, D.L., Salgueiro, C.A., LeGall, J., and Xavier, A.V., *Structural studies of* Desulfovibrio vulgaris *ferrocytochrome* c_3 *by two-dimensional NMR.* Eur J Biochem, 1992. **210**: 931-6.

11. Guntert, P., Mumenthaler, C., and Wuthrich, K., *Torsion angle dynamics for NMR structure calculation with the new program DYANA.* J Mol Biol, 1997. **273**: 283-98.

12. Turner, D.L., Brennan, L., Chamberlin, S.G., Louro, R.O., and Xavier, A.V., *Determination of solution structures of paramagnetic proteins by NMR.* Eur Biophys J, 1998. **27**: 367-75.

13. Havel, T.F., Kuntz, I.D., and Crippen, G.M., *The combinatorial distance geometry method for the calculation of molecular conformation. I. A new approach to an old problem.* J Theor Biol, 1983. **104**: 359-81.

14. Braun, W., Bosch, C., Brown, L.R., Go, N., and Wuthrich, K., *Combined use of proton-proton Overhauser enhancements and a distance geometry algorithm for determination of polypeptide conformations. Application to micelle-bound glucagon.* Biochim Biophys Acta, 1981. **667**: 377-96.

15. Braun, W. and Go, N., *Calculation of protein conformations by proton-proton distance constraints. A new efficient algorithm.* J Mol Biol, 1985. **186**: 611-26.

16. Braun, W., *Distance geometry and related methods for protein structure determination from NMR data.* Q Rev Biophys, 1987. **19**: 115-57.

17. Havel, T. and Wüthrich, K., *A distance geometry program for determining the structures of small proteins and other macromolecules from nuclear magnetic resonance measurements of intramolecular* $^1H-^1H$ *proximities in solution.* Bull Math Biol, 1984. **46**: 673-98.

18. Nerdal, W., Hare, D.R., and Reid, B.R., *Solution structure of the EcoRI DNA sequence: refinement of NMR-derived distance geometry structures by NOESY spectrum back-calculations.* Biochemistry, 1989. **28**: 10008-21.

19. Guntert, P., Braun, W., and Wuthrich, K., *Efficient computation of three-dimensional protein structures in solution from nuclear magnetic resonance data using the program DIANA and the supporting programs CALIBA, HABAS and GLOMSA.* J Mol Biol, 1991. **217**: 517-30.

20. Jain, A., Vaidehi, N., and Rodriguez, G., *A fast recursive algorithm for molecular dynamics simulation.* J Comput Phys, 1993. **106**: 258-68.

21. Stein, E.G., Rice, L.M., and Brünger, A.T., *Torsion-Angle Molecular Dynamics as a New Efficient Tool for NMR Structure Calculation.* J Magn Reson, 1997. **124**: 154-64.

22. Mathiowetz, A.M., Jain, A., Karasawa, N., and Goddard, W.A., 3rd, *Protein simulations using techniques suitable for very large systems: the cell multipole method for nonbond interactions and the Newton-Euler inverse mass operator method for internal coordinate dynamics.* Proteins, 1994. **20**: 227-47.

23. Rice, L.M. and Brunger, A.T., *Torsion angle dynamics: reduced variable conformational sampling enhances crystallographic structure refinement.* Proteins, 1994. **19**: 277-90.

24. Nilges, M., Clore, G.M., and Gronenborn, A.M., *Determination of three-dimensional structures of proteins from interproton distance data by hybrid distance geometry-dynamical simulated annealing calculations.* FEBS Lett, 1988. **229**: 317-24.

25. Kalk, A. and Berendsen, H.J.C., *Proton magnetic relaxation and spin diffusion in proteins.* J Magn Reson, 1976. **24**: 343-66.

26. Keepers, J.W. and James, T.L., *A theoretical study of distance determinations from NMR. Two-dimensional nuclear overhauser effect spectra.* J Magn Reson, 1984. **57**: 404-26.

27. Olejniczak, E.T., Gampe, R.T.J., and Fesik, S.W., *Accounting for Spin Diffusion in the Analysis of 2D NOE Data.* J Magn Reson, 1986. **67**: 28-41.

28. Boelens, R., Koning, T.M.G., and Kaptein, R., *Determination of biomolecular structures from proton-proton NOE's using a relaxation matrix approach.* J Mol Struct, 1988. **173**: 299-311

29. Boelens, R., Koning, T.M.G., van der Marel, G.A., van Boom, J.H., and Kaptein, R., *Iterative procedure for structure determination from proton-proton NOEs using a full relaxation matrix approach. Application to a DNA octamer.* J Magn Reson, 1989. **82**: 290-308.

30. Borgias, B.A. and James, T.L., *Two-dimensional nu-*

clear Overhauser effect: Complete relaxation matrix analysis.
Methods in Enzymol, 1989. **176**: 169-83

3

REDOX LINKED CONFORMATIONAL CHANGES IN CYTOCHROME C_3 FROM *DESULFOVIBRIO DESULFURICANS* ATCC 27774

Results published in:
Paixao, V. B., Vis H., and Turner, D. L. (2010) *Redox linked conformational changes in cytochrome* c_3 *from* Desulfovibrio desulfuricans *ATCC 27774*, Biochemistry 49, 9620-9.

CONTENTS

ABSTRACT

Cytochrome c_3 from *Desulfovibrio desulfuricans* ATCC 27774 appears to be capable of receiving two protons and two electrons from hydrogenase for transport to the membrane, and converting electronic energy into proton motive force. Detailed studies of the mechanism require control both of the redox state and of the protonation state of the protein; hence structure determination of the protein in solution by NMR is the preferred method. This work compares the structures of the protonated protein in the fully oxidised and fully reduced states as a first step towards elucidating the pH-dependent and redox-state-dependent conformational changes that drive the energy transduction.

These high-resolution structures revealed significant localized differences upon change of redox state, even though the global folds of the two families of structures are similar.

There are concerted redox-linked motions within the protein that bring Glu^{61} and Lys^{75} closer to haem II in the oxidised form. This is consistent with an electrostatically driven movement that may provide an important contribution to the previous measured positive cooperativity between haems I and II. No significant conformational changes were observed that might be related to redox-Bohr effects; the families of structures represent the protonated forms and so pH dependence should not play a role in the observed structural rearrangements.

INTRODUCTION

Cytochromes c_3 isolated from *Desulfovibrio* spp. are periplasmic proteins which play a central role in energy transduction by coupling the transfer of electrons and protons from hydrogenase.By receiving both electrons and protons that result from the conversion of H_2, the redox-Bohr effect in cytochromes c_3 allows part of the free energy of the conversion to be used to release protons in the more acidic environment of the periplasm [1, 2].

Due to their small size (ca. 13-14 kDa) and proximity of the haems, cytochromes c_3 display homo- and hetero-cooperative effects arising from redox interactions between neighbouring haems (redox-redox interactions) and redox-Bohr interactions between haems and protonatable centres [3-7] which allow them to work as small energy transduction devices [8, 9]. These interactions are responsible for the fine modulation of the redox potentials of the haem groups so that each cytochrome can be functionally optimized.

Despite their structural homology, the thermodynamic characterization of these proteins revealed that their redox and redox-Bohr interactions show significant variations [2, 5, 9-13]. Indeed, reduction potentials ranging from -352 to -62 mV, redox interactions from 59 to -52 mV, and redox-Bohr interactions from -88 to -4 mV were determined for several cytochromes c_3 [11, 14].

The oxidized and reduced solution structures for cytochromes c_3 from *D. vulgaris* and *D. gigas* have been determined and used to probe the structural basis for the network of functional cooperativities in these cytochromes [15-18].

Of all the cytochromes c_3 characterized so far, the one isolated from *Desulfovibrio desulfuricans* ATCC 27774 (*Dd27c*$_3$ hereafter) is distinctive since the pH dependence of its redox potentials involves two separate pK_a values [11, 12] in contrast with the other cytochromes c_3 studied so far which have just one. Crystal structures of *Dd27c*$_3$ have been determined by X-ray diffraction [19, 20] and the microscopic thermodynamic properties are well established [11]. The first haem to oxidise is haem I followed by haems II, IV and III. No positive redox cooperativity is found between haems, in contrast with *D.gigas* and *D.vulgaris*, but positive cooperativity is observed between the acid-base centres and the haems, as expected from electrostatics. However, 21 thermodynamic parameters are needed to characterise the four redox centres and two protonatable groups in *D.desulfuricans* together with their pairwise interac-

tions. Some of these could not be defined with the available data and were set to zero, namely the proton-proton interaction, the interaction of the first acid-base centre with haem I, and the interactions between the second acid-base centre and haems II, III and IV [11].

Deviations from simple electrostatic interactions occur as a result of conformational changes that alter the distance between charges or modify the local dielectric constant. The oxidised protein should be deprotonated at pH 7.6 used for the crystal structures and the reduced protein would be in a mixed protonation state. However, it is necessary to map the conformational changes that accompany reduction and protonation separately in order to understand the functional significance of the interactions. To that end, the solution structures of fully oxidised and reduced forms of *Dd27c*$_3$ were determined in this work. In each case, the pH of the sample was set below that of the groups involved in the redox-Bohr interactions (pH 4.2 and pH 6.4 respectively) to ensure that any conformational change depended only on the redox state.

MATERIALS AND METHODS

Sample preparation

Cytochrome c_3 was purified from *D. desulfuricans* ATCC 27774 as described in the literature [14, 21].

For NMR experiments in H_2O the protein was lyophilised from H_2O and suspended in 92% H_2O / 8% ^2H_2O to a final concentration of approximately 2 mM. The pH was adjusted to 6.4 in an anaerobic chamber (Mbraun MB 150 I) by addition of 0.1 M NaO^2H or ^2HCl for ^2H_2O samples and 0.1 M NaOH or HCl for H_2O samples. The pH values measured are direct meter readings without correction for isotope effects [22]. Complete reduction of the samples was achieved by the reaction with hydrogen gas in the presence of catalytic amounts of hydrogenase isolated from *Desulfovibrio gigas* and *Desulfovibrio vulgaris*.

To prevent bacterial growth an antibiotic cocktail (70 μm ampicillin, 50 μm kanamycin and 50 μm chloramphenicol) was added to the sample in H_2O.

For the preparation of the oxidised sample the protein was dissolved in 90% H_2O/10% ^2H_2O and in 100% ^2H_2O to a final concentration of 1.8-2 mM. The pH was adjusted to 4.2 for the structure determination (uncorrected pH reading).

NMR spectroscopy

Reduced state spectra

^{1}H-NMR spectra were obtained on a Bruker DRX-500 spectrometer equipped with a 5 mm inverse detection probe head with internal B_0 gradient coil and on a Bruker AV-800 equipped with a z-gradient cryo-probe.

2D NMR spectra were acquired at 298 K. Acquisition was made in the phase sensitive mode by the States-TPPI method [23] collecting 4096 (t_2)×1024 (t_1) data points to cover a sweep width of 10 kHz, with 64 scans per increment in 500 MHz spectra and, 2048 (t_2) ×1024 (t_1) data points for a sweep width of 12 kHz with 64 scans per increment in the 800 MHz spectra.

NOESY spectra were acquired with mixing times of 80 and 100 ms [24-26] with the SCUBA sequence [24] for the 500 MHz spectra and with the WATERGATE sequence [27] for water suppression in the 800 MHz spectra. Total correlation spectra were acquired using the clean TOCSY pulse sequence [28-30] with spin lock periods of 40 and 60 ms. COSY [23, 31] and DQF-COSY [32, 33] spectra were also recorded. Raw data were multiplied by a pure sine-squared function in both dimensions. 2D spectra were typically processed to a final size of 2k × 2k points. Polynomial baseline corrections were applied in both dimensions of each spectrum.

Data were processed using XWINNMR and TopSpin software (Bruker, Rheinstetten). Proton chemical shifts are referenced to the resonances of the methyl groups in DSS at 0.0 p.p.m. using water as the internal reference.

Oxidised state spectra

A series of two dimensional spectra were recorded on a Bruker DRX 500 Spectrometer at 283, 298, 305, 310, and 315 K.

NOESY spectra [25, 26] were acquired at 298 K with 20 ms and 120 ms mixing times using standard pulse sequences with WATERGATE [27] and SCUBA [24] techniques. The short mixing time spectra were used for the analysis of haem and haem ligand resonances as well as for some protons very close to the haems. TOCSY spectra were acquired with mixing times of 40 ms and 70 ms using the clean TOCSY sequence [28-30]. COSY spectra were also recorded [31]. The spectra were processed in a similar way to that used for the reduced state spectra.

Assignment and integration

Reduced state

The software package XEASY (version 1.2; ETH, Zurich) [34] was used to display and annotate spectra. The assigned NOESY cross peaks were integrated and converted into volume restraints with the program SPARKY [35]. NOE volumes were measured in the 80 ms NOESY spectra at pH 6.4, cross-peaks involving protons separated by fixed distances and all intra-haem cross-peaks except those involving the propionate groups were excluded. Integration was performed by Gaussian and Lorentzian function fitting for isolated peaks and with sum data heights in a box or ellipse surrounding the peak for more overlapped peaks. The baseline around each individual peak was determined and used to correct the measured volume.

Oxidised state

The same software was used for spectral analysis of the oxidised spectra. Integration was performed with XEASY version 1.2; ETH, Zurich [34] either by manual integration for isolated peaks or with line-shape integration for overlapped peaks with baseline correction. Cross-peaks involving protons separated by fixed distances and all intra-haem cross-peaks, except these involving the propionate groups and the thioether groups, were excluded from integration. Measured volumes were used to obtain an overall scaling factor relating the 120 ms mixing time NOESY spectra of samples in H_2O and D_2O [17].

At later stages of the assignment procedure, pseudocontact shifts were obtained by subtraction of the chemical shifts in the reduced state from those of the same protons in the oxidised state and were used to calculate the magnetic susceptibility tensors. The predicted dipolar shifts were used as a guide for further assignment, in the elimination of misassignments and helped to extend the assignment of the reduced form [36].

Determination of restraints

Reduced state

The minimum uncertainty in any measured volume (δV) was estimated from the intensity of the smallest recognisable peaks in the H_2O spectrum and used as input for the program INDYANA [37]. The program computes upper limit volumes (upv) as $\langle V \rangle + \max(\Delta V, \delta V)$, and lower limit volumes (lov) as $\langle V \rangle - \delta V$, where $\langle V \rangle$ and ΔV are the average and difference of volumes for each pair of symmetrical cross-peaks, respectively. If one peak in a pair could not be measured, its volume is treated as zero. The inclusion of upvs, and hence lower limit distance constraints, makes automatic calibration of the NOEs possible and ensures that structures do not have protons in close proximity in the absence of experimental evidence. The conservative approach of applying

a cut-off volume effectively limits these constraints to about 4 Å, which minimises the risk of distorting structures through anomalously weak NOEs [15-18].

For degenerate or completely overlapped peaks upper volume limits (lower distance constraints) were applied to both protons. At later stages of structure calculation, some of the potentially overlapping peaks could be specifically assigned as the various possibilities were eliminated by reference to the structure, therefore providing a lower volume limit also. For the degenerate H^{δ} and H^{ε} ring protons of fast-flipping residues, it is often possible to identify which side of the ring is involved because the pair of degenerate protons has a separation of 4.3 Å, which is large with respect to the distances that give rise to strong NOEs. In the preliminary stages of structure calculation, all cross-peaks from degenerate ring protons are treated as non-specific, with the exception of one chosen to distinguish the two sides of the ring. During structure refinement, individual NOEs were assigned specifically as in the case of non-degenerate protons, with the aid of the program GLOMSA [38].

Oxidised state

Due to paramagnetic relaxation some cross-peaks that were visible in the 20 ms NOESY spectrum disappear at 120 ms, as a consequence, all cross-peaks involving haem groups and haem ligands were measured from the 20 ms H_2O spectrum.

In some cases, integrals were taken from the spectrum in which the cross-peak was more intense, and a separate calibration was used for the two mixing times, with a single additional parameter determining the ratio of scaling factors for each class of peaks. Instead of integrating every peak in both spectra, the cross-peak volumes at both mixing times were calculated with respect to preliminary structures to indicate which spectrum was appropriate for each cross-peak. Peaks with intensities predicted to increase by less than a factor of two between 20 ms and

120 ms were measured at both mixing times, and the largest volume was used in each case.

The two sets of integrals (20 ms and 120 ms) were processed separately to convert them into upper and lower volumes using the algorithm described previously and used in the program INDYANA [37]. Before being used in the final structure calculations, these four sets of values (20 ms and 120 ms, upper and lower volumes) were corrected for reduction of the NOE intensities by electron-nuclear dipolar relaxation caused by the paramagnetic haem groups [15].

Additional restraints

Three non-standard residues were used for both structure calculations: fast-flipping aromatic residues with pseudo-atoms to define the orientations of the planes [17, 39, 40], flexible haem groups and proline residues with fixed upper limit distances for ring closure [17, 37, 41]. In addition, for the oxidised state, two types of histidine axial ligands were defined to take into account the iron–nitrogen bond [17, 41], the magnetic axes [41] and the torsion angle that defines the orientation of the histidine ring plane with respect to the haem plane [37].

The torsion angles were not constrained but provide a convenient measure of ligand geometry. In the final stages of structure refinement, the calculated structures were checked for short (less than 2.5 Å) distances between assigned protons that should give rise to significant NOEs. Even if no peaks were visible at the predicted frequencies, the volume was measured and used in further calculations. In this way, a lower limit distance restraint defines a minimum distance between protons if there is no NOE in the spectra.

Correction of volume restraints for the oxidised state

In paramagnetic proteins the NOE intensities of protons near the haem groups are reduced due to relaxation caused by the dipolar coupling to the unpaired electrons on the iron atoms of the haems. Correction for this paramagnetic leakage has been shown to increase the resolution of calculated structures in regions close to the paramagnetic centre [42, 43].

The contribution to longitudinal relaxation from the dipolar interaction between a nuclear spin and each unpaired electron is described by the following equation [44]:

$$\rho_I^{\text{para}} = \frac{1}{10}\left(\frac{\mu_0}{4\pi}\right)^2 \frac{\gamma_I^2 g_e^2 \mu_B^2}{r^6}\left(\frac{3\tau_S}{1+\omega_I^2\tau_S{}^2} + \frac{\tau_S}{1+(\omega_I-\omega_S)^2\tau_S{}^2} + \frac{6\tau_S}{1+(\omega_I+\omega_S)^2\tau_S{}^2}\right)$$

where γ_I is the nuclear gyromagnetic ratio, r is the distance between the proton and the metal centre, τ_S is the correlation time for electron spin relaxation, μ_B the Bohr magneton and ω_I and ω_S are the Larmor frequencies of the proton and the electron. Assuming that the unpaired electrons are localised on the iron atoms, the constants can be combined in a parameter k such that $\rho_i = kr^6$. For simplicity τ_S is assumed to be equal for the four haem groups. The value of k was estimated from the ratio of cross-peak intensities in the 20 ms and 120 ms spectra. By adding this electron-nucleus dipolar contribution to the diagonal elements of the internuclear dipole-dipole relaxation matrix calculation, the NOE intensity can be obtained [45, 46].

Cross peak intensities were then calculated with and without paramagnetic effects using $k=6\times10^5$ Å^{6}s^{-1} for the paramagnetic relaxation and τ_R=8 ns for the diamagnetic terms, with averaged distances from a family of preliminary structures. A correction factor was obtained for each cross-peak from the ratio of the two calculated values, $I_{ij}^{\text{para}}/I_{ij}^{\text{dia}}$, and each upper and lower volume limit was divided by its correction factor [42, 43]. Using constraints obtained with different mixing times reduces

the need for correction: the largest calculated volume ratios were less than 10.

Since this approach is approximate, all distance restraints were softened by a percentage to allow a margin for error and for the effects of spin diffusion. For this purpose, the cross-peak intensities calculated with the inclusion of paramagnetic relaxation were replaced by scaled measured values and back-transformed to give theoretical distances. Those distances that were outside the range obtained from the maximum and minimum experimental volumes were used to calculate a ratio that was used to relax all distance restraints.

Dipolar shifts as restraints for the oxidised state

Dipolar (pseudocontact) shifts are useful for structure determination and refinement for paramagnetic proteins [36] due to the dependence on the position of the nucleus relative to the paramagnetic centres and their magnetic axes. Simultaneous calculation of the structure and the magnetic susceptibility tensors to fit dipolar shifts is implemented in the program PARADYANA [41].

Approximate dipolar shifts were obtained by subtracting the shifts of the reduced protein from those observed in the oxidised protein.

To ensure that the use of dipolar shifts would not undermine the detection of any change in structural or protonation state between the oxidised and the reduced forms, some shifts were not considered in the calculation; namely shifts of non specifically-assigned diastereotopic pairs of protons (except when the values for both protons of the pair differ by less than 0.2 p.p.m.), as well as shifts for H^N. Diamagnetic shifts were calculated for the family of structures in the reduced form and for a family of oxidised structures obtained without dipolar shifts and protons for which the difference in shifts from the two forms was greater than 0.2 ppm were excluded from the list of dipolar shifts.

As a further test, the remaining dipolar shifts were used to fit the magnetic susceptibility tensor parameters to the coordinates of a preliminary set of twenty structures obtained without the use of dipolar shifts [47], with the uncertainty for the dipolar shifts set to ±0.2 p.p.m. and the uncertainty for the atomic coordinates set to ±0.25 Å. Those dipolar shifts which were not accommodated by these uncertainties in more than ten out of the twenty structures were rejected. Finally, if a side-chain proton was excluded then so were the shifts of all protons further from the backbone.

Structure calculations

The final reduced and oxidised structures were calculated with the program PARADYANA [41], as in the case of *Desulfovibrio gigas* [15], *Desulfovibrio vulgaris* [16, 17] and *Shewanella fridigimarina* [48]. The program uses corrected NOE volumes, angle restraints and dipolar shifts, as described above, and optimises magnetic susceptibility tensors together with the parameters of the structure in the presence of paramagnetic centres.

A complete relaxation matrix analysis was used to estimate the error that might be induced by spin diffusion. Theoretical NOEs were replaced by scaled measured NOEs and the combined NOE matrix was back-transformed to obtain inter-proton distances that take account of spin diffusion. The RMSD of the ratio between those calculated distances that deviated from the maximum or minimum distances obtained by automatic calibration in PARADYANA was used to loosen all of the distance restraints in subsequent structure calculations.

Structure analysis

CHIMERA (version 1.24) [49] was used for visual interpretation with the preliminary structure calculations, as an aid to assignment, during structure refinement. The program MOLMOL (version 2.0) [50] was

used for superimposition, visual inspection, calculation of mean structure and of root-mean-square deviations from the mean structure. Stereochemical analysis of the structures was performed with the program WHAT IF (version 20030529-0952)[51]. Identification and classification of the consensus secondary structure elements in the NMR structure ensemble, defined as those present in at least 50% of the structures was accomplished with the program PROMOTIF (version 2.0)[52]. Secondary structural shifts, which are dominated by the effect of haem ring currents, were calculated for the structures using the program TOTAL [53]

Diamagnetic chemical shift calculations

Proton chemical shifts were calculated for the ensemble of the best NMR structures for both the oxidised and reduced states using the program TOTAL [53].

RESULTS

Structure determination for the reduced state

Assignment and integration

Amino acid assignment was performed using the approach described by Wüthrich [54], assisted by predicted chemical shifts for the reduced protein, based on the preliminary structures of the oxidised form as well the X-ray structure of the reduced structure of *Dd27c*$_3$ [19]. Spin systems were identified through analysis of the TOCSY and COSY spectra of ^2H_2O and H_2O solutions, and sequence-specific assignment was performed by analysing NOESY spectra of the protein in H_2O and identifying sequential connectivities.

Sequential connectivities between H^N, H^α and H^β protons are shown in Figure 3.1. All of the residues, with exception of prolines (residues 2, 5,

8, 21, 24, 91, and 107) show at least one of the sequential connectivities between its H^N and the H^N, H^α or H^β of the preceding residue. For the proline residues, connectivities were obtained at least between the H^δ protons of the prolines and the H^α or H^β of the preceding residue. Two of the exchangeable hydroxyl group protons of Thr and Ser residues were also found (Thr[98] and Ser[63]).

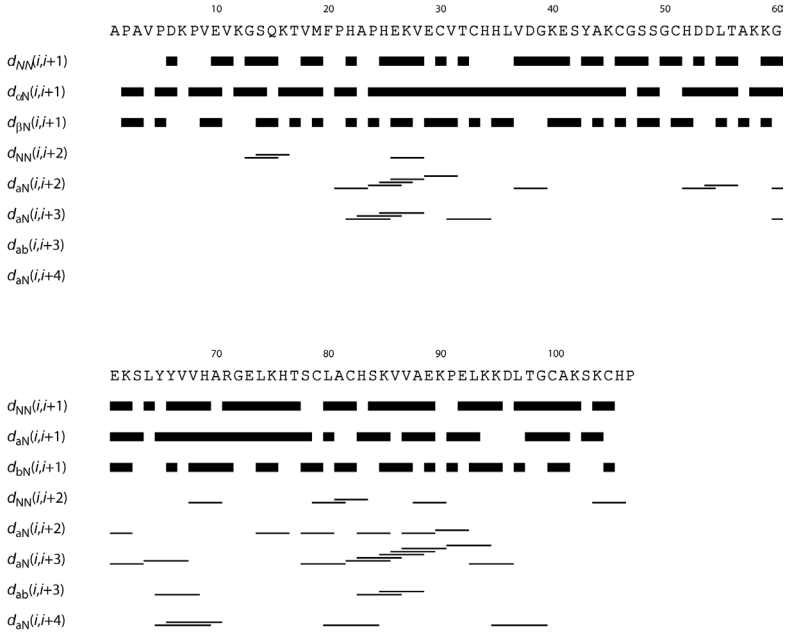

FIGURE 3.1 - Sequential NOE connectivities involving H^N, H^α and H^β observed in the NOESY spectrum for the reduced cytochrome c_3 from *D. desulfuricans* ATCC 27774. The line thickness is indicative of the NOE intensity.

In total, 77% of all the protons in this protein after excluding exchangeable protons other than backbone H^N were assigned. The chemical shifts have been deposited in the BioMagResBank database (http://www.bmrb.wisc.edu) under accession number BMRB – 16674.

Calculation and analysis of structures

Assigned cross-peaks in the H_2O NOESY spectra were integrated and converted into volume restraints, resulting in 1107 lower limits (lovs) and 1339 upper limits (upvs). These were used as input for the program

PARADYANA [41] together with a set of 133 fixed upper limit distances associated with ring closure in the flexible proline residues and haem groups, and the attachment of Histidine ligands [17, 37, 41].

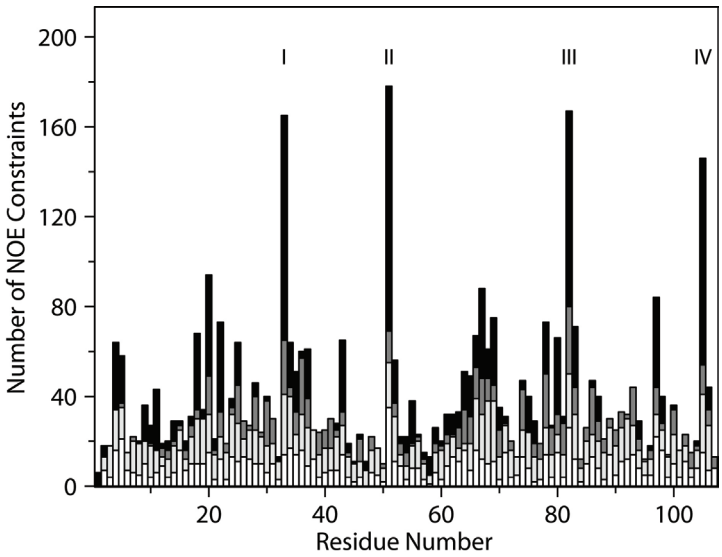

FIGURE 3.2 - Number of constraints per residue used for the calculation of the reduced structure of cytochrome c_3 from *D. desulfuricans*. Bars are white, light grey, dark grey and black for intra residue, sequential, medium and long range restraints, respectively. Residues 33, 51, 82 and 105 also include restraints to haems I, II, III and IV, respectively.

The preliminary calculated structures were analysed using the program GLOMSA [55] modified to take NOE volumes as input and 26 stereospecific assignments were made for diastereotopic pairs of protons or methyl groups. The conversion of experimental data to distance constraints has an intrinsic uncertainty due to the spin diffusion effect, which was simulated by complete relaxation matrix calculations based on the initial protein structures, with τ_R=8 ns. Calculated spin diffusion effects have errors that arise from the uncertainties in the atomic coordinates. Hence we adopt a statistical approach in which all constraints are loosened far enough to eliminate the majority of distortions.

Accordingly, a parameter was set in the program PARADYANA to loosen all distance restraints by 4%. An average of 23 NOE restraints per amino acid residue (10 lovs and 13 upvs) and 122 per haem residue (55 lovs and 67 upvs) were used for the final calculation (Figure 3.2).

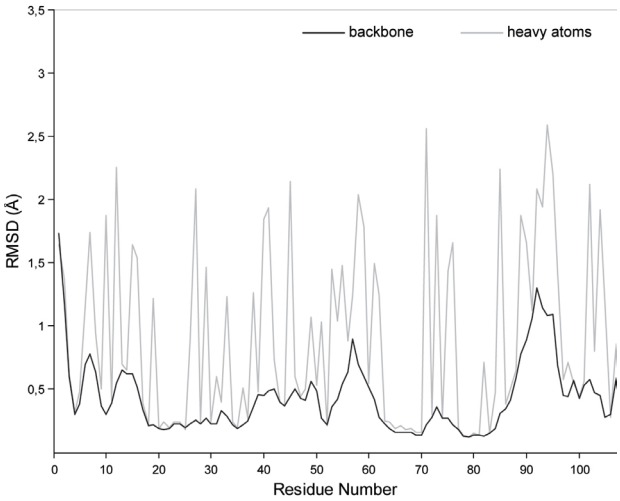

FIGURE 3.3 - Average backbone and heavy atom RMSD values per residue with respect to the mean structure of the families of *Dd27c*$_3$ conformers for the reduced state.

A total of 500 random conformers were used as starting points for annealing by the PARADYANA program. The 20 structures with lowest target function values (from 2.40 Å^2 to 2.80 Å^2, average value 2.66 Å^2, range 17% from the lowest value) were selected as being representative of the solution structure of the protein. The structures superimpose with an average backbone RMSD of 0.58 Å and a heavy atom RMSD of 1.28 Å with respect to the mean structure (Figure 3.3); the statistics for the family of structures are shown in Table 3.2.

The Ramachandran plot [56] shows 59.5% of the residues in the most favoured regions, 36.9% in the additionally allowed, 2.4% in the generously allowed and 1.1% in the disallowed regions. Residues in the disallowed regions include Lys^{58} and Lys^{95} which show a low number of restraints per residue. A total of 108 hydrogen bonds were identified in the family of 20 structures with the program WHAT IF (using routine HBO), 25 of which were present in at least 50% of the structures. Chemical shifts were calculated for each proton in the NMR structures and compared with experimental values as described in Materials and Methods (Figure 3.9a).

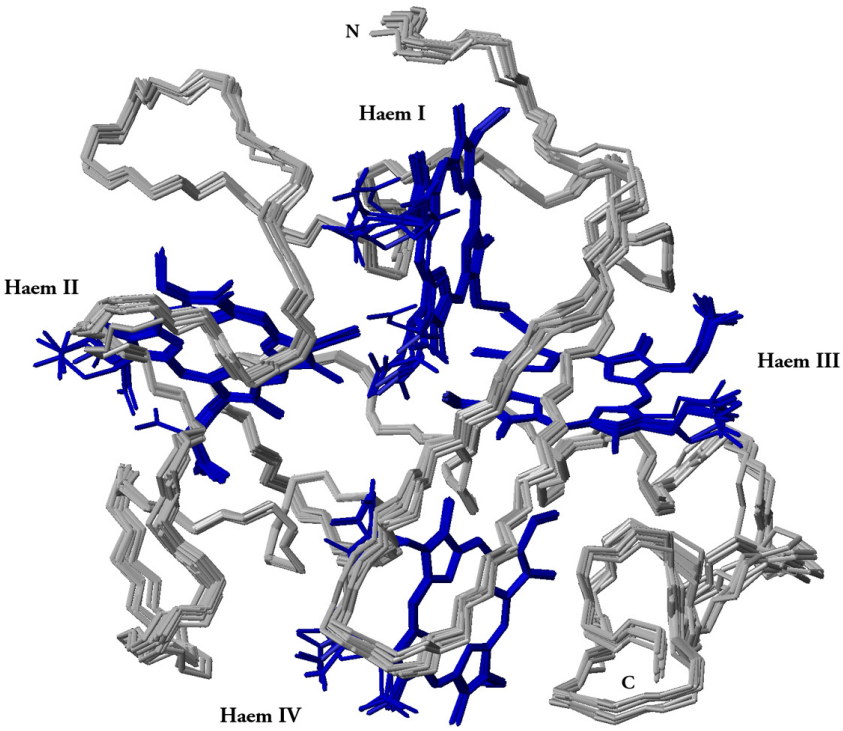

FIGURE 3.4 - Backbone and haems of the 20 lowest energy NMR structures of *D. desulfuricans* cytochrome c_3 for the reduced state. The peptide chain and the haems are colour-coded grey and blue respectively. In this orientation the C-terminus is at the bottom-right and haems are disposed from the left to the right in the following order: II, I, III, and IV. The figure was produced using MOLMOL [50].

Structure determination for the oxidised state

Assignment and integration

Assignments were obtained for the 107 residues and the four haem groups, using a combination of NOESY, TOCSY and COSY experiments at different mixing times and temperatures. The axial histidine residues experience large paramagnetic shifts: the His ring protons were not observed and the H^N, H^α and H^β protons show large downfield shifts. Two of the exchangeable hydroxyl protons of Ser residues were found (Ser^{63} and Ser^{103}). In total, 89% of the proton resonances after excluding exchangeable protons other than the backbone H^N atoms were assigned.

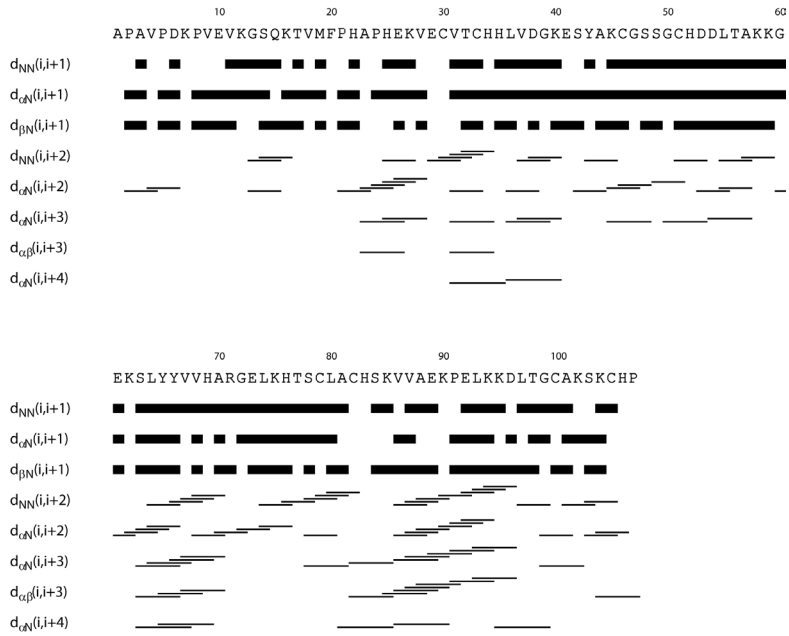

FIGURE 3.5 - Sequential NOE connectivities involving H^N, H^α and H^β observed in the NOESY spectrum for the oxidised cytochrome c_3 from *D. desulfuricans* ATCC 27774. The line thickness is indicative of the NOE intensity.

Figure 3.5 shows the sequential connectivities between H^N, H^α and H^β protons observed in the NOESY spectrum of the oxidised protein.

Restraints

A total of 1453 lower volume limits and 1774 upper volume limits were obtained from the NOESY spectra with a 120 ms mixing time. The spectra with a 20 ms mixing time yielded a further 191 lovs and 282 upvs. More restraints were obtained for the oxidized form than the reduced, mainly because of the reduced spectral overlap in the presence of paramagnetic shifts. The detection of two hydroxyl protons in slow exchange with water in each of the forms suggests that the rigidity of the structure is unchanged.

Stereospecific assignments were obtained using the program GLOMSA. Out of the 200 stereopairs with non-degenerate chemical shifts, 73 were stereospecifically assigned and 55% of the restraints to fast-flipping aromatic residues were pseudo-stereospecifically assigned to one or the other side of the ring. A summary of the restraints used is presented in Table 3.1 and the number of restraints per residue is shown in Figure 3.6.

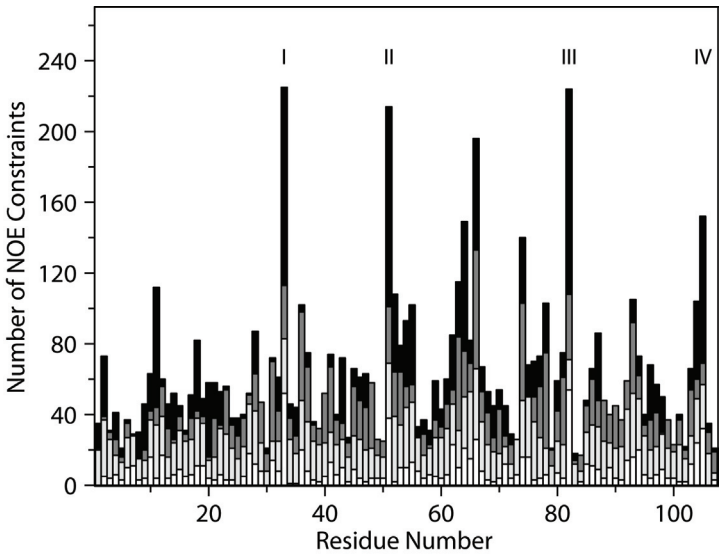

FIGURE 3.6 - Number of constraints per residue used for the calculation of the oxidised structure of cytochrome c_3 from *D. desulfuricans*. White, light grey, dark grey and black bars are for intra residue, sequential, medium and long range restraints, respectively. Residues 33, 51, 82 and 105 also include restraints to haems I, II, III and IV, respectively.

Initial structures calculated with uncorrected NOE volumes were used as input for relaxation matrix calculations. Correction factors for paramagnetic leakage [42, 43] were obtained as described in Materials and Methods.

Structures calculated with these corrected restraints were used as input for relaxation matrix calculations, calculations to assess the influence of spin diffusion. The back-calculated distances exceeded the range of experimental restraints with an RMSD of 4% for the 20 ms data and 8% for the 120 ms data, and these values were used to soften all distance restraints in the final structure calculations.

TABLE 3.1 - Restraints used for calculation of reduced and oxidised cytochrome c_3 from *D. desulfuricans* ATCC 27774.

Distance restraints (Reduced)	Upper distance limits	Lower distance limits
Intra-residual	333	416
Sequential (|1 - j| = 1)	275	350
Medium range (2≤ | i - j | <5)	190	240
Long range (|1 - j| ≥ 5)	313	410
Total	1111	1416

Distance restraints (Oxidised)	Upper distance limits	Lower distance limits
Intra-residual	294	352
Sequential (|1 - j| = 1)	502	624
Medium range (2≤ | i - j | <5)	504	550
Long range (|1 - j| ≥ 5)	557	594
Total	1857	2120

Dipolar shifts contain important long-range structural information, since they depend on the inverse cube of the distance from the metal centres as well as the orientation and anisotropy of the magnetic susceptibility tensors [44]. Therefore they can be used together with the other experimental restraints such as paramagnetic relaxation [57] and nuclear Overhauser enhancements [58], or even used by themselves as restraints for structure refinement [59]. Conversely, anomalous dipolar shifts may indicate misassignments; predictions of shifts from calculations and experimental temperature dependences were used as a guide for further assignment once preliminary structures were available [36]. Experimental dipolar shifts were determined by subtracting the observed reduced protein shifts from the observed oxidised shifts.

However, to allow for possible changes in the diamagnetic contribution to the shifts of the oxidised and reduced forms due to structural differences, the shifts of some protons were excluded as described in Materials and Methods.

TABLE 3.2 - Summary of scaling factors, restraint violations and quality analysis for the final families of structures for reduced and oxidised cytochrome c_3 from *D. desulfuricans*.

Parameter	Reduced	Oxidised
Scaling factors		
Proton-proton	29.89 ± 0.15	7.36 ± 0.03
Proton-methyl	36.42 ± 0.15	8.78 ± 0.06
Methyl-methyl	46.82 ± 0.28	11.79 ± 0.35
Backbone proton-proton	28.64 ± 0.05	7.23 ± 0.03
Dyana Target function		
Average total (Å)	2.66 ± 0.12	3.43 ± 0.31
Upper distance limit violations		
Average maximum	0.28 ± 0.06	0.24 ± 0.06
Number of consistent violations (>0.2 Å)	0	0
Lower distance limit violations		
Average maximum	0.27 ± 0.04	0.29 ± 0.05
Number of consistent violations (>0.2 Å)	0	1
Van de Waals violations		
Average maximum	0.28 ± 0.01	0.26 ± 0.03
Number of consistent violations (>0.2 Å)	0	1
Dipolar shifts violations		
Average maximum	-	0.48± 0.07
Number of consistent violations (>0.2 Å)	-	1
Ramachandran Plot (%)		
Most favoured	59.5	71.4
Additionally allowed	36.9	26.2
Generously allowed	2.4	2.4
Disallowed	1.1	-
Precision		
RMSD backbone (Å)	0.58 ± 0.10	0.48 ± 0.07
RMSD heavy atoms (Å)	1.28 ± 0.10	1.18 ± 0.08

The NOE volume limits, together with dipolar shifts and the fixed upper limit distances were used as input for the program PARADYANA. With this program, the anisotropies of the magnetic susceptibility ten-

sors as well as the orientation of their principal axes are optimised simultaneously with the annealing of each structure, such that the final family of structures reflects the uncertainty in all of the tensor parameters as well as the atomic coordinates.

Calculation and analysis of structures

Six hundred random conformers were used as starting points for annealing and the structures with lowest target function values were selected as representative of the solution structure of the protein. The final family consists of 20 structures with 34% target function variation (ranging from 2.83 Å^2 to 3.82 Å^2, average value 3.48 Å^2) from the first to the last. The structures superimpose with an average backbone RMSD of 0.48 Å and a heavy atom RMSD of 1.18 Å with respect to the mean structure (Figure 3.7); the statistics for the family of structures are shown in Table 3.2. For the oxidised structure a total of 109 hydrogen bonds were identified in the family of 20 structures using the program WHAT IF (routine HBO), 30 of which were present in at least 50% of the structures.

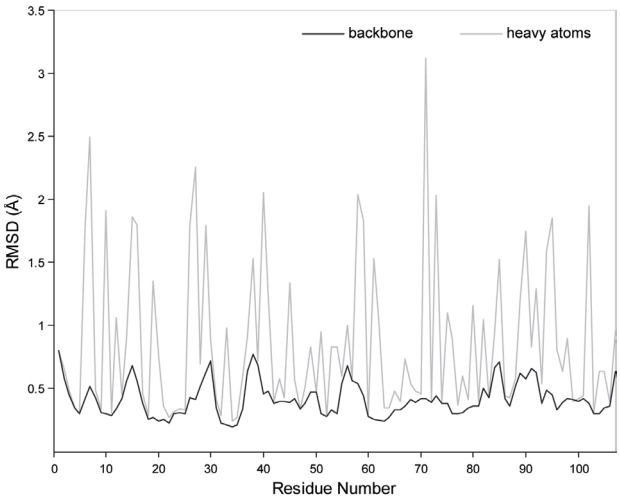

FIGURE 3.7 - Average backbone and heavy atom RMSD values per residue with respect to the mean structure of the families of *Dd27c*$_3$ conformers for the oxidised state.

The Ramachandran plot for all the relevant residues gave 71.4% residues in the most favoured regions, 26.2% in the additionally allowed and 2.4% in the generously allowed.

TABLE 3.3 - Properties of the magnetic susceptibility tensors of the four haems in *D. desulfuricans* cytochrome c_3. The in-plane rotation is given for the y-axis to allow direct comparison with the orientations of the imidazole planes as defined by [61]; note the opposite sign of the angle.

Haems	I	II	III	IV
$\Delta\chi_{ax}$ x 10^{32} (m^3)	3.8 (0.2)	3.5 (0.1)	2.0 (0.1)	3.0 (0.4)
$\Delta\chi_{eq}$ x 10^{32} (m^3)	-1.8 (0.1)	-0.8 (0.2)	-1.8 (0.2)	-2.4 (0.2)
In-plane rotation of χ_y (deg)	-52.5 (2.8)	-74.4 (8.8)	-158.5 (2.4)	-52.0 (4.1)
Tilt angle of χ_z (deg)	3.9 (2.0)	5.0 (2.0)	7.0 (3.8)	5.2 (3.1)
Average imidazole orientation φ	49.1 (2.9)	85.6 (3.6)	160.1 (5.6)	58.7 (4.4)
	48.6[a]	89.6[a]	156.7[a]	51.6[a]
Angle between imidazole planes β	5.5 (8.2)	73.0 (8.1)	21.8 (14.2)	29.1 (10.5)
	11.3[a]	60.6[a]	25.3[a]	8.9[a]

[a]Predicted from chemical shifts using equation 5 of [61].

The average magnetic susceptibility tensors obtained for the family of structures are shown in Table 3.3. Besides providing a refinement of atomic coordinates through the dipolar shifts, the tensors can also be used to estimate the orientation of the axial ligands [60]. In fact, for low-spin bis-histidinyl haem proteins it is predicted that the magnetic axes will rotate about the perpendicular to the haem in the opposite sense to the axial ligands. The data of Table 3.3 shows that the counter-rotation of the magnetic y-axis in the plane of the haem in the opposite sense to the axial ligand orientations holds for this protein as in several other cases of Dc_3 [60]. This provides an independent test for the consistency of the chemical shifts used in this calculation as well as the proton structural coordinates and the geometry of the haem ligands. This internal consistency is further supported by the low value of the equatorial anisotropy for haem II that is associated with the large dihedral angle between the His ring planes. Yet another test is provided by comparing the geometry obtained by analysing the paramagnetic shifts of the haem methyl groups [61].

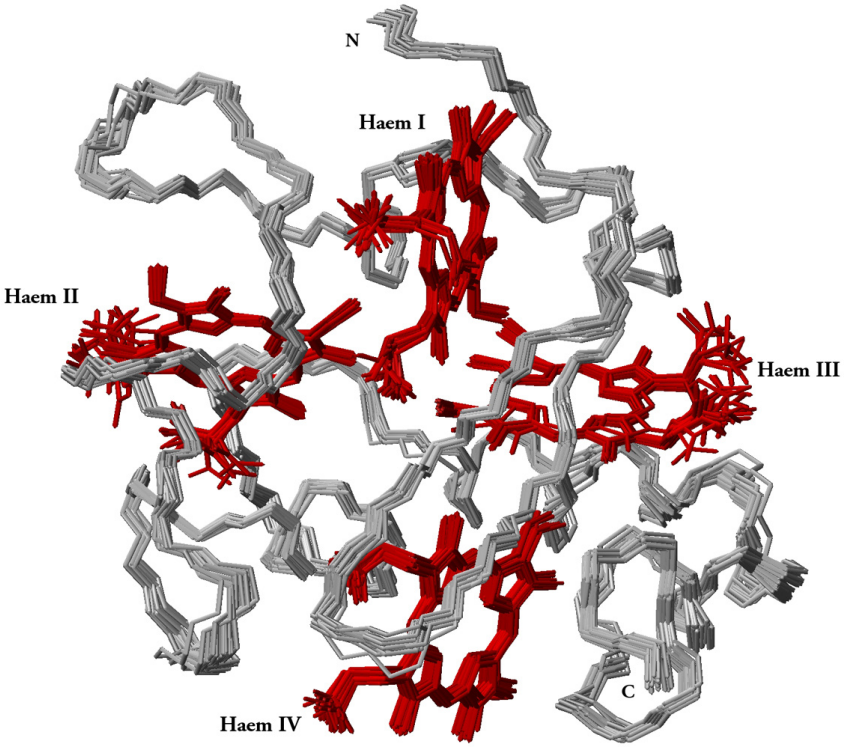

FIGURE 3.8 - Backbone and haems of the 20 lowest energy NMR structures of *D. desulfuricans* cytochrome c_3 for the oxidised state. The peptide chain and the haems are colour-coded grey and red respectively. In this orientation the C-terminus is at the bottom-right and haems are disposed from the left to the right in the following order: II, I, III, and IV. The figure was produced using MOLMOL [50].

DISCUSSION

Comparison between the solution structures of the reduced and oxidised states

Calculated diamagnetic shifts may be used to test the accuracy of the reduced structures: shifts were calculated for each unique non-exchangeable proton in the reduced NMR structures and compared with the experimental values (Figure 3.9a). These shifts are dominated by large ring current contributions from the haems, and the good overall agreement is an assurance of the quality of the structures. Dipolar shifts were fitted as part of the structure determination for the oxidised protein

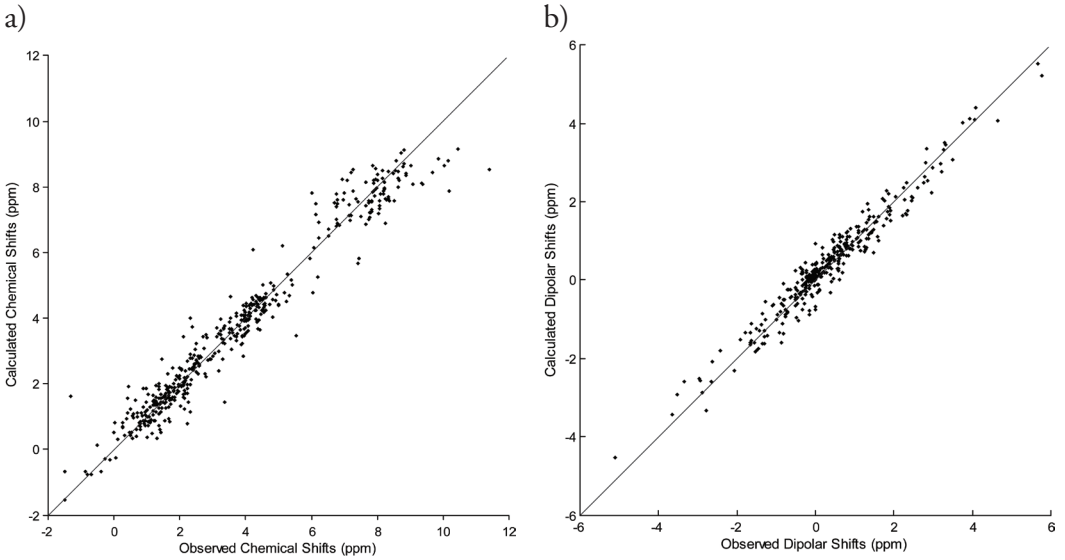

FIGURE 3.9 - a) Average calculated chemical shifts for protons in the 20 best *Dd27c*$_3$ NMR reduced structures versus observed chemical shifts. b) Calculated dipolar shifts for the family of oxidised structures against the observed shifts.

(Figure 3.9b) and therefore do not provide a completely independent test. However, the quality of the fit, and the relationship between the magnetic susceptibility tensors, the haem ligand orientations, and the Fermi contact shifts of the haem methyl groups demonstrate the quality of the structure (see Table 3.3). Also, despite the expectation that the magnetic susceptibility tensors of the haems will have different temperature dependences, the simple measurement of the temperature dependence of chemical shifts provides a good estimate of the dipolar shifts of individual protons that correlates well with the observed values (Figure 3.11).

The global RMSD of the superimposition of the mean structures of each family is 0.98 Å for backbone atoms and 1.34 Å for heavy atoms respectively, which is larger than might be expected on the basis of the uncertainty of the individual structures. The overall fold of the oxidised and reduced structures is very similar, with the position of the haem groups and Fe distances showing good agreement (Figures 3.4 and 3.8) and only minor differences between the consensus secondary structure

elements were identified. The two-stranded antiparallel β-sheet (Val^{9}-Lys^{12} and Thr^{17}-Phe^{20}) and one of the 3_{10}-helices (Ala^{23}-His^{25}) were found in both states of the structures. The α-helix (Ala^{81}-Ser^{84}) in the reduced form was found as a π-helix in the oxidised form and the second 3_{10}-helix (Val^{86}-Ala^{88}) in the reduced form was found as an α-helix in the oxidised state (Figure 3.10.

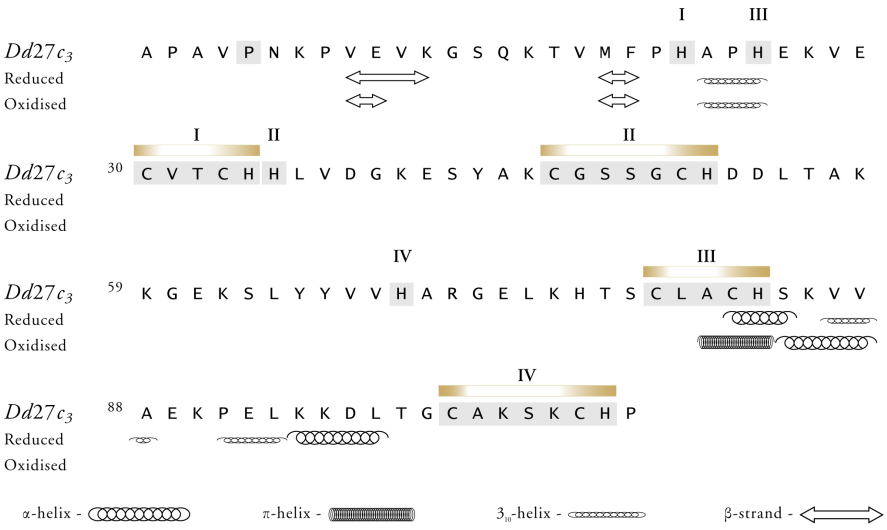

FIGURE 3.10 - Secondary structure elements of the reduced and oxidised forms of *D. desulfuricans* cytochrome c_3 in solution. The roman numbers indicate the haem binding motifs (CXX(XX)CH) and the sixth axial ligand of each haem..

A few regions of the protein show differences between the reduced and oxidised form that are significantly larger than the global RMSD values, which may indicate redox-related structural changes (Figure 3.13). The largest differences are observed in the segments 11-20, 47-63, and 71-75. It is important to note that the haem core region is virtually unchanged between the two forms with only a few of the propionate groups showing some conformational disorder, usually related to higher solvent exposure. The segment comprising residues Val^{11}-Phe^{20} shows a slight but significant (with respect to the global RMSD) movement towards the propionates of haem IV upon reduction.

All these residues are well defined in the solution structure families with many NOEs involving the side chain atoms. The two small beta strands identified in this zone are also conserved in both solution structures as well as in the X-ray structures of the reduced (1UP9) and oxidised (1UPD) forms [19]. The backbone of the segment Gly[47]-Ser[63] also moves, with Leu[55], Thr[56] and Lys[59] closer to the propionates of Haem IV in the oxidised cytochrome. This rearrangement brings Glu[61] within hydrogen-bonding distance of propionate D of haem II (Figure 3.12). Earlier simulations identified Glu[61] and propionate D of haem II as showing important contributions to the redox cooperativity of this cytochrome [19, 20].

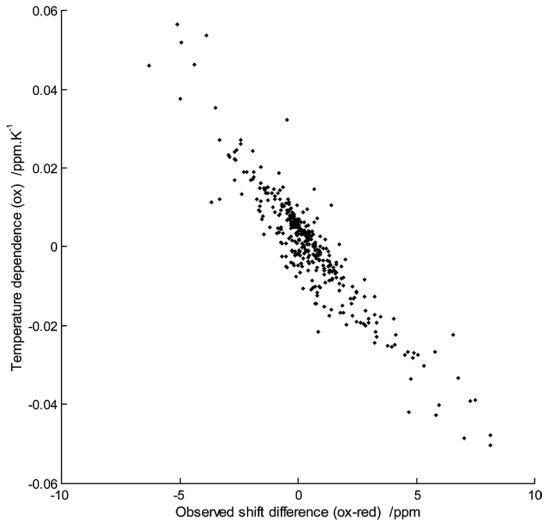

FIGURE 3.11 - Correlation of the measured temperature dependence of proton shifts on the oxidized protein against the observed dipolar shifts.

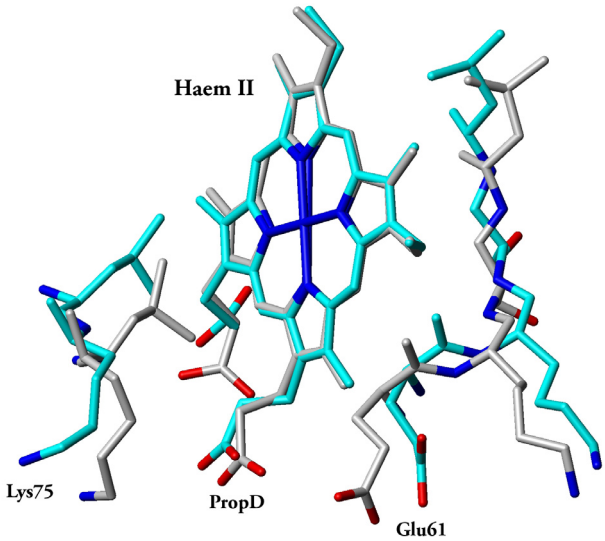

FIGURE 3.12 - Conformations of haem II propionate D and residues Glu 61 and Lys 75 in the overall best NMR structures of reduced (cyan) and oxidised (grey) cytochrome c_3 from *D. desulfuricans*. Note that the orientations of the Lys N^{ζ} and Glu carboxylate are not well defined. The figure was produced using MOLMOL [50].

The X-ray structures of reduced and oxidised *Dd27c*$_3$ showed conformational changes involving residues Lys[75], His[76] and also propionate D of haem II as possible participants in the functional cooperativities of this protein. In solution we also find a flexible region between Arg[71] and Lys[75] moving slightly closer to haem II upon oxidation, with Lys[75] within H-bond distance of propionate D of haem II. The free histidine His[76] has been identified as a likely redox-Bohr group [19], but it should be largely protonated in both forms studied here; it shows a high degree of conformational variability among the structures of each state and so the conformational changes are not significant.

Structural basis for the redox and redox-Bohr couplings

Several cytochromes c_3 show positive redox cooperativity between haems; the most positive effect in *Dd27c*$_3$ is between haems I and II which have a near-zero redox interaction despite their proximity: i.e. the electrostatic interaction is cancelled by changes in conformation. As mentioned above, Glu[61] shows a significant redox-linked conformational change with its charged carboxylate side chain moving closer to haem II upon oxidation, which is consistent with an electrostatically driven movement. A distinct cluster in the vicinity of haem II, comprising Leu[74], Lys[75], and the propionates of haem II, shows redox linked changes in conformation. A movement of Leu[74] towards propionate A of haem II is observed with reduction while Lys[75] shifts closer to the same propionate upon oxidation. These changes may make an important contribution to the positive cooperativity observed for haems I and II, which essentially titrate together. However, it is not possible to attribute the effect to isolated groups; it appears to involve concerted motions within the structure upon reduction (Figure 3.13).

The thermodynamic properties of *Dd27c*$_3$ reported in the literature have shown that the reduction potentials of the four haems are pH dependent, the so-called redox-Bohr effect.

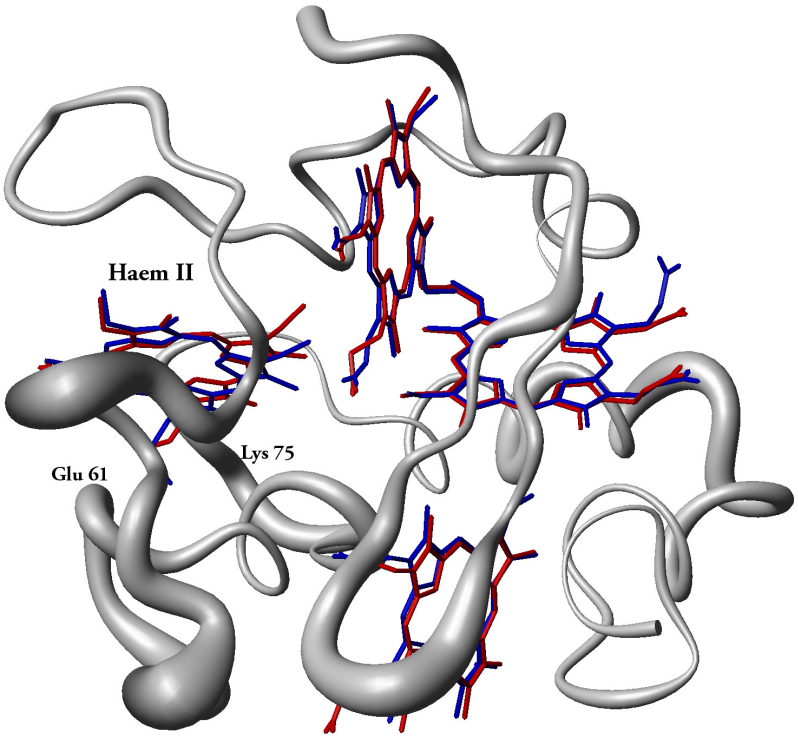

FIGURE 3.13 - Redox state dependent conformational changes in cytochrome c_3 from *D. desulfuricans*. The diameter of the tube is proportional to the RMS displacement between the mean oxidised structure and the mean reduced structure. The haems of the reduced structure are colored blue and those of the oxidised structure are red. The orientation is the same as in Figures 3.4 and 3.8 The figure was produced using MOLMOL [50].

This pH dependence in the range 5-9 is mediated by two distinct pK_a fitted with pK_a^{red}=7.4 and 6.4 and pK_a^{ox}=4.9 and 4.9 (the two are not distinguishable in the oxidised form) [11]. Propionate D of haem I has been shown to play an important role in the functional cooperativities of cytochromes c_3 from several *Desulfovibrio* species [11, 15-17, 62] and from the structural, thermodynamic and theoretical data it has also been suggested that the propionates of haem I play a similar role in *Dd27*c_3 [19]. In particular, the acid-base centre denoted H2 [11]) shows a strong influence on the reduction potential of haem I. However, when comparing the oxidised and reduced structures in solution the propionates of haem I, which are relatively disordered, or its neighbouring residues

show no significant conformational modifications. In fact both propionates are expected to be protonated at the chosen pH values (4.2 and 6.4 respectively).

CONCLUSIONS

High quality solution structures of reduced and oxidised cytochrome c_3 from *D. desulfuricans* ATCC 27774 have been solved from NMR data obtained from samples at pH values chosen to ensure that both forms were in similar states of protonation with respect to the redox-Bohr protons.

The standard stereochemical checks as well as the good agreement with the experimental constraint data and between the calculated and experimental diamagnetic shifts is a good indication of the accuracy of the reduced structure. The structure of the oxidised *Dd27c*$_3$ was calculated together with its magnetic properties: the magnetic susceptibility tensors obtained from the calculated family of structures provide an independent test for the structural geometry

Comparison between the structures of tetrahaem cytochrome c_3 in the reduced and oxidised states showed that the general backbone conformation is maintained as well as the orientation and position of the haems. The segments involving residues 11-20, 47-63 and 71-75 show significant differences between the two forms, with a combined rearrangement of these regions leading to the movement of Glu^{61} towards hydrogen-bond distance of Propionate D of Haem II, in agreement with the proposed contributions of Glu^{61} and haem II to the redox properties of *Dd27c*$_3$ [19, 20]. In fact the redox-linked movement of Glu^{61} and of a cluster involving Lys^{75} and the propionates of haem II may play an important role in the positive cooperativity observed between haems I and II.

The reduction potentials of the four haems of *Dd27c*$_3$ are pH dependent and several previous studies link the propionates of haem I to an impor-

tant role in the functional properties of this cytochrome. In solution, at the chosen pH values of the oxidised and the reduced samples (4.2 and 6.4 respectively), the ionisable centres involved in the redox-Bohr effect are essentially protonated in the structures obtained in this work and no significant conformational changes are observed for haem I or neighbouring residues when comparing the oxidised and reduced structures. The same situation occurs for the free histidine His^{76} which has been described as a likely redox-Bohr group [19]: it is partly protonated in the reduced and oxidised forms, and shows no significant conformational changes in solution.

In conclusion, comparing the reduced and oxidised structures in solution in the same protonation state allowed us to identify the redox related conformational changes that are important in the haem-haem cooperativity observed in this protein. This emerged as a concerted motion upon reduction involving several zones and is not attributable to isolated groups. Furthermore, the fact that the redox-Bohr effects are not observed could make this analysis more significant since the possible interference from pH dependent conformational changes is absent.

Acknowledgment

This work was initiated and inspired by António Xavier (1943-2006).

REFERENCES

1. Odom, J.M. and Peck, H.D., *Hydrogen cycling as a general mechanism for energy coupling in the sulfate-reducing bacteria,* Desulfovibrio *sp.* FEMS Microbiol Letters, 1981. **12**: 47-50.

2. Louro, R.O., Catarino, T., LeGall, J., and Xavier, A.V., *Redox-Bohr effect in electron/proton energy transduction: cytochrome* c_3 *coupled to hydrogenase works as a 'proton thruster' in* Desulfovibrio vulgaris*.* J Biol Inorg Chem, 1997. **2**: 488-91.

3. Fan, K.J., Akutsu, H., Kyogoku, Y., and Niki, K., *Estimation of microscopic redox potentials of a tetraheme protein, cytochrome* c_3 *of* Desulfovibrio vulgaris*, Miyazaki F, and partial assignments of heme groups.* Biochemistry, 1990. **29**: 2257-63.

4. Turner, D.L., Salgueiro, C.A., Catarino, T., LeGall, J., and Xavier, A.V., *Homotropic and heterotropic cooperativity in the tetrahaem cytochrome* c_3 *from* Desulfovibrio vulgaris*.* Biochim Biophys Acta, 1994. **1187**: 232-5.

5. Turner, D.L., Salgueiro, C.A., Catarino, T., Legall, J., and Xavier, A.V., *NMR studies of cooperativity in the tetra-*

haem cytochrome c$_3$ *from* Desulfovibrio vulgaris. Eur J Biochem, 1996. **241**: 723-31.

6. Salgueiro, C.A., Turner, D.L., Gall, J.L., Xavier, A.V., and LeGall, J., *Reevaluation of the redox and redox-Bohr cooperativity in tetrahaem* Desulfovibrio vulgaris *(Miyazaki F) cytochrome* c$_3$. J Biol Inorg Chem, 1997. **2**: 343-9.

7. Park, J.S., Ohmura, T., Kano, K., Sagara, T., Niki, K., Kyogoku, Y., and Akutsu, H., *Regulation of the redox order of four hemes by pH in cytochrome* c$_3$ *from* D. vulgaris *Miyazaki F.* Biochim Biophys Acta, 1996. **1293**: 45-54.

8. Louro, R.O., Catarino, T., Salgueiro, C.A., LeGall, J., and Xavier, A.V., *Redox-Bohr effect in the tetrahaem cytochrome* c$_3$ *from* Desulfovibrio vulgaris*: a model for energy transduction mechanisms.* J Biol Inorg Chem, 1996. **1**: 34-8.

9. Louro, R.O., Catarino, T., Turner, D.L., Picarra-Pereira, M.A., Pacheco, I., LeGall, J., and Xavier, A.V., *Functional and mechanistic studies of cytochrome* c$_3$ *from* Desulfovibrio gigas*: thermodynamics of a "proton thruster".* Biochemistry, 1998. **37**: 15808-15.

10. Paquete, C.M., Pereira, P.M., Catarino, T., Turner, D.L., Louro, R.O., and Xavier, A.V., *Functional properties of type I and type II cytochromes* c$_3$ *from* Desulfovibrio africanus. Biochim Biophys Acta, 2007. **1767**: 178-88.

11. Paquete, C.M., Turner, D.L., Louro, R.O., Xavier, A.V., and Catarino, T., *Thermodynamic and kinetic characterisation of individual haems in multicentre cytochromes* c$_3$. Biochim Biophys Acta, 2007. **1767**: 1169-79.

12. Louro, R.O., Catarino, T., LeGall, J., Turner, D.L., and Xavier, A.V., *Cooperativity between electrons and protons in a monomeric cytochrome* c$_3$*: the importance of mechanochemical coupling for energy transduction.* Chembiochem, 2001. **2**: 831-7.

13. Correia, I.J., Paquete, C.M., Louro, R.O., Catarino, T., Turner, D.L., and Xavier, A.V., *Thermodynamic and kinetic characterization of trihaem cytochrome* c$_3$ *from* Desulfuromonas acetoxidans. Eur J Biochem, 2002. **269**: 5722-30.

14. Coutinho, I.B. and Xavier, A.V., *Tetraheme cytochromes.* Methods Enzymol, 1994. **243**: 119-40.

15. Brennan, L., Turner, D.L., Messias, A.C., Teodoro, M.L., LeGall, J., Santos, H., and Xavier, A.V., *Structural basis for the network of functional cooperativities in cytochrome* c$_3$ *from* Desulfovibrio gigas*: solution structures of the oxidised and reduced states.* J Mol Biol, 2000. **298**: 61-82.

16. Messias, A.C., Aguiar, A.P., Brennan, L., Salgueiro, C.A., Saraiva, L.M., Xavier, A.V., and Turner, D.L., *Solution structures of tetrahaem ferricytochrome* c$_3$ *from* Desulfovibrio vulgaris *(Hildenborough) and its K45Q mutant: the molecular basis of cooperativity.* Biochim Biophys Acta, 2006. **1757**: 143-53.

17. Messias, A.C., Kastrau, D.H., Costa, H.S., LeGall, J., Turner, D.L., Santos, H., and Xavier, A.V., *Solution structure of* Desulfovibrio vulgaris *(Hildenborough) ferrocytochrome c$_3$: structural basis for functional cooperativity.* J Mol Biol, 1998. **281**: 719-39.

18. Harada, E., Fukuoka, Y., Ohmura, T., Fukunishi, A., Kawai, G., Fujiwara, T., and Akutsu, H., *Redox-coupled conformational alternations in cytochrome* c$_3$ *from* D. vulgaris *Miyazaki F on the basis of its reduced solution structure.* J Mol Biol, 2002. **319**: 767-78.

19. Bento, I., Matias, P.M., Baptista, A.M., da Costa, P.N., van Dongen, W.M., Saraiva, L.M., Schneider, T.R., Soares, C.M., and Carrondo, M.A., *Molecular basis for redox-Bohr and cooperative effects in cytochrome* c$_3$ *from* Desulfovibrio desulfuricans *ATCC 27774: crystallographic and modeling studies of oxidized and reduced high-resolution structures at pH 7.6.* Proteins, 2004. **54**: 135-52.

20. Louro, R.O., Bento, I., Matias, P.M., Catarino, T., Baptista, A.M., Soares, C.M., Carrondo, M.A., Turner, D.L., and Xavier, A.V., *Conformational component in the coupled transfer of multiple electrons and protons in a monomeric tetraheme cytochrome.* J Biol Chem, 2001. **276**: 44044-51.

21. Liu, M.C., Costa, C., Coutinho, I.B., Moura, J.J., Moura, I., Xavier, A.V., and LeGall, J., *Cytochrome components of nitrate- and sulfate-respiring* Desulfovibrio desulfuricans *ATCC 27774.* J Bacteriol, 1988. **170**: 5545-51.

22. Glasoe, P.K. and Long, F.A., *Use of glass electrodes to measure acidities in deuterium oxide.* J Phys Chem, 1960. **64**: 188-90.

23. Marion, D. and Wuthrich, K., *Application of phase*

sensitive two-dimensional correlated spectroscopy (COSY) for measurements of ^{1}H-^{1}H spin-spin coupling constants in proteins. Biochem Biophys Res Commun, 1983. **113**: 967-74.

24. Brown, S.C., Weber, P.L., and Mueller, L., *Toward complete ^{1}H NMR spectra in proteins.* J Magn Reson, 1988. **77**: 166-9.

25. Jeener, J., Meier, B.H., Bachmann, P., and Ernst, R.R., *Investigation of exchange processes by two-dimensional NMR spectroscopy.* J Chem Phys, 1979. **71**: 4546-53.

26. Kumar, A., Ernst, R.R., and Wuthrich, K., *A two-dimensional nuclear Overhauser enhancement (2D NOE) experiment for the elucidation of complete proton-proton cross-relaxation networks in biological macromolecules.* Biochem Biophys Res Commun, 1980. **95**: 1-6.

27. Piotto, M., Saudek, V., and Sklenar, V., *Gradient-tailored excitation for single-quantum NMR spectroscopy of aqueous solutions.* J Biomol NMR, 1992. **2**: 661-5.

28. Bearden, D.W., Macura, S., and Brown, L.R., *Suppression of cross relaxation in TOCSY experiments on macromolecules.* J Magn Reson, 1988. **80**: 534-8.

29. Briand, J. and Ernst, R.R., *Computer-optimized homonuclear TOCSY experiments with suppression of cross relaxation.* Chem Phys Lett, 1991. **185**: 276-85.

30. Griesinger, C., Otting, G., Wuethrich, K., and Ernst, R.R., *Clean TOCSY for proton spin system identification in macromolecules.* J Am Chem Soc, 1988. **110**: 7870-2.

31. Aue, W.P., Bartholdi, E., and Ernst, R.R., *Two-dimensional spectroscopy. Application to nuclear magnetic resonance.* J Chem Phys, 1976. **64**: 2229-46.

32. Derome, A.E. and Williamson, M.P., *Rapid-pulsing artifacts in double-quantum-filtered COSY.* J Magn Reson, 1990. **88**: 177-85.

33. Rance, M., Sorensen, O.W., Bodenhausen, G., Wagner, G., Ernst, R.R., and Wuthrich, K., *Improved spectral resolution in cosy ^{1}H NMR spectra of proteins via double quantum filtering.* Biochem Biophys Res Commun, 1983. **117**: 479-85.

34. Bartels, C., Xia, T.-h., Billeter, M., Güntert, P., and Wüthrich, K., *The program XEASY for computer-supported NMR spectral analysis of biological macromolecules.* J Biomol NMR, 1995. **6**(1): 1-10.

35. Goddard, T.D. and Kneller, D.G., *SPARKY 3*, University of California: San Francisco.

36. Salgueiro, C.A., Turner, D.L., and Xavier, A.V., *Use of paramagnetic NMR probes for structural analysis in cytochrome* c_3 *from* Desulfovibrio vulgaris. Eur J Biochem, 1997. **244**: 721-34.

37. Turner, D.L., Brennan, L., Meyer, H.E., Lohaus, C., Siethoff, C., Costa, H.S., Gonzalez, B., Santos, H., and Suarez, J.E., *Solution structure of plantaricin C, a novel lantibiotic.* Eur J Biochem, 1999. **264**: 833-9.

38. Guntert, P. and Wuthrich, K., *Improved efficiency of protein structure calculations from NMR data using the program DIANA with redundant dihedral angle constraints.* J Biomol NMR, 1991. **1**: 447-56.

39. Wareham, R.S., Kilburn, J.D., Rees, N.H., Turner, D.L., Leach, A.R., and Holmes, D.S., *Synthesis and Solution Conformation of a C2 Symmetric Macrobicycle.* Tetrahedron Lett, 1995. **36**: 3047-50.

40. Wareham, R.S., Kilburn, J.D., Turner, D.L., Rees, N.H., and Holmes, D.S., *Homeomorphic Isomerism in a Peptidic Macrobicycle.* Angew Chem Int Ed Engl, 1996. **34**: 2660-2.

41. Turner, D.L., Brennan, L., Chamberlin, S.G., Louro, R.O., and Xavier, A.V., *Determination of solution structures of paramagnetic proteins by NMR.* Eur Biophys J, 1998. **27**: 367-75.

42. Bertini, I., Donaire, A., Felli, I.C., Rosato, A., and Luchinat, C., *From NOESY Cross Peaks to Structural Constraints in a Paramagnetic Metalloprotein.* Magn Reson Chem, 1996. **34**: 948-50.

43. Bertini, I., Felli, I.C., Luchinat, C., and Rosato, A., *A complete relaxation matrix refinement of the solution structure of a paramagnetic metalloprotein: reduced HiPIP I from* Ectothiorhodospira halophila. Proteins, 1996. **24**: 158-64.

44. Bertini, I. and Luchinat, C., *NMR of paramagnetic molecules in biological systems.* Phys Bioinorg Chem Ser, 3. 1986, Menlo Park, Calif.: Benjamin/Cummings Pub. Co.

45. Boelens, R., Koning, T.M.G., and Kaptein, R., *Determination of biomolecular structures from proton-proton NOE's using a relaxation matrix approach.* J Mol Struct,

1988. **173**: 299-311

46. Boelens, R., Koning, T.M.G., van der Marel, G.A., van Boom, J.H., and Kaptein, R., *Iterative procedure for structure determination from proton-proton NOEs using a full relaxation matrix approach. Application to a DNA octamer.* J Magn Reson, 1989. **82**: 290-308.

47. Turner, D.L., *Evaluation of ^{13}C and ^{1}H Fermi contact shifts in horse cytochrome* c. *The origin of the anti-Curie effect.* Eur J Biochem, 1993. **211**: 563-8.

48. Paixao, V.B., Salgueiro, C.A., Brennan, L., Reid, G.A., Chapman, S.K., and Turner, D.L., *The solution structure of a tetraheme cytochrome from* Shewanella frigidimarina *reveals a novel family structural motif.* Biochemistry, 2008. **47**: 11973-80.

49. Pettersen, E.F., Goddard, T.D., Huang, C.C., Couch, G.S., Greenblatt, D.M., Meng, E.C., and and Ferrin, T.E., *CSF Chimera - A Visualization System for Exploratory Research and Analysis.* J Comput Chem, 2004. **25**: 1605-12.

50. Koradi, R., Billeter, M., and and Wüthrich, K., *MOLMOL: a program for display and analysis of macromolecular structures.* J Mol Graphics, 1996. **14**: 51-5.

51. Vriend, G., *WHAT IF: A molecular modeling and drug design program.* J Mol Graph, 1990. **8**: 52-6.

52. Hutchinson, E.G. and Thornton, J.M., *PROMOTIF--A program to identify and analyze structural motifs in proteins.* Protein Sci, 1996. **5**: 212-20.

53. Williamson, M.P. and Asakura, T., *Empirical Comparisons of Models for Chemical-Shift Calculation in Proteins.* J Magn Reson, Ser B, 1993. **101**: 63-71.

54. Wüthrich, K., *NMR of Proteins and Nucleic Acids*. 1986, John Wiley and Sons: NY. 30-1, 130-61.

55. Guntert, P., Braun, W., and Wuthrich, K., *Efficient computation of three-dimensional protein structures in solution from nuclear magnetic resonance data using the program DIANA and the supporting programs CALIBA, HABAS and GLOMSA.* J Mol Biol, 1991. **217**: 517-30.

56. Ramachandran, G.N., Ramakrishnan, C., and Sasisekharan, V., *Stereochemistry of polypeptide chain configurations.* J Mol Biol, 1963. **7**: 95-9.

57. Barry, C.D., North, A.C., Glasel, J.A., Williams, R.J., and Xavier, A.V., *Quantitative determination of mononucleotide conformations in solution using lanthanide ion shift and broadenine NMR probes.* Nature, 1971. **232**: 236-45.

58. Barry, C.D., Martin, D.R., Williams, R.J., and Xavier, A.V., *Quantitative determination of the conformation of cyclic 3',5'-adenosine monophosphate in solution using lanthanide ions as nuclear magnetic resonance probes.* J Mol Biol, 1974. **84**: 491-502.

59. Gochin, M. and Roder, H., *Protein structure refinement based on paramagnetic NMR shifts: applications to wild-type and mutant forms of cytochrome* c. Protein Sci, 1995. **4**: 296-305.

60. Turner, D.L., Brennan, L., Messias, A.C., Teodoro, M.L., and Xavier, A.V., *Correlation of empirical magnetic susceptibility tensors and structure in low-spin haem proteins.* Eur Biophys J, 2000. **29**: 104-12.

61. Turner, D.L., *Obtaining ligand geometries from paramagnetic shifts in low-spin haem proteins.* J Biol Inorg Chem, 2000. **5**: 328-32.

62. Baptista, A.M., Martel, P.J., and Soares, C.M., *Simulation of electron-proton coupling with a Monte Carlo method: application to cytochrome* c_3 *using continuum electrostatics.* Biophys J, 1999. **76**: 2978-98.

4

SOLUTION STRUCTURE OF A TETRAHAEM CYTOCHROME FROM *SHEWANELLA FRIGIDIMARINA*

Results published in:
Paixao, V. B., Salgueiro, C. A., Brennan, L., Reid, G. A., Chapman, S. K., and Turner, D. L. (2008) *The solution structure of a tetraheme cytochrome from* Shewanella frigidimarina *reveals a novel family structural motif*, Biochemistry **47**, 11973-80.

CONTENTS

ABSTRACT

The bacteria belonging to *Shewanella* genus are facultative anaerobes that utilize a variety of terminal electron acceptors which includes soluble and insoluble metal oxides. The tetrahaem *c*-type cytochrome isolated during anaerobic growth of *Shewanella frigidimarina* NCIMB400 (*Sfc*) contains 86 residues and is involved in the Fe (III) reduction pathways.

Although the functional properties of *Sfc* redox centres are quite well described, no structures are available for this protein. In this work we report the solution structure of the reduced form of *Sfc*. The overall fold is completely different from those of the tetrahaem cytochromes c_3 and instead has similarities with the tetrahaem cytochrome recently isolated from *Shewanella oneidensis* (*Soc*).

Comparison of the tetrahaem cytochromes from *Shewanella* show a considerable diversity in their primary structure and haem reduction potentials and yet have highly conserved haem geometry, as is the case for the family of tetrahaem cytochromes isolated from *Desulfovibrio* spp.

INTRODUCTION

Bacterial tetrahaem *c*-type cytochromes were first discovered in *Desulfovibrio* spp. [1, 2]. These proteins have approximately 30 amino acids per haem and each co-factor has bis-histidinyl axial coordination, and is therefore low spin in the oxidised and reduced forms.

Several structures of tetrahaem cytochromes isolated from *Desulfovibrio* spp. (Dc_3) have been determined either by X-ray crystallography or NMR and show that the haem groups are arranged in very close proximity in a roughly circular fashion (for a review see [3]).

More recently, the bacterial genome sequence of *Geobacter sulfurreducens* and *Shewanella oneidensis* revealed that soluble small multihaem proteins are not exclusive to the *Desulfovibrio* genus [4-7]. Moreover,

cytochromes containing three or four haem groups have been identified in bacteria that have the ability to reduce metal oxides (most of them located in the cellular exterior) which suggests an important role for these small proteins in transferring electrons from the cytoplasm to the outer membrane and/or to be used as alternative devices to assist the energy transduction process [8, 9].

Gene disruption experiments have shown that PpcA (a trihaem cytochrome containing 71 amino acids from *G. sulfurreducens*) and *Sfc* (a small tetrahaem cytochrome with 86 residues from *S. frigidimarina*) are both involved in metabolic pathways leading to the reduction of Fe(III) [6, 10].

Structural data reported for PpcA and its homologue cytochrome c_7 isolated from *Desulfuromonas acetoxidans* showed that both proteins share structural homologies with Dc_3 [11-13]. Indeed, the arrangement of the three haems is closely similar to the haem core of tetrahaem cytochromes c_3 isolated from the *Desulfovibrionacea* family but with haem II deleted together with the region of polypeptide responsible for its binding.

The periplasmic tetrahaem cytochrome produced by the bacteria *S. frigidimarina* (*Sfc*) is even smaller than Dc_3. It contains only approximately 20 amino acid residues per haem group and is the smallest tetrahaem cytochrome described to date. Sequence analysis of this cytochrome showed that the haem binding motifs are different from those of Dc_3 [14].

Little structural information is available for *Sfc* and only a preliminary model determined with a limited number of distance constraints was used to predict the haem arrangement in solution [14]. However it was possible to show that in *Sfc* the haem groups have a linear arrangement instead of the circular one found in Dc_3. A similar disposition of haems has only been found in the N-terminal cytochrome domain of a flavocytochrome c_3 ($Sffcc_3$) isolated from the same bacterium [15, 16] and in a

small tetrahaem cytochrome isolated from *S. oneidensis* (*Soc*) [17].

Harada and co-workers [18] determined the haem redox potentials for *Soc* and the order in which the haems become oxidised. The thermodynamic properties of the *Sfc* redox centres were also determined [19] showing that the co-factors are not structurally or functionally equivalent, with negative and different reduction potentials. As with Dc_3, the reduction potentials of the haems in *Sfc* are modulated by redox interactions between the four haems and by redox-Bohr interactions between the haems and a protonatable centre.

Most importantly, the thermodynamic properties of *Soc* and *Sfc* are quite different. Significant differences were also observed for Dc_3 isolated from different species. In fact, from eight different Dc_3 only two very closely related ones showed the same order of oxidation of the haem groups [3, 20]. The wide variations in the sequences and properties of these multihaem proteins makes the high degree of conservation of the haem geometry still more surprising.

To rationalise the thermodynamic parameters of *Sfc* and to establish how closely the haem geometry is conserved between *Sfc* and *Soc* it is necessary to obtain more detailed structural information. Attempts to crystallize *Sfc* were unsuccessful and in this study we report the solution structure of the reduced form of *Sfc* and the structural basis for the network of cooperativities observed in this protein are discussed.

MATERIALS AND METHODS

Bacterial growth and protein purification

Shewanella frigidimarina cells were grown and the tetrahaem cytochrome was purified as previously described [6].

NMR sample preparation.

For NMR experiments in H_2O the protein was lyophilised from H_2O and suspended in 92% H_2O / 8% ^2H_2O to a final concentration of approximately 3 mM.

For NMR experiments in ^2H_2O the protein was lyophilised several times from ^2H_2O and then dissolved in ^2H_2O (99.96%) to a final concentration of approximately 3 mM.

The pH was adjusted to 6.1 in an anaerobic chamber (Mbraun MB 150 I) by addition of 0.1 M NaO^2H or ^2HCl for ^2H_2O samples and 0.1 M NaOH or HCl for H_2O samples. The pH values measured are direct meter readings without correction for isotope effects [21].

Complete reduction of the samples was achieved by the reaction with hydrogen gas in the presence of catalytic amounts of hydrogenase isolated from *Desulfovibrio gigas* and *Desulfovibrio vulgaris*. An antibiotic cocktail (70 μm ampicillin, 50μm kanamycin and 50 μm chloramphenicol) was added to the sample in H_2O to prevent bacterial growth.

NMR spectroscopy

All ^{1}H-NMR spectra were obtained on a Bruker DRX-500 spectrometer equipped with a 5 mm inverse detection probe head with internal B_0 gradient coil and a Eurotherm 818 temperature control unit.

All 2D NMR spectra were acquired at 303 K. Acquisition was made in the phase sensitive mode by the States-TPPI method [22] collecting 4096 (t_2)x1024 (t_1) data points to cover a sweep width of 8 kHz, with 32 scans per increment.

NOESY spectra [23, 24] were recorded with 40, 60, 80 and 100 ms mixing times. NOESY spectra of the ^2H_2O spectra were recorded with standard pulse sequences with continuous low-power water presaturation during the relaxation delay and the mixing time. NOESY spectra of the H_2O sample were recorded with presaturation of the water resonance

by a composite 180º inversion pulse followed by a SCUBA sequence to facilitate recovery of potentially saturated alpha protons [25].

Total correlation spectra were acquired using the clean TOCSY pulse sequence [26-28] with spin-lock times of 40 and 60 ms. DQF-COSY spectra were also acquired [29, 30]. Data were processed using XWIN-NMR software (Bruker, Rheinstetten). Proton chemical shifts were calibrated using the water signal as internal reference.

Assignment and integration

The software package XEASY (version 1.2; ETH, Zurich) [31] was used to display and annotate spectra.

Amino acid residue assignment was performed using the classical approach described by Wüthrich [32]. Examination of TOCSY and COSY spectra in H_2O and ^2H_2O allowed spin-system identification. Further analysis of the NOESY spectra and identification of H^N-H^N, H^N-H^α and H^N-H^β connectivities between different spin-systems allowed the sequential assignment.

Stereospecific assignments were obtained in the process of structure calculation with the aid of the program GLOMSA [33]. The assigned NOESY cross peaks were integrated and converted into volume restraints with the program SPARKY [34]. All NOEs were measured in the 80 ms NOESY spectra at 303 K and pH 6.1. Cross-peaks due to protons separated by fixed distances and all intra-haem cross-peaks, except those involving the propionate groups, were excluded.

Integration was performed by Gaussian and Lorentzian function fitting for isolated peaks and with sum data heights in a box or ellipse surrounding the peak for more overlapped peaks. The baseline around each individual peak was determined and used to correct the measured volume.

Determination of restraints

Signals from H^{α} protons close to the H_2O frequency, whenever possible were taken from the ^2H_2O spectra only, except for H^N-H^{α} cross-peaks. NOE cross-peaks involving non-exchangeable protons were integrated both in H_2O and in ^2H_2O spectra. These calculated volumes were also used to obtain an overall scaling factor relating the spectra [35]; the volumes were then combined into a single data set.

The smallest recognizable peaks in the H_2O spectra were used to assess the minimum uncertainty volume (δV) for input in the program INDYANA [36] for structure calculation. The program generates upper limit volumes (upv) as $<V> + \max(\Delta V, \delta V)$, and lower limit volumes (lov) as $<V> - \delta V$, where $<V>$ and ΔV are the average and difference of volumes for each pair of symmetrical cross-peaks, respectively.

For overlapping peaks involving protons not separated by a fixed distance, upper volume limits (lower distance constraints) were applied to each possible proton pair. When the structure was calculated, some of the potentially overlapping peaks were specifically assigned as the various possibilities were eliminated by reference to the structure. Hence a lower limit could also be applied.

For the degenerate H^{δ} and H^{ε} ring protons of fast-flipping residues, it is often possible to identify which side of the ring is involved because of the large distance between them. In the preliminary stages of structure calculation, all cross-peaks from degenerate ring protons are treated as non-specific, with the exception of one chosen to distinguish the two sides of the ring. During structure refinement, individual NOEs were assigned specifically as in the case of non-degenerate protons, with the aid of the program GLOMSA [37].

Additional restraints

Three non-standard residues were used for structure calculations: fast-

flipping aromatic residues with pseudo-atoms to limit the orientations of the planes [35, 38, 39]. Flexible haem groups and proline residues with fixed upper limit distances for ring closure [35, 36, 40].

In the final stages of structure refinement, the calculated structures were checked for short (less than 2.5 Å) distances between assigned protons that should give rise to significant NOEs. Even if no peaks were visible at the predicted frequencies, the volume was measured and used in further calculations. In this way, a lower limit distance restraint defines a minimum distance between protons if there is no NOE in the spectra.

Structure calculation and analysis

Structure calculations were performed using the extended version of the program DYANA [41], called PARADYANA. This version of DYANA is modified to accept peak volumes as input and pseudocontact shifts for paramagnetic proteins.

The functionality of the original DYANA program remains, as well as the extensions introduced in the program INDYANA [36] for the fully automatic conversion of peak volumes into distance constraints.

The program CHIMERA (version 1.24) [42] was used for visual interpretation with the preliminary structure calculations, as an aid to assignment, during structure refinement. The program MOLMOL (version 2.0) [43] was used for superimposition, visual inspection, calculation of mean structure and of root-mean-square deviations from the mean structure. It was also used for calculation of solvent accessible surfaces using a radius of 1.4 Å for the H_2O molecule. Stereochemical analysis of the structures was performed with the program WHAT IF (version 20030529-0952)[44].

Identification and classification of the consensus secondary structure elements in the NMR structure ensemble, defined as those present in at least 50% of the structures was accomplished with the program

PROMOTIF (version 2.0) [45]. Secondary structural shifts, which are dominated by the effect of haem ring currents, were calculated for the structures using the program TOTAL [46].

RESULTS

Sequential assignment

Sequence-specific assignment was straightforward, but no connectivities involving residue 1 were assigned, probably because of the high flexibility of the N-terminus.

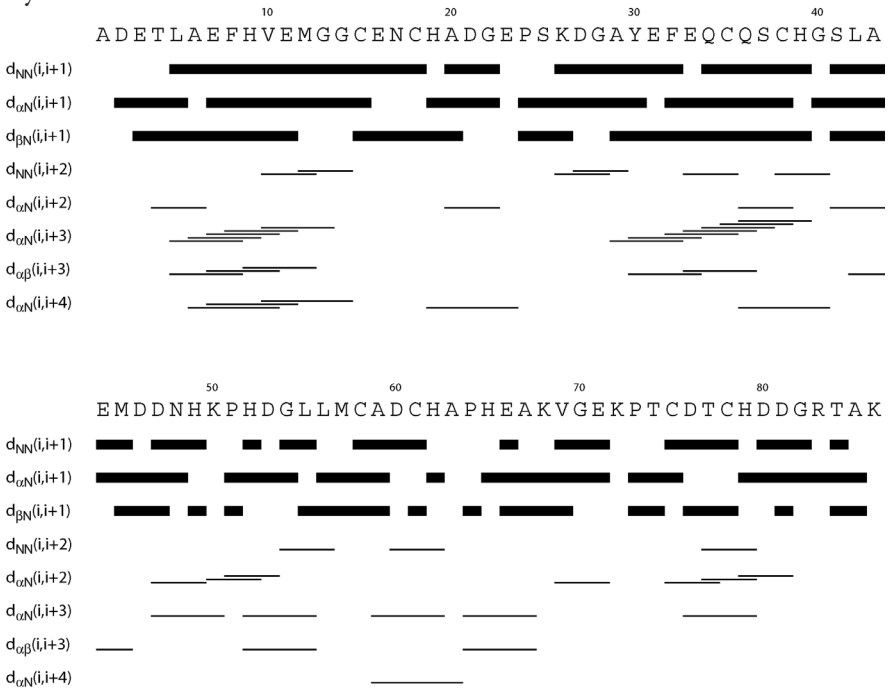

FIGURE 4.1 - Sequential NOE connectivities involving H^N, H^α and H^β observed in the NOESY spectrum for tetrahaem cytochrome from *S. frigidimarina*. The line thickness is indicative of the NOE intensity.

Sequential connectivities between H^N, H^α and H^β protons are shown in Figure 4.1. All of the residues, with exception of prolines (residues 24, 51, 64 and 73) show at least one of the sequential connectivities

between its H^N and the H^N, H^α or H^β of the preceding residue. For the proline residues, connectivities were obtained at least between the H^δ protons of the prolines and the H^α or H^β of the preceding residue.

In total 86% of all protons in the protein were assigned. This corresponds to 92% of the protons after excluding exchangeable protons other than the backbone HN. The chemical shifts have been deposited in the BioMagResBank database (http://www.bmrb.wisc.edu) under accession number BMRB – 15765.

Restraints and structure calculations

Assigned cross-peaks in the H_2O and ^2H_2O NOESY spectra were integrated and converted into volume restraints, resulting in 1153 lower limits for volumes (lovs) and 1366 upper limits (upvs). These were used as input for the program PARADYANA together with a set of 88 fixed upper limit distances (associated with ring closure in the flexible proline residues and haem groups, and the attachment of His ligands)[35, 36, 40].

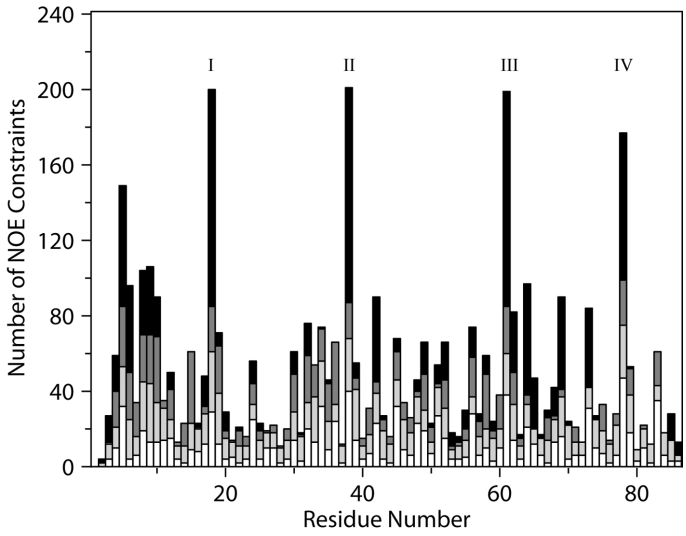

FIGURE 4.2 - Number of constraints per residue used for the calculation of the structure of *S. frigidimarina* tetrahaem cytochrome. Bars are white, light grey, dark grey and black for intra residue, sequential, medium and long range restraints, respectively. Residues 18, 38, 61 and 78 also include restraints to haems I, II, III and IV, respectively.

The preliminary structures were also analysed using the program GLOMSA [33] modified to take NOE volumes as input and 29 stereospecific assignments were made for diastereotopic pairs of protons or methyl groups.

The effect of spin diffusion introduces an uncertainty into the conversion of experimental data to distance constraints. These effects were simulated by complete relaxation matrix calculations based on the initial protein structures and, accordingly, a parameter was set in the program PARADYANA to loosen all distance restraints by 5%. An average of 29 NOE restraints per amino acid residue (13 lovs and 16 upvs) and 126 per haem residue (58 lovs and 68 upvs) was used for the final calculation (Figure 4.2).

Quality analysis of the structures

The final family consists of 20 structures with the target function increasing by 11% from the first to the last. The structures superimpose with an average backbone RMSD of 0.60 Å and a heavy atom RMSD of 0.95 Å with respect to the mean structure; the values for each residue are shown in Figure 4.3.

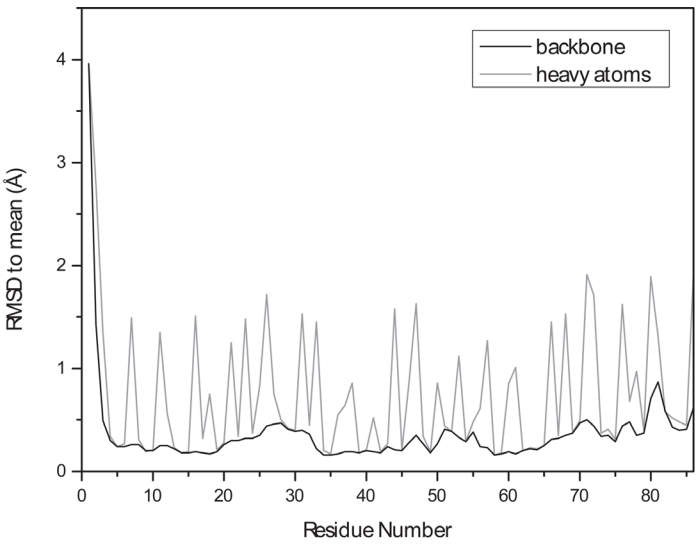

FIGURE 4.3 - Average backbone and heavy atom RMSD values per residue with respect to the mean structure of the family of 20 conformers obtained for Sfc.

The Ramachandran plot shows 59% of the residues in the most favoured regions, 35% in the additionally allowed and 6% in the generously allowed. A total of 90 hydrogen bonds were identified in the family of 20 structures with the program WHAT IF (using routine HBO), 35 of which were present in at least 50% of the structures.

The NMR structure models presented in Figure 4.4 are, in general well defined. Some amino acid side-chains or haem ligand propionate groups show a larger conformational variability probably because of the reduction in the number of restraints due to higher solvent exposure.

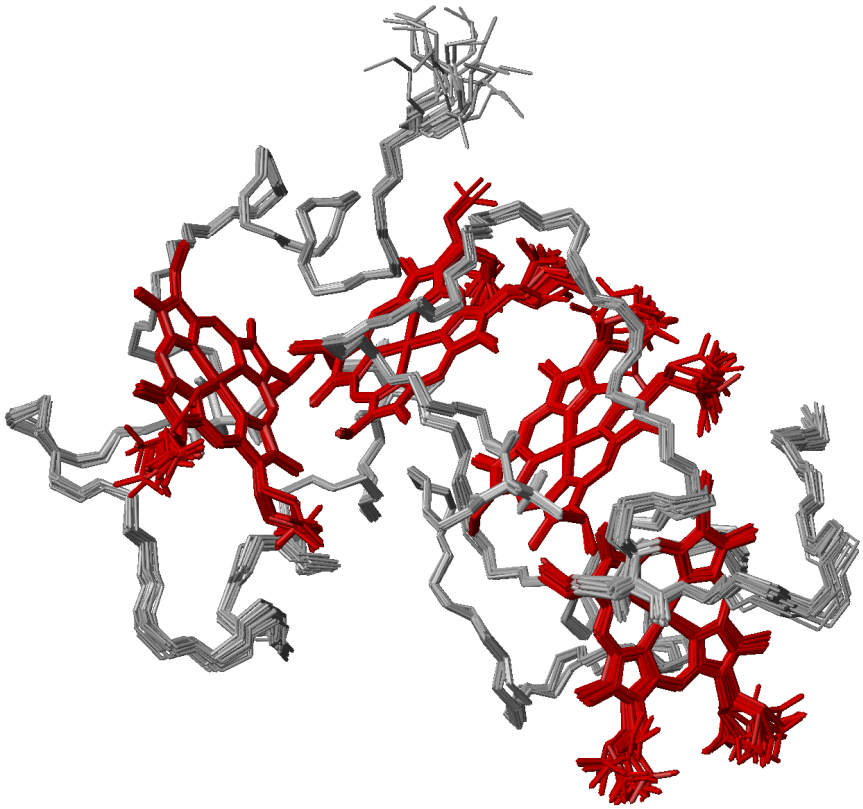

FIGURE 4.4 - Overlay of the 20 lowest energy NMR structures of *S. frigidimarina* tetrahaem cytochrome at pH 6.1. Superimposition was performed using all the heavy-atoms. The peptide chain and the haems are color-coded grey and red, respectively. In this orientation the N-terminus is at the top-left and haems are disposed from the left to the right in the following order: I, II, III, and IV. The figure was produced using MOLMOL [42].

DISCUSSION

Comparison of the *Sfc* and *Soc* structures

The *Sfc* is folded in a series of helices connected by extended loop regions; there are no β-strands (Figure 4.5). Three α-helices are established between residues Ala^{5}-Val^{10} (A), Ala^{29}-Gln^{34} (B), and Cys^{58}-Cys^{61} (C), and there are three additional 3_{10} helical regions between residues Cys^{15}-Asn^{17}, Leu^{42}-Glu^{44}, and Cys^{75}-Thr^{77}. The four bis-histidinyl haem groups are arranged in a linear fashion with haems I-II and III-IV exhibiting a perpendicular orientation of haem planes, whereas the planes of the central haems II-III are roughly parallel to each other.

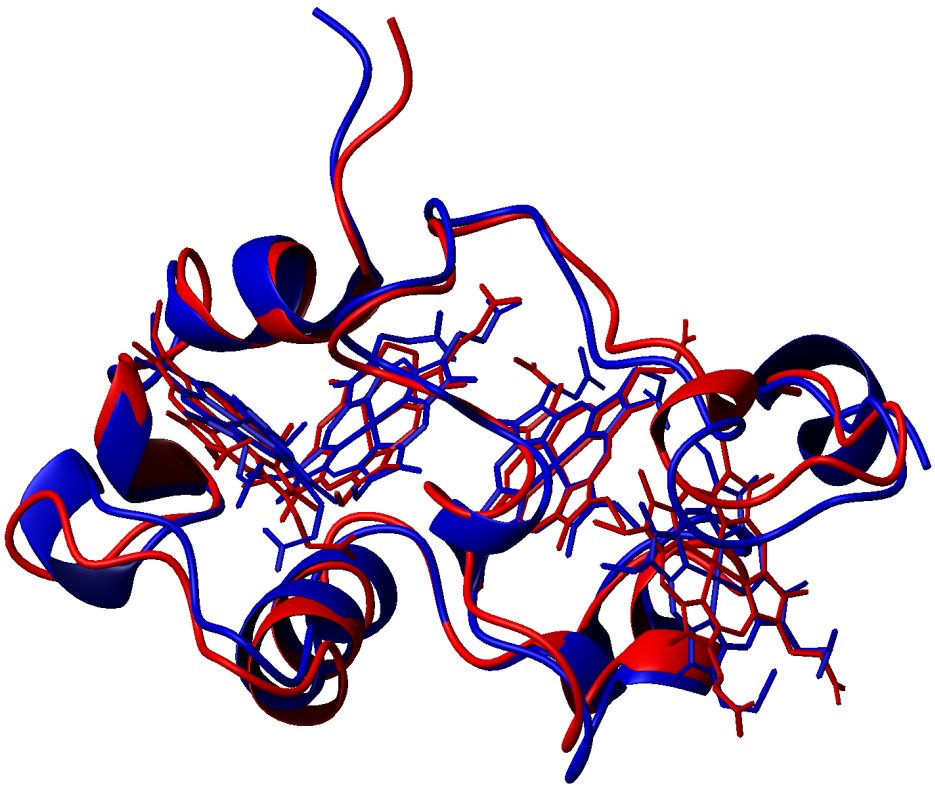

FIGURE 4.5 - Comparison of the *Sfc* (red) and *Soc* (blue) structures. The lowest energy NMR structure of *Sfc* is superimposed on the X-ray structure of *Soc*. The figure was generated using program MOLMOL (42).

When comparing the available sequences for *Sfc* and *Soc*, 27 residues are different, plus the 5 extra residues at the *Soc* C-terminus (Figure 4.6).

Comparison of the reduced NMR structures of *Sfc* with the X-ray structure of *Soc* [17] reveals that the general fold of the proteins, as well as the relative position of the four haem groups, are similar (Figure 4.5 and Table 4.1). However, differences are observed in the helical regions. The α-helices in *Soc* are established between residues Leu[5]-Ala[10] (A), Ala[29]-His[39] (B), and Ser[85]-Leu[89] (C) and there are 3_{10} helical regions between residues Leu[42]-Glu[44], Lys[50]-His[52], Cys[58]-Asp[60] (Figure 4.6).

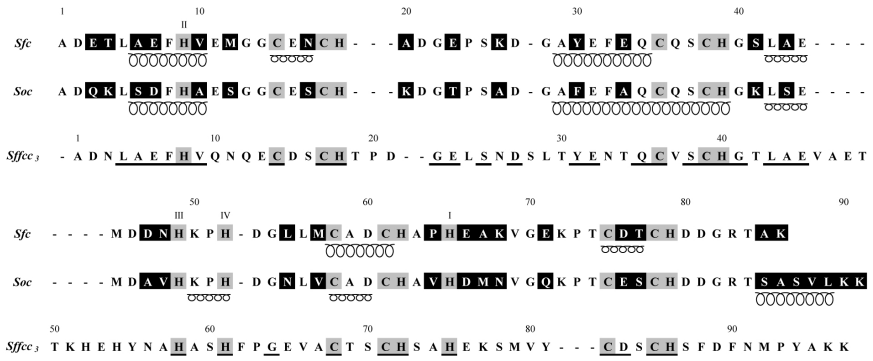

FIGURE 4.6 - Sequence alignment of tetrahaem cytochromes from *S. frigidimarina* (*Sfc*), *S. oneidensis* (*Soc*) and *S. frigidimarina* flavocytochrome c_3 (*Sffcc*$_3$). Large and small coils denote α-helices and 3_{10} helices, respectively. The non-conserved residues between the *Sfc* and *Soc* proteins are indicated by black boxes. The cysteines and histidines that bind to the haems are boxed in grey and Roman numbers (I-IV) refer to the sixth haem axial ligand. The conserved residues between *Sfc* and *Sffcc*$_3$ are underlined in the latter sequence.

The first two α-helices are formed in the same region of the two proteins. However the α-helix B in *Soc* is 5 residues longer and the *Soc* α-helix C is formed at the C-terminal end of the protein and involves three out of the five extra residues which are not present in *Sfc*. In *Sfc* α-helix C is established between the two Cys residues that form the haem III binding motif. Both proteins have three 3_{10} helical regions but only that involving the residues Leu[42]-Glu[44] is conserved.

The haem spatial disposition in *Sfc* and *Soc* is highly conserved with average iron-iron distances differing by less than 6% between the structures (Table 4.1).

TABLE 4.1 - Average iron-iron distances (Å) in the NMR (*Sfc*) and X-ray (*Soc*) reduced structures. Values in parenthesis correspond to the standard deviation for the family of 20 NMR conformers. The iron-iron distances of the highly homologous N-terminal domain of flavocytochrome c_3 (*Sffcc*$_3$) are also given for comparison.

		Haem I	Haem II	Haem III
Haem II	*Sfc*	12.8 (0.03)		
	Soc	12.0		
	Sffcc$_3$	12.5		
Haem III	*Sfc*	17.2 (0.07)	9.6 (0.1)	
	Soc	16.3	9.2	
	Sffcc$_3$	17.3	9.5	
Haem IV	*Sfc*	23.2 (0.11)	20.0 (0.08)	11.0 (0.03)
	Soc	23.1	19.9	11.2
	Sffcc$_3$	29.8	25	15.6

However important differences were detected in the orientation of the rings of the axial haem ligands and the dihedral angles formed between them. Indeed, with the exception of haem II where the angles are similar, at least one His axial ligand of each haem has a different orientation in *Sfc* and *Soc*. This is the case of His^{67} (haem I), His^{64} (haem III) and both His^{52} and His^{79} in haem IV. These differences are likely to affect the redox properties of the haem groups and the rates of haem-haem electron transfer (see below).

Comparison of the *Sfc* and N-terminal domain of flavocytochrome c_3 structures

Sequence comparison of *Sfc* and the N-terminal domain of flavocytochrome c_3, an enzyme with fumarate reductase activity (42% identity), also isolated from *S. frigidimarina* (*Sffcc*$_3$) showed that the haem binding motifs (CXXCH) and the sixth haem axial ligands are strictly conserved (Figure 4.6).

The X-ray structure of *Sffcc*$_3$ was determined [15] and comparison with the *Sfc* structure shows remarkably similar distances among haems I, II and III, with differences less than 2%. However, whereas the polypep-

tide chain traces of *Sfc* and *Sffcc*$_3$ are similar from the N-terminus up to Ala[67], the C-terminal region of *Sfc* is unlike *Sffcc*$_3$ because of the interaction with the FAD binding domain, which results in a nearly 60° angle difference between the haem IV planes of the two proteins and differences of up to 29% are observed for distances to haem IV.

In view of the differences in thermodynamic properties of *Sfc* and *Soc* that exist despite the close similarity in their structures, it would be unwise to use these properties to model the behaviour of the N-terminal domain of *Sffcc*$_3$ with its much larger structural differences. Indeed, the order of oxidisation of the haems in *Sffcc*$_3$ has been determined [47] and shows no correlation with that of *Sfc* [14].

Structural basis for the electrostatic origin of the *Sfc* redox interactions

The thermodynamic properties of the haems in *Sfc*, including the reduction potentials and haem-redox (haem-haem) interactions, have been determined [19].

The values obtained for the haem redox-interactions suggest that they are dominated by electrostatic effects, rather than conformational changes between redox stages. Indeed, the redox interactions between the haem groups are all positive such that the oxidation of a particular haem makes the oxidation of its neighbours more difficult (negative homo-cooperativity).

On the other hand, the redox interactions with the redox-Bohr centre are all negative, i.e. the oxidation of the haems facilitates deprotonation of the redox centre and vice-versa (positive hetero-cooperativity). The correlation obtained for the distance and the redox interactions between pairs of haems (Figure 4.7) further supports the electrostatic origin of the redox interactions. The correlation between the redox-interaction values obtained for *Soc* by Harada and co-workers [18] and the Fe-Fe

distances taken from the *Soc* X-ray structure [17] is not so clearly electrostatic in origin (Figure 4.7).

However, it should be noted that Harada *et al.* observed some pH dependence but the redox-Bohr interactions were not separated from haem-haem interactions in their analysis.

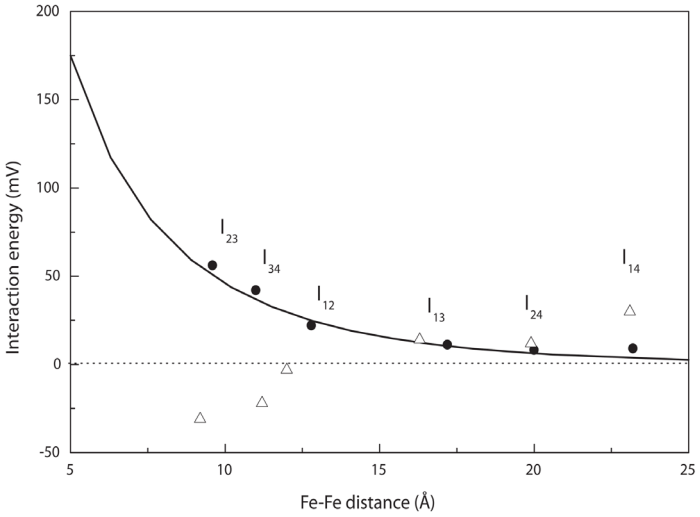

FIGURE 4.7 - Distance dependence of the pairwise interaction energies between the iron centres (Iij, interaction between haems i and j; i,j=1-4; i>j). The filled circles indicate the correlations obtained for *Sfc*. Triangles correlate the pairwise interactions values obtained by Harada and co-workers [18] for *Soc* and distances taken from the *Soc* crystal structure [16]. The solid line was obtained with an exponentially decaying Coulomb interaction considering an effective dielectric constant of 8.6 (0.6) and Debye length of 7.7 (0.3), as previously reported [19].

Structural mapping of the haem reduction potentials

As described above, haem-redox interactions modulate the redox potentials of the haem groups during the oxidation of the protein such that the order of oxidation is not necessarily the same as the order of potentials in the fully reduced protein. The order in which the haems oxidize is different in *Sfc* and *Soc*: it is IV-II-I-III for *Sfc* [19] and I-II-(III,IV) for *Soc* [18]. Of the 27 residues where the two proteins differ, 11 residues involve charge alteration: residues 3, 23, 26, 33, 47, 68, 71 and 86 are potentially charged in *Sfc* and are not charged in *Soc*, whereas residues 4, 20, and 41 become charged in *Soc*. Additionally, *Soc* has also two extra

positive residues at the C-terminus (Figure 4.6).

Overall, compared with *Soc*, *Sfc* has four extra negatively charged residues and three fewer positively charged. The substitutions are not localized in any particular region of the protein and most of them occur at protein surface, but the protein is small and the more negatively charged protein surface in *Sfc* might contribute to the differences observed in the haem reduction potentials.

The midpoint reduction potentials of *Sfc* at pH 7 are -215, -190, -175, and -125 mV for haems IV, II, I and III, respectively [19]. The reduction potential of haem III is clearly the least negative, so it dominates the last oxidation step of *Sfc*. Assuming that there is little change in conformation between the reduced and oxidised forms, this correlates well with the fact that haem III is by far the least solvent exposed (345, 305, 196 and 385 $Å^2$ for haems I, II, III and IV, respectively). Haem III also has the lowest solvent exposure in *Soc*, but its reduction potential in the last step of oxidation is more negative (-186 mV) than in *Sfc* and similar to that of haem IV [18].

The higher reduction potential of haem III in *Sfc* in comparison with that of *Soc* may be influenced by the replacement of residue Asn^{55} in *Soc* with the hydrophobic residue (Leu^{55}) in *Sfc*. This residue forces the side chain of the conserved residue Leu^{56} to orient toward haem III, creating a more hydrophobic environment (Figure 4.8).

Another important change between the two proteins is observed in the side chain orientation of the conserved residue Lys^{72}. This residue in the reduced *Soc* protein is hydrogen bonded to propionate group P17 of haem II (P_{17}^{II}), whereas the side chain of Lys^{72} in *Sfc* is reoriented towards propionate P13 of haem III (P_{13}^{III}) (Figure 4.9). Placing a positive charge close to haem III of *Sfc* helps to stabilize the reduced form of this haem and thus contributes to the high reduction potential of haem III in *Sfc*.

The solvent exposure of the remaining haem groups is similar and much greater than that of haem III. Since the reduction potentials of the haems I, II, and IV differ by less than 40 mV both in *Sfc* and *Soc*, a variety of subtle effects could easily be as important as the solvent effect. One possible effect is the geometry of the dihedral angle of the His rings and the haem porphyrin planes. Indeed, studies carried out in several cytochromes showed that changes in the angle formed between the His ring planes and those of the haem porphyrin may account for changes up to 30 mV in the haem redox potentials [38, 48-50].

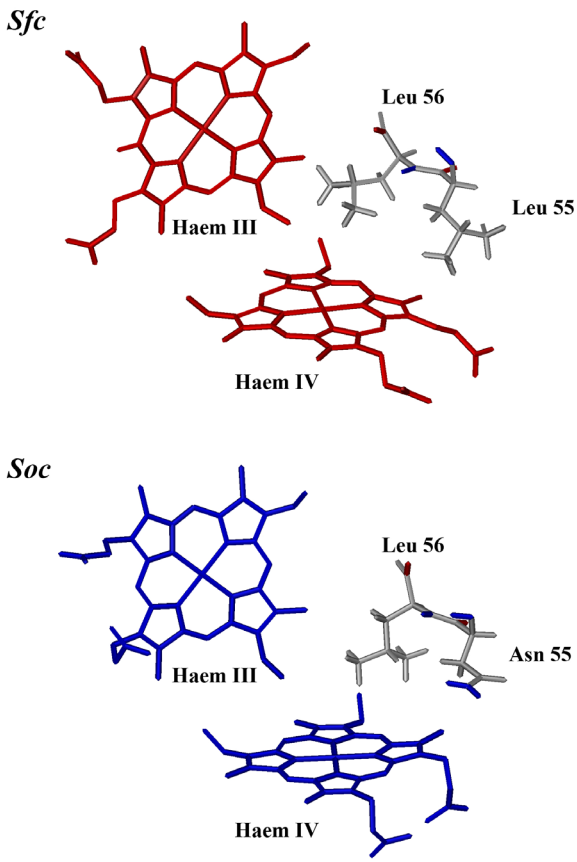

FIGURE 4.8 - Relative position of haems III and IV and residues 55-56 for the *Sfc* (best NMR structure) and *Soc* (X-ray structure [16]). Haems III and IV have the same orientations in both structures.

Structural mapping of the redox-Bohr center

Previous studies showed the individual reduction potentials of the haem groups (microscopic potentials) in *Sfc* are pH dependent, with haem III being by far the most affected. The redox-Bohr interaction, *i.e.* the measure of the effect of the redox-Bohr centre deprotonation on the reduction potential of the haems, is -36 mV for haem III, whereas for haems I, II, and IV are -9, -11, and -4 mV respectively [19], and the sign of the interactions is that expected for an electrostatic effect between an electron and a proton.

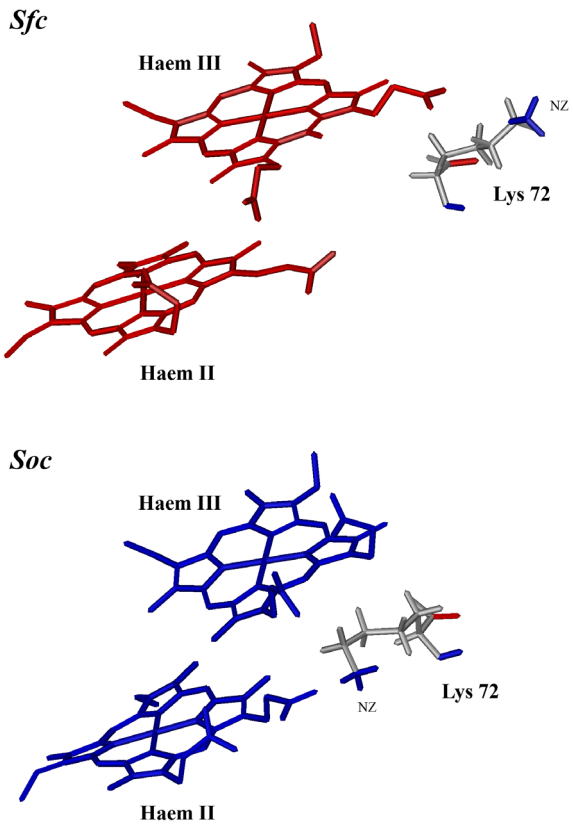

FIGURE 4.9 - Relative position of haems II and III and the conserved positively charged residue Lys72 for *Sfc* (best NMR structure) and *Soc* (X-ray structure [16]). Haems III and IV have the same orientations in both structures.

Thus, the ionisable centre responsible for the redox-Bohr effect in *Sfc* is close to haem III and may well be a propionate group of that haem. In the case of *Soc,* it was suggested that the redox-Bohr centre should be located close to haem II since Lys^{72} is hydrogen bonded to propionate group P_{17}^{II} in the reduced form [17] and moves toward haem III in the oxidised form (Figure 4.9). It is interesting to note that the conserved residue Lys^{72} adopts a completely different orientation in *Sfc*. Indeed in the reduced structure of *Sfc* the N^Z protons of Lys^{72} are pointing even further away from P_{17}^{II} than in the oxidised form of *Soc* (Figure 4.9).

CONCLUSIONS

The structure of the reduced tetrahaem cytochrome from *S. frigidimarina* is the first solution structure of a multihaem cytochrome isolated from *Shewanella* spp. The protein folds in a series of helices with no β-strands present. The haem groups are arranged in a linear fashion with haems I-II and III-IV exhibiting a perpendicular orientation of haem planes, whereas the planes of the central haems II-III are nearly parallel to each other. The structure shows close similarities with the X-ray structure determined for the tetrahaem cytochrome from *S. oneidensis* [17], with rearrangements of the side chains of two conserved residues (Leu^{56} and Lys^{72}) that influence the properties of the redox centres in the two proteins.

Comparison of the structures suggests that the small tetrahaem cytochromes isolated from *Shewanella* spp. represent a new structural motif that is distinct from that of the tetrahaem (and trihaem) cytochromes c_3 from the *Desulfovibrionacea* family (Dc_3). A similar motif, with some rearrangement of haem IV, is found in the N-terminal cytochrome domain of a flavocytochrome c_3 ($Sffc_3$) isolated from *S. frigidimarina* [15, 16]. The most remarkable feature of these motifs is that the architecture of the haem core is highly conserved despite low sequence homology. The purpose of this conserved geometry is certainly not obvious because

the thermodynamic properties of the haems, including homo- and hetero-cooperativities as well as the reduction potentials, differ substantially among Dc_3 and are also variable within the *Shewanella* spp. structural motif.

In the case of Dc_3, which are thought to transport pairs of electrons between the periplasmic hydrogenases and transmembrane electron transfer complexes, the geometry is likely to be important for the efficient transfer of consecutive electrons. Although the Dc_3 may be adapted to the specific conditions of different organisms, their properties within the electron transfer complexes are also likely to depend on those of their partners.

Understanding the diverse properties within the new family of *Shewanella* tetrahaem cytochromes will probably also require a detailed study of their electron transfer partners.

REFERENCES

1. Postgate, J.R., *Presence of cytochrome in a obligate anaerobe.* Biochem J, 1954. **56**: xi-xii.

2. Ishimoto, M.K., Koyama, J., and Nagai, Y., *A cytochrome and a green pigment of sulphate-reducing bacteria.* Bull Chem Soc Jap 1954. **27**: 564.

3. Louro, R.O., *Proton thrusters: overview of the structural and functional features of soluble tetrahaem cytochromes* c_3. J Biol Inorg Chem, 2007. **12**: 1-10.

4. Seeliger, S., Cord-Ruwisch, R., and Schink, B., *A periplasmic and extracellular* c*-type cytochrome of* Geobacter sulfurreducens *acts as a ferric iron reductase and as an electron carrier to other acceptors or to partner bacteria.* J Bacteriol, 1998. **180**: 3686-91.

5. Afkar, E. and Fukumori, Y., *Purification and characterization of triheme cytochrome* c_7 *from the metal-reducing bacterium,* Geobacter metallireducens. FEMS Microbiol Lett, 1999. **175**: 205-10.

6. Gordon, E.H., Pike, A.D., Hill, A.E., Cuthbertson, P.M., Chapman, S.K., and Reid, G.A., *Identification and characterization of a novel cytochrome* c_3 *from* Shewanella frigidimarina *that is involved in Fe(III) respiration.* Biochem J, 2000. **349**: 153-8.

7. Tsapin, A.I., Nealson, K.H., Meyers, T., Cusanovich, M.A., Van Beuumen, J., Crosby, L.D., Feinberg, B.A., and Zhang, C., *Purification and properties of a low-redox-potential tetraheme cytochrome* c_3 *from* Shewanella putrefaciens. J Bacteriol, 1996. **178**: 6386-8.

8. Mahadevan, R., Bond, D.R., Butler, J.E., Esteve-Nunez, A., Coppi, M.V., Palsson, B.O., Schilling, C.H., and Lovley, D.R., *Characterization of metabolism in the Fe(III)-reducing organism* Geobacter sulfurreducens *by constraint-based modeling.* Appl Environ Microbiol, 2006. **72**: 1558-68.

9. Pessanha, M., Morgado, L., Louro, R.O., Londer, Y.Y., Pokkuluri, P.R., Schiffer, M., and Salgueiro, C.A., *Thermodynamic characterization of triheme cytochrome PpcA from* Geobacter sulfurreducens*: evidence for a role played in*

e^-/H^+ energy transduction. Biochemistry, 2006. **45**: 13910-7.

10. Lloyd, J.R., Leang, C., Hodges Myerson, A.L., Coppi, M.V., Cuifo, S., Methe, B., Sandler, S.J., and Lovley, D.R., *Biochemical and genetic characterization of PpcA, a periplasmic* c*-type cytochrome in* Geobacter sulfurreducens. Biochem J, 2003. **369**: 153-61.

11. Pokkuluri, P.R., Londer, Y.Y., Duke, N.E., Long, W.C., and Schiffer, M., *Family of cytochrome* c_7*-type proteins from* Geobacter sulfurreducens*: structure of one cytochrome* c_7 *at 1.45 A resolution.* Biochemistry, 2004. **43**: 849-59.

12. Czjzek, M., Arnoux, P., Haser, R., and Shepard, W., *Structure of cytochrome* c_7 *from* Desulfuromonas acetoxidans *at 1.9 A resolution.* Acta Crystallogr D Biol Crystallogr, 2001. **57**: 670-8.

13. Coutinho, I.B., Turner, D.L., Liu, M.Y., LeGall, J., and Xavier, A.V., *Structure of the three-haem core of cytochrome* $c_{551.5}$ *determined by* ^1H *NMR.* J Biol Inorg Chem, 1996. **1**: 305-11.

14. Pessanha, M., Brennan, L., Xavier, A.V., Cuthbertson, P.M., Reid, G.A., Chapman, S.K., Turner, D.L., and Salgueiro, C.A., *NMR structure of the haem core of a novel tetrahaem cytochrome isolated from* Shewanella frigidimarina*: identification of the haem-specific axial ligands and order of oxidation.* FEBS Lett, 2001. **489**: 8-13.

15. Taylor, P., Pealing, S.L., Reid, G.A., Chapman, S.K., and Walkinshaw, M.D., *Structural and mechanistic mapping of a unique fumarate reductase.* Nat Struct Biol, 1999. **6**: 1108-12.

16. Leys, D., Tsapin, A.S., Nealson, K.H., Meyer, T.E., Cusanovich, M.A., and Van Beeumen, J.J., *Structure and mechanism of the flavocytochrome* c *fumarate reductase of* Shewanella putrefaciens *MR-1.* Nat Struct Biol, 1999. **6**: 1113-7.

17. Leys, D., Meyer, T.E., Tsapin, A.S., Nealson, K.H., Cusanovich, M.A., and Van Beeumen, J.J., *Crystal structures at atomic resolution reveal the novel concept of "electron-harvesting" as a role for the small tetraheme cytochrome* c. J Biol Chem, 2002. **277**: 35703-11.

18. Harada, E., Kumagai, J., Ozawa, K., Imabayashi, S., Tsapin, A.S., Nealson, K.H., Meyer, T.E., Cusanovich, M.A., and Akutsu, H., *A directional electron transfer regulator based on heme-chain architecture in the small tetraheme cytochrome* c *from* Shewanella oneidensis. FEBS Lett, 2002. **532**: 333-7.

19. Pessanha, M., Louro, R.O., Correia, I.J., Rothery, E.L., Pankhurst, K.L., Reid, G.A., Chapman, S.K., Turner, D.L., and Salgueiro, C.A., *Thermodynamic characterization of a tetrahaem cytochrome isolated from a facultative aerobic bacterium,* Shewanella frigidimarina*: a putative redox model for flavocytochrome* c_3. Biochem J, 2003. **370**: 489-95.

20. Paquete, C.M., Pereira, P.M., Catarino, T., Turner, D.L., Louro, R.O., and Xavier, A.V., *Functional properties of type I and type II cytochromes* c_3 *from* Desulfovibrio africanus. Biochim Biophys Acta, 2007. **1767**: 178-88.

21. Glasoe, P.K. and Long, F.A., *Use of glass electrodes to measure acidities in deuterium oxide.* J Phys Chem, 1960. **64**: 188-90.

22. Marion, D. and Wuthrich, K., *Application of phase sensitive two-dimensional correlated spectroscopy (COSY) for measurements of* ^1H-^1H *spin-spin coupling constants in proteins.* Biochem Biophys Res Commun, 1983. **113**: 967-74.

23. Jeener, J., Meier, B.H., Bachmann, P., and Ernst, R.R., *Investigation of exchange processes by two-dimensional NMR spectroscopy.* J Chem Phys, 1979. **71**: 4546-53.

24. Kumar, A., Ernst, R.R., and Wuthrich, K., *A two-dimensional nuclear Overhauser enhancement (2D NOE) experiment for the elucidation of complete proton-proton cross-relaxation networks in biological macromolecules.* Biochem Biophys Res Commun, 1980. **95**: 1-6.

25. Brown, S.C., Weber, P.L., and Mueller, L., *Toward complete* ^1H *NMR spectra in proteins.* J Magn Reson, 1988. **77**: 166-9.

26. Bearden, D.W., Macura, S., and Brown, L.R., *Suppression of cross relaxation in TOCSY experiments on macromolecules.* J Magn Reson, 1988. **80**: 534-8.

27. Briand, J. and Ernst, R.R., *Computer-optimized homonuclear TOCSY experiments with suppression of cross relaxation.* Chem Phys Lett, 1991. **185**: 276-85.

28. Griesinger, C., Otting, G., Wuethrich, K., and Ernst, R.R., *Clean TOCSY for proton spin system identification in*

macromolecules. J Am Chem Soc, 1988. **110**: 7870-2.

29. Rance, M., Sorensen, O.W., Bodenhausen, G., Wagner, G., Ernst, R.R., and Wuthrich, K., *Improved spectral resolution in cosy ^{1}H NMR spectra of proteins via double quantum filtering.* Biochem Biophys Res Commun, 1983. **117**: 479-85.

30. Derome, A.E. and Williamson, M.P., *Rapid-pulsing artifacts in double-quantum-filtered COSY.* J Magn Reson, 1990. **88**: 177-85.

31. Bartels, C., Xia, T.-h., Billeter, M., Güntert, P., and Wüthrich, K., *The program XEASY for computer-supported NMR spectral analysis of biological macromolecules.* J Biomol NMR, 1995. **6**: 1-10.

32. Wüthrich, K., *NMR of Proteins and Nucleic Acids*. 1986, John Wiley and Sons: NY. 30-1, 130-61.

33. Guntert, P., Braun, W., and Wuthrich, K., *Efficient computation of three-dimensional protein structures in solution from nuclear magnetic resonance data using the program DIANA and the supporting programs CALIBA, HABAS and GLOMSA.* J Mol Biol, 1991. **217**: 517-30.

34. Goddard, T.D. and Kneller, D.G., SPARKY 3, University of California: San Francisco.

35. Messias, A.C., Kastrau, D.H., Costa, H.S., LeGall, J., Turner, D.L., Santos, H., and Xavier, A.V., *Solution structure of* Desulfovibrio vulgaris *(Hildenborough) ferrocytochrome* c_3*: structural basis for functional cooperativity.* J Mol Biol, 1998. **281**: 719-39.

36. Turner, D.L., Brennan, L., Meyer, H.E., Lohaus, C., Siethoff, C., Costa, H.S., Gonzalez, B., Santos, H., and Suarez, J.E., *Solution structure of plantaricin C, a novel lantibiotic.* Eur J Biochem, 1999. **264**: 833-9.

37. Guntert, P. and Wuthrich, K., *Improved efficiency of protein structure calculations from NMR data using the program DIANA with redundant dihedral angle constraints.* J Biomol NMR, 1991. **1**: 447-56.

38. Wareham, R.S., Kilburn, J.D., Rees, N.H., Turner, D.L., Leach, A.R., and Holmes, D.S., *Synthesis and Solution Conformation of a C2 Symmetric Macrobicycle.* Tetrahedron Lett, 1995. **36**: 3047-50.

39. Wareham, R.S., Kilburn, J.D., Turner, D.L., Rees, N.H., and Holmes, D.S., *Homeomorphic Isomerism in a Peptidic Macrobicycle.* Angew Chem, Int Ed Engl, 1996. **34**: 2660-2.

40. Turner, D.L., Brennan, L., Chamberlin, S.G., Louro, R.O., and Xavier, A.V., *Determination of solution structures of paramagnetic proteins by NMR.* Eur Biophys J, 1998. **27**: 367-75.

41. Guntert, P., Mumenthaler, C., and Wuthrich, K., *Torsion angle dynamics for NMR structure calculation with the new program DYANA.* J Mol Biol, 1997. **273**: 283-98.

42. Pettersen, E.F., Goddard, T.D., Huang, C.C., Couch, G.S., Greenblatt, D.M., Meng, E.C., and and Ferrin, T.E., *CSF Chimera - A Visualization System for Exploratory Research and Analysis.* J Comput Chem, 2004. **25**: 1605-12.

43. Koradi, R., Billeter, M., and and Wüthrich, K., *MOLMOL: a program for display and analysis of macromolecular structures.* J Mol Graphics, 1996. **14**: 51-5.

44. Vriend, G., *WHAT IF: A molecular modeling and drug design program.* J. Mol. Graph., 1990. **8**: 52-6.

45. Hutchinson, E.G. and Thornton, J.M., *PROMOTIF--A program to identify and analyze structural motifs in proteins.* Protein Sci, 1996. **5**: 212-20.

46. Williamson, M.P. and Asakura, T., *Empirical Comparisons of Models for Chemical-Shift Calculation in Proteins.* J of Magn Reson, 1993. **101**: 63-71.

47. Pessanha, M., Londer, Y.Y., Long, W.C., Erickson, J., Pokkuluri, P.R., Schiffer, M., and Salgueiro, C.A., *Redox characterization of* Geobacter sulfurreducens *cytochrome* c_7*: physiological relevance of the conserved residue F15 probed by site-specific mutagenesis.* Biochemistry, 2004. **43**: 9909-17.

48. Sarma, S., DiGate, R.J., Goodin, D.B., Miller, C.J., and Guiles, R.D., *Effect of axial ligand plane reorientation on electronic and electrochemical properties observed in the A67V mutant of rat cytochrome* b_5*.* Biochemistry, 1997. **36**: 5658-68.

49. Xue, L.L., Wang, Y.H., Xie, Y., Yao, P., Wang, W.H., Qian, W., Huang, Z.X., Wu, J., and Xia, Z.X., *Effect of mutation at valine 61 on the three-dimensional structure, stability, and redox potential of cytochrome* b_5*.* Biochemistry, 1999. **38**: 11961-72.

50. Sarma, S., Dangi, B., Yan, C., DiGate, R.J., Banville, D.L., and Guiles, R.D., *Characterization of a site-directed*

mutant of cytochrome b_5 *designed to alter axial imidazole ligand plane orientation.* Biochemistry, 1997. **36**: 5645-57.

5

INTEGRATED OVERVIEW

CONTENTS

INTEGRATED OVERVIEW

Our understanding of the structural-functional role of small periplasmic tetrahaem cytochromes is still rather limited.

Cytochromes c_3 from *Desulfovibrio* spp. (Dc_3) are the best studied members of the tetrahaem cytochrome family. These cytochromes have approximately 30 amino acids per haem and have been suggested to play a fundamental role in the bioenergetic metabolism of the host organisms. Various metabolic models propose that Dc_3 act as mediators between periplasmic hydrogenases and transmembrane electron complexes.

Several Dc_3 were thermodynamically characterized in detail using NMR and visible spectroscopic techniques [1-6]. The structural characterization of these proteins by X-ray and NMR techniques revealed a conserved general folding and haem core architecture in spite of the low amino-acid sequence homology between the members of this family [7-18].

Until late 1990's only tetrahaem cytochromes c_3 from *Desulfovibrio* spp. were reported in the literature, however, in the year 2000 an even smaller tetrahaem cytochrome with only approximately 20 amino acid residues per haem group was identified in a different bacteria: *Shewanella frigidimarina* NCIMB400 [19]. This finding revealed new functional involvements for tetrahaem cytochromes in the metabolic pathways leading to the reduction of extracellular metal oxides. One basic question emerges. What are the structural features of this new tetrahaem cytochrome and how does it compare with cytochromes c_3 from *Desulfovibrio* spp.?

In this Thesis we have attempted to contribute to a better understanding of the structural features of these two types of tetrahaem cytochromes by determining the solution structure of cytochrome c_3 from *Desulfovibrio desulfuricans* ATCC 27774 (Chapter 3) and the tetrahaem cytochrome isolated from *Shewanella frigidimarina* (Chapter 4).

In the case of cytochrome c_3 from *D. desulfuricans* (*Dd27*c_3) which belongs to a structurally well characterized family of cytochromes in which the four haem groups adopt a nearly circular disposition, the detailed thermodynamic characterization revealed the presence of two redox-Bohr centres, a distinct feature never reported for this family. On the contrary, for the tetrahaem cytochrome isolated from *S. frigidimarina* (*Sfc*), preliminary studies suggested that it might have a completely different disposition of the haem groups [20].

Solution structures of fully reduced and oxidised forms of *Dd27*c_3 have been determined to assess the conformational changes arising upon reduction and protonation. This allowed us to interpret the functional significance of the deviations from simple electrostatic interactions. To ensure that any conformational change would depend only on the redox state, the pH of the samples was set below that of the groups involved in the redox-Bohr interactions.

The comparison of the reduced and oxidised structures showed a conserved general fold, with the haem core region and iron-iron distances virtually unchanged and only minor differences between the consensus secondary structure elements. A few regions however show significant differences between the reduced and oxidized forms, indicating redox-related structural changes. In fact, a concerted movement of several regions leads to the rearrangement of Glu^{61} and Lys^{75} in conformity with previous simulations that have identified these residues as playing an important role in the redox properties of *Dd27*c_3 [12, 21].

As in the case of tetrahaem cytochromes c_3 from *D. vulgaris* and *D. gigas* that show positive cooperativity between haems, *Dd27*c_3 shows nearly zero redox interaction between haems I and II in spite of their close proximity, which indicates an electrostatic interaction cancellation. This is consistent with the aforementioned redox-linked rearrangements of Glu^{61} and the other two residues near haem II, which seem to make an important contribution to the observed positive cooperativity between haem I and II.

The four reduction potentials of *Dd27c*$_3$ show pH dependence mediated by two distinct pK_a. Previous studies have identified the key residues for the redox-Bohr effect [12, 21], but no significant conformational changes are observed in these regions. This is expected since the protonatable centres involved in the redox-Bohr effect are essentially protonated at the pH values chosen. As a consequence, the analysis of the redox-related structural changes should be more robust due to the absence of the redox-Bohr contribution.

The small tetrahaem cytochrome *Sfc* from *S. frigidimarina* shows a distinct structural motif from that of the tetrahaem cytochromes from the *Desulfovibrionacea* family (*Dc*$_3$), with the four haem groups oriented in a quasi-linear architecture instead of the circular arrangement found in *Dc*$_3$. The *Sfc* structure shows close similarities with the three-dimensional structure determined for the highly homologous (69% sequence identity) tetrahaem cytochrome from *S. oneidensis* (*Soc*) [22] both for the haem spatial disposition and the general fold.

A similar haem motif is also found in the N-terminal domain of periplasmic tetrahaem flavocytochromes isolated from *S. frigidimarina* [23] and *S. oneidensis* [24]. Flavocytochromes are composed of three domains: the N-terminal haem domain containing four *c*-type haems with bis-histidinyl axial coordination; the flavin domain containing a non-covalently bound FAD and the clamp domain, which consists of a four stranded antiparallel β-sheet surrounded by several α-helices [23, 24]. The haem binding motifs, as well as the histidines providing the distal axial coordination of the iron in the N-terminal domain of flavocytochromes *c*$_3$ from *S. frigidimarina* and *S. oneidensis* are also conserved with exception of haem IV, which controls the passage of electrons to the flavin domain.

This shows that the small tetrahaem cytochromes isolated from *Shewanella* spp. represents a new structural motif distinct from that of *Dc*$_3$. As in the case of *Dc*$_3$, the most remarkable feature of these motifs is that

the architecture of the haem core is highly conserved despite their low sequence homology, considerable diversity in their primary structure and different haem reduction potentials.

In summary, the studies carried out for this Thesis elucidated the structural features for the unique cytochrome c_3 with two redox-Bohr centres controlling its functional properties. Comparison between the structures in the reduced and oxidised state showed that, redox-linked localized modifications are evident, allowing the identification of the conformational changes involved in the positive cooperativities and responsible for the counter electrostatic effects. This was an important issue missing in the structural characterization of the members of the cytochrome c_3 family.

On the other hand the structural characterization of a tetrahaem cytochrome isolated from *S. frigidimarina* revealed a completely different structural motif for the haem architecture that is distinct from that of Dc_3. The structural data now available for the members of *Shewanellacea* family suggests that, as for Dc_3, the haem geometry is conserved, in spite of the diversity encountered for the thermodynamic properties of their members.

REFERENCES

1. Correia, I.J., Paquete, C.M., Louro, R.O., Catarino, T., Turner, D.L., and Xavier, A.V., *Thermodynamic and kinetic characterization of trihaem cytochrome* c_3 *from* Desulfuromonas acetoxidans. Eur J Biochem, 2002. **269**: 5722-30.

2. Turner, D.L., Salgueiro, C.A., Catarino, T., Legall, J., and Xavier, A.V., *NMR studies of cooperativity in the tetrahaem cytochrome* c_3 *from* Desulfovibrio vulgaris. Eur J Biochem, 1996. **241**: 723-31.

3. Louro, R.O., Catarino, T., LeGall, J., Turner, D.L., and Xavier, A.V., *Cooperativity between electrons and protons in a monomeric cytochrome* c_3*: the importance of mechanochemical coupling for energy transduction.* Chembiochem, 2001. **2**: 831-7.

4. Louro, R.O., Catarino, T., Turner, D.L., Picarra-Pereira, M.A., Pacheco, I., LeGall, J., and Xavier, A.V., *Functional and mechanistic studies of cytochrome* c_3 *from* Desulfovibrio gigas*: thermodynamics of a "proton thruster".* Biochemistry, 1998. **37**: 15808-15.

5. Paquete, C.M., Pereira, P.M., Catarino, T., Turner, D.L., Louro, R.O., and Xavier, A.V., *Functional properties of type I and type II cytochromes* c_3 *from* Desulfovibrio africanus. Biochim Biophys Acta, 2007. **1767**: 178-88.

6. Paquete, C.M., Turner, D.L., Louro, R.O., Xavier,

A.V., and Catarino, T., *Thermodynamic and kinetic characterisation of individual haems in multicentre cytochromes* c_3. Biochim Biophys Acta, 2007. **1767**: 1169-79.

7. Brennan, L., Turner, D.L., Messias, A.C., Teodoro, M.L., LeGall, J., Santos, H., and Xavier, A.V., *Structural basis for the network of functional cooperativities in cytochrome* c_3 *from* Desulfovibrio gigas*: solution structures of the oxidised and reduced states.* J Mol Biol, 2000. **298**: 61-82.

8. Matias, P.M., Frazao, C., Morais, J., Coll, M., and Carrondo, M.A., *Structure analysis of cytochrome* c_3 *from* Desulfovibrio vulgaris *Hildenborough at 1.9 A resolution.* J Mol Biol, 1993. **234**: 680-99.

9. Matias, P.M., Morais, J., Coelho, R., Carrondo, M.A., Wilson, K., Dauter, Z., and Sieker, L., *Cytochrome* c_3 *from* Desulfovibrio gigas*: crystal structure at 1.8 A resolution and evidence for a specific calcium-binding site.* Protein Sci, 1996. **5**: 1342-54.

10. Messias, A.C., Kastrau, D.H., Costa, H.S., LeGall, J., Turner, D.L., Santos, H., and Xavier, A.V., *Solution structure of* Desulfovibrio vulgaris *(Hildenborough) ferrocytochrome* c_3*: structural basis for functional cooperativity.* J Mol Biol, 1998. **281**: 719-39.

11. Nørager, S., Legrand, P., Pieulle, L., Hatchikian, C., and Roth, M., *Crystal structure of the oxidised and reduced acidic cytochrome* c_3 *from* Desulfovibrio africanus. J Mol Biol, 1999. **290**: 881-902.

12. Bento, I., Matias, P.M., Baptista, A.M., da Costa, P.N., van Dongen, W.M., Saraiva, L.M., Schneider, T.R., Soares, C.M., and Carrondo, M.A., *Molecular basis for redox-Bohr and cooperative effects in cytochrome* c_3 *from* Desulfovibrio desulfuricans *ATCC 27774: crystallographic and modeling studies of oxidized and reduced high-resolution structures at pH 7.6.* Proteins, 2004. **54**: 135-52.

13. Correia, I.J., Paquete, C.M., Coelho, A., Almeida, C.C., Catarino, T., Louro, R.O., Frazao, C., Saraiva, L.M., Carrondo, M.A., Turner, D.L., and Xavier, A.V., *Proton-assisted two-electron transfer in natural variants of tetraheme cytochromes from* Desulfomicrobium *Sp.* J Biol Chem, 2004. **279**: 52227-37.

14. Coutinho, I.B., Turner, D.L., Legall, J., and Xavier, A.V., *Revision of the haem-core architecture in the tetraheam cytochrome* c_3 *from* Desulfovibrio baculatus *by two-dimensional* ^1H *NMR.* Eur J Biochem, 1992. **209**: 329-33.

15. Czjzek, M., Payan, F., Guerlesquin, F., Bruschi, M., and Haser, R., *Crystal structure of cytochrome* c_3 *from* Desulfovibrio desulfuricans *Norway at 1·7 Å resolution.* J Mol Biol, 1994. **243**: 653-67.

16. Einsle, O., Foerster, S., Mann, K., Fritz, G., Messerschmidt, A., and Kroneck, P.M., *Spectroscopic investigation and determination of reactivity and structure of the tetraheme cytochrome* c_3 *from* Desulfovibrio desulfuricans *Essex 6.* Eur J Biochem, 2001. **268**: 3028-35.

17. Morais, J., Palma, P.N., Frazao, C., Caldeira, J., LeGall, J., Moura, I., Moura, J.J., and Carrondo, M.A., *Structure of the tetraheme cytochrome from* Desulfovibrio desulfuricans *ATCC 27774: X-ray diffraction and electron paramagnetic resonance studies.* Biochemistry, 1995. **34**: 12830-41.

18. Simões, P., Matias, P.M., Morais, J., Wilsonc, K., Dauterc, Z., and Carrondo, M.A., *Refinement of the three-dimensional structures of cytochrome* c_3 *from* Desulfovibrio vulgaris *Hildenborough at 1.67 Å resolution and from* Desulfovibrio desulfuricans *ATCC 27774 at 1.6 Å resolution.* Inorg Chim Acta, 1998. **273**: 213-24.

19. Gordon, E.H., Pike, A.D., Hill, A.E., Cuthbertson, P.M., Chapman, S.K., and Reid, G.A., *Identification and characterization of a novel cytochrome* c_3 *from* Shewanella frigidimarina *that is involved in Fe(III) respiration.* Biochem J, 2000. **349**: 153-8.

20. Pessanha, M., Brennan, L., Xavier, A.V., Cuthbertson, P.M., Reid, G.A., Chapman, S.K., Turner, D.L., and Salgueiro, C.A., *NMR structure of the haem core of a novel tetrahaem cytochrome isolated from* Shewanella frigidimarina*: identification of the haem-specific axial ligands and order of oxidation.* FEBS Lett, 2001. **489**: 8-13.

21. Louro, R.O., Bento, I., Matias, P.M., Catarino, T., Baptista, A.M., Soares, C.M., Carrondo, M.A., Turner, D.L., and Xavier, A.V., *Conformational component in the coupled transfer of multiple electrons and protons in a monomeric tetraheme cytochrome.* J Biol Chem, 2001. **276**: 44044-51.

22. Leys, D., Tsapin, A.S., Nealson, K.H., Meyer, T.E.,

Cusanovich, M.A., and Van Beeumen, J.J., *Structure and mechanism of the flavocytochrome* c *fumarate reductase of* Shewanella putrefaciens *MR-1.* Nat Struct Biol, 1999. **6**: 1113-7.

23. Taylor, P., Pealing, S.L., Reid, G.A., Chapman, S.K., and Walkinshaw, M.D., *Structural and mechanistic mapping of a unique fumarate reductase.* Nat Struct Biol, 1999. **6**: 1108-12.

24. Page, C.C., Moser, C.C., Chen, X., and Dutton, P.L., *Natural engineering principles of electron tunnelling in biological oxidation-reduction.* Nature, 1999. **402**: 47-52.

APPENDIX

CONTENTS

APPENDIX

Tables with the thermodynamic parameters determined for various *Dc*$_3$ and *Sfc*

The fully reduced and protonated protein was taken as reference state for all the haems.

Diagonal values (in bold) correspond to oxidation energies of the haems and deprotonating energy of the redox-Bohr center. Off-diagonal values are the redox and redox-Bohr interactions energies.

All energies are reported in meV and standard errors are given in parenthesis.

Energies (meV)					
D. africanus [1]					
	Haem I	Haem II	Haem III	Haem IV	Redox-Bohr centre
Haem I	**-280 (2)**	11 (2)	-	-13 (1)	-36 (1)
Haem II		**-267 (3)**	-	8 (1)	-20 (1)
Haem III			**-84 (4)**	-	-10 (9)
Haem IV				**-280 (2)**	-26 (1)
Redox-Bohr centre					**483 (12)**

Energies (meV)					
D. vulgaris (Hildenborough) [2]					
	Haem I	Haem II	Haem III	Haem IV	Redox-Bohr centre
Haem I	**-252 (2)**	-39 (1)	19 (1)	3 (3)	-74 (3)
Haem II		**-284 (2)**	1 (1)	10 (2)	-36 (1)
Haem III			**-343 (1)**	34 (2)	-23 (2)
Haem IV				**-293 (2)**	-14 (2)
Redox-Bohr centre					**454 (3)**

Energies (meV)					
D. vulgaris (Miyazaki F) [3]					
	Haem I	Haem II	Haem III	Haem IV	Redox-Bohr centre
Haem I	**-259 (2)**	-32 (2)	17 (3)	14 (2)	-54 (2)
Haem II		**-325 (2)**	25 (2)	21 (3)	-28 (2)
Haem III			**-352 (2)**	39 (2)	-19 (2)
Haem IV				**-318 (2)**	-12 (2)
Redox-Bohr centre					**467 (5)**

Energies (meV)					
D. gigas [2]					
	Haem I	Haem II	Haem III	Haem IV	Redox-Bohr centre
Haem I	**-279 (2)**	-15 (3)	51 (3)	-16 (7)	-62 (2)
Haem II		**-262 (2)**	-52 (4)	59 (4)	-25 (2)
Haem III			**-240 (3)**	22 (3)	-38 (2)
Haem IV				**-202 (7)**	-18 (3)
Redox-Bohr centre					**491 (4)**

Energies (meV)						
D. desulfuricans ATCC 27774 [1]						
	Haem I	Haem II	Haem III	Haem IV	Redox-Bohr centre I	Redox-Bohr centre II
Haem I	**-237 (2)**	3 (2)	62 (6)	20 (5)	-	-88 (5)
Haem II		**-279 (2)**	40 (10)	12 (6)	-63 (3)	-
Haem III			**-215 (9)**	48 (2)	-55 (6)	-
Haem IV				**-206 (6)**	-33 (4)	-
Redox-Bohr centre I					**440 (3)**	-
Redox-Bohr centre II						**377 (4)**

Energies (meV)					
Dsmn [4]					
	Haem I	Haem II	Haem III	Haem IV	Redox-Bohr centre
Haem I	**-257 (2)**	15 (2)	-	12 (6)	-37 (3)
Haem II		**-312 (2)**	-	20 (3)	-24 (2)
Haem III			**-62 (2)**	-	-53 (8)
Haem IV				**-274 (2)**	-13 (3)
Redox-Bohr centre					**413 (4)**

Energies (meV)					
Dsmb [4]					
	Haem I	Haem II	Haem III	Haem IV	Redox-Bohr centre
Haem I	**-293 (2)**	13 (2)	-	14 (2)	-23 (3)
Haem II		**-336 (2)**	-	18 (2)	-13 (2)
Haem III			**-79 (2)**	-	-31 (10)
Haem IV				**-294 (3)**	-9 (3)
Redox-Bohr centre					**413 (5)**

Energies (meV)					
Sfc [5]					
	Haem I	Haem II	Haem III	Haem IV	Redox-Bohr centre
Haem I	**-190 (3)**	22 (1)	11 (1)	9 (1)	-9 (2)
Haem II		**-212 (3)**	56 (2)	8 (1)	-11 (2)
Haem III			**-199 (3)**	42 (2)	-36 (2)
Haem IV				**-229 (2)**	-4 (2)
Redox-Bohr centre					**443 (5)**

Tables with the macroscopic pK_as for the ionisable centres for various Dc_3 and *Sfc*

Macroscopic pK_as for the ionisable(s) centre(s) associated with each of the five stages of oxidation determined for various Dc_3 and *Sfc*. From [2].

	Stage 0	Stage 1	Stage 2	Stage 3	Stage 4
D. gigas	8.3	7.4	7.0	6.2	5.9
D. vulgaris	7.7	7.2	6.5	5.6	5.2
D. desulfuricans ATCC 27774	7.4	7.0	6.4	5.8	4.9
	6.4	6.2	5.3	5.0	4.9
Dsmb	6.4	6.2	5.9	5.6	5.1
Dsmn	7.0	6.6	6.2	5.7	4.8
D. vulgaris (Miyazaki F)	7.8	7.4	6.9	6.2	5.9
D. africanus	8.2	7.7	7.2	6.8	6.6
Sfc	7.5	7.3	7.1	6.9	6.5

REFERENCES

1. Paquete, C.M., Pereira, P.M., Catarino, T., Turner, D.L., Louro, R.O., and Xavier, A.V., *Functional properties of type I and type II cytochromes* c_3 *from* Desulfovibrio africanus. Biochim Biophys Acta, 2007. **1767**: 178-88.

2. Paquete, C.M., Turner, D.L., Louro, R.O., Xavier, A.V., and Catarino, T., *Thermodynamic and kinetic characterisation of individual haems in multicentre cytochromes* c_3. Biochim Biophys Acta, 2007. **1767**: 1169-79.

3. Salgueiro, C.A., Turner, D.L., LeGall, J., and Xavier, A.V., *Reevaluation of the redox and redox-Bohr cooperativity in tetrahaem* Desulfovibrio vulgaris *(Miyazaki F) cytochrome* c_3. J Biol Inor Chem, 1997. **2**: 343-9.

4. Correia, I.J., Paquete, C.M., Coelho, A., Almeida, C.C., Catarino, T., Louro, R.O., Frazao, C., Saraiva, L.M., Carrondo, M.A., Turner, D.L., and Xavier, A.V., *Proton-assisted two-electron transfer in natural variants of tetraheme cytochromes from* Desulfomicrobium *Sp.* J Biol Chem, 2004. **279**: 52227-37.

5. Pessanha, M., Louro, R.O., Correia, I.J., Rothery, E.L., Pankhurst, K.L., Reid, G.A., Chapman, S.K., Turner, D.L., and Salgueiro, C.A., *Thermodynamic characterization of a tetrahaem cytochrome isolated from a facultative aerobic bacterium,* Shewanella frigidimarina*: a putative redox model for flavocytochrome* c_3. Biochem J, 2003. 370: 489-95.

Apoio financeiro da FCT e do FSE no âmbito do Quadro Comunitário de Apoio,
Grant SFRH / BD / 5830 / 2001 financiada pelo POCTI – Formar e Qualificar – Medida 1.1º